Alma Mater Studiorum - Università di Bologna

Facoltà di Chimica Industriale
Dipartimento di Chimica Industriale e dei Materiali

Structural changes and dynamic behaviour of vanadium oxide-based catalysts for gas-phase selective oxidations

Tesi di Dottorato di Ricerca

Presentata da:
Dott.ssa **Silvia Luciani**

Relatore:
Prof. **Fabrizio Cavani**

Co-relatore:
Dott. **Nicola Ballarini**

Coordinatore:
Chiar.mo Prof. **Luigi Angiolini**

Dottorato di Ricerca in
Chimica Industriale (settore CHIM/04)
ciclo XXI

Esame finale anno 2009

INDEX

ABSTRACT

Selective oxidation is one of the simplest functionalization methods and essentially all monomers used in manufacturing artificial fibers and plastics are obtained by catalytic oxidation processes. Formally, oxidation is considered as an increase in the oxidation number of the carbon atoms, then reactions such as dehydrogenation, ammoxidation, cyclization or chlorination are all oxidation reactions. In this field, most of processes for the synthesis of important chemicals use vanadium oxide-based catalysts. These catalytic systems are used either in the form of multicomponent mixed oxides and oxysalts, e.g., in the oxidation of *n*-butane (V/P/O) and of benzene (supported V/Mo/O) to maleic anhydride (MA), or in the form of supported metal oxide, e.g., in the manufacture of phthalic anhydride by o-xylene oxidation, of sulphuric acid by oxidation of SO_2, in the reduction of NO_x with ammonia and in the ammoxidation of alkyl aromatics. In addition, supported vanadia catalysts have also been investigated for the oxidative dehydrogenation of alkanes to olefins, the oxidation of pentane to MA and the selective oxidation of methanol to formaldehyde or methyl formate [1].

During my PhD I focused my work on two gas phase selective oxidation reactions. The work was done at the Department of Industrial Chemistry and Materials (University of Bologna) in collaboration with Polynt SpA. Polynt is a leader company in the development, production and marketing of catalysts for gas-phase oxidation.

In particular, I studied the catalytic systems for *n*-butane oxidation to MA (fluid bed technology) and for o-xylene oxidation to phthalic anhydride. Both reactions are catalyzed by systems based on vanadium, but catalysts are completely different. Part A deals with the study of the V/P/O catalyst for *n*-butane selective oxidation, while in Part B the results of an investigation on TiO_2-supported V_2O_5 catalyst for o-xylene oxidation are reported.

Part A reports an introduction about the importance of MA, its uses, the industrial processes and the catalytic system. The oxidation of *n*-butane is the only industrial example of direct transformation of an alkane into an intermediate. MA is produced using either a fixed bed or a fluid bed technology; in both cases, the catalyst is the vanadyl pyrophosphate (VPP). Notwithstanding the good performances, the yield value doesn't exceed 60% and the system is continuously studied to improve activity and selectivity.

The main open problem is the understanding of the real active phase that develops under reaction conditions. Several articles deal with the role of different crystalline and/or amorphous vanadium/phosphorus (VPO) compounds. In all cases, bulk VPP is assumed to constitute the core of the active phase, while two different hypotheses have been formulated concerning the catalytic surface. In one case the development of surface amorphous layers that play a direct role in the reaction is described, in the second case specific planes of crystalline VPP are assumed to contribute to the reaction pattern, and the redox process occurs reversibly between VPP and $VOPO_4$. Both hypotheses are supported also by *in-situ* characterization techniques, but the experiments have been performed with different catalysts and probably under slightly different working conditions. Due to the complexity of the system, these differences could be the cause of the contradictions in the literature.

Under the hypothesis that a key role might be played by the P/V atomic ratio, I prepared, characterized and tested two samples with different P/V ratio. The transformations occurring on catalytic surfaces under different conditions of temperature and gas-phase composition were studied by means of *in-situ* Raman spectroscopy, trying to investigate the changes that VPP undergoes during reaction. The goal is to find out which compound constituting the catalyst surface is the most active and selective for *n*-butane oxidation, and also which features the catalyst should possess to ensure the development of this catalytically active surface (e.g. catalyst composition). Starting from the results from this study, we designed a new V/P/O-based catalyst, with the aim of developing a more active and selective system than those currently used.

In fact, the second topic investigated was the attempt to reproduce the surface active layer of VPP in a supported catalyst, that is, the spreading of the active phase onto a support. In general, supporting is a way to improve the mechanical

properties of catalysts, to overcome problems associated to the development of local hot spot temperatures, which might cause a decrease of selectivity at high conversion, and finally to lower the cost of the catalyst. In literature, it is possible to find several works dealing with the preparation of supported catalysts, but in general the intrinsic characteristics of VPP are worsened due to the chemical interaction with the support. Moreover all published works deal with the deposition of VPP on various types of supports. On the contrary, my work was aimed at the build-up of the V/P/O active layer on the surface of a zirconia support by thermal treatment of a precursor, the latter having been obtained by impregnation of a V^{5+} salt and of H_3PO_4. *In-situ* Raman analysis during the thermal treatment, as well as reactivity tests were used to investigate on the parameters that may influence the generation of the active phase.

Part B deals with the study of *o*-xylene oxidation of phthalic anhydride; industrially, the reaction is carried out in gas-phase using a supported catalyst made of V_2O_5 deposited on TiO_2.

The V/Ti/O system is quite complex; different vanadium species can be present on the titania surface, in function of the vanadium content and of the titania surface area: (i) a V species which is chemically bound to the support via oxo bridges (isolated V in octahedral or tetrahedral coordination, depending on the hydration degree), (ii) a polymeric species spread over titania, and (iii) bulk vanadium oxide, either amorphous or crystalline. The different species have different catalytic properties; therefore changing the relative amount of V species can be a tool to optimize the catalytic performance. For this reason, samples containing increasing amount of vanadium were prepared and tested in the selective oxidation of o-xylene, with the aim of searching for relationships between V/Ti/O reactivity propeortesi, chemical-physical features and amount of the different vanadium species.

The second topic investigated is the role of steam as a gas-phase promoter for the reaction. Catalytic surface changes under working conditions; temperature and gas-phase composition may affect the nature of the V species. Furthermore, in the industrial practice, the vanadium oxide-based catalysts need the addition of gas-phase promoters in the feed stream, that although do not have a direct role

in the reaction stoichiometry, when present leads to considerable improvement of catalytic performance.

Starting point of my investigation is the possibility that, under reaction conditions, steam (a component always present during oxidation reactions) may modify the catalytic surface. For this reason, the dynamic phenomena occurring at the surface of a 7wt% V_2O_5 on TiO_2 catalyst, in the presence of steam, were investigated by means of in-situ Raman spectroscopy. Moreover, a relationship between the amount of the different vanadium species and catalytic performance have been searched for.

Finally, I studied the role of dopants on catalytic performance. The industrial V/Ti/O system contains several dopants; the nature and the relative amount of promoters may vary depending on catalyst supplier and on the technology used, either a single-bed or a multi-layer catalytic fixed-bed. Promoters have quite a remarkable effect on both activity and selectivity to phthalic anhydride. Their role is crucial, and the proper control of the relative amount of each component is fundamental for the process performance. Furthermore, it can not be excluded that the same promoter may play different role depending on reaction conditions (T, composition of gas phase..). The reaction network of phthalic anhydride formation is very complex and includes several parallel and consecutive reactions; for this reason a proper understanding of the role of each dopant cannot be separated from the analysis of the reaction scheme. One of the most important promoters at industrial level, which is always present in the composition of V/Ti/O catalysts, is caesium. It is known that Cs plays an important role on selectivity to phthalic anhydride, but the reasons of this are not clear. Therefore the effect of Cs on the reaction scheme has been investigated at two different temperatures, with the aim of highlighting in which step of the reaction network does this promoter play its role.

[1] I. E. Wachs, B. M. Weckhuysen, Appl. Catal. A: General 157 (1997) 67

Part A

Selective oxidation of *n*-butane to maleic anhydride

1

INTRODUCTION

1.1 MALEIC ANHYDRIDE: PRODUCTION AND USES

Maleic Anhydride (MA) is the anhydride of cis-butenedioic acid (maleic acid); this molecule has a cyclic structure with a ring containing four carbon atoms and one oxygen atom, as shown in Figure 1.1.

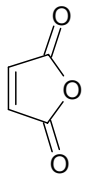

Figure 1.1: Maleic Anhydride structure.

At room temperature, MA is a white solid with pungent odour. The most important physical-chemical characteristics are summarized in Table 1.1.

Table 1.1: Physical-chemical features of MA [1, 2].

Molecular Weight (g/mol)	98.01
Melting Point (°C)	52.85
Boiling Point (°C)	202
Combustion heat (kJ/mol)	1391.2
Explosion limits (%V)	Lower: 1.4 Upper: 7.1
Solubility in xylene (g/l at 30°C)	163.2
Solubility in water (g/l at 30°C)	572
Solubility in benzene (g/l at 35°C)	439.4

Other names of MA are:

- 2,5-Furandione
- Dihydro-2,5-dioxofuran
- cis-Butanedioic anhydride

1.1.1 Maleic anhydride uses [1]

About 1.5 million tons of MA are consumed each year in the world and global demand is expected to grow 3.7%/year through 2015 [3]. Global production is just over 1.6 million tons/year and more than 50% of MA is used to produce unsaturated polyester resins. Applications include boat hulls, car parts, furniture and pipes. MA is also used to produce copolymers (such as MA-styrene, MA-acrylic acid), paints, lubricants, pesticides, and other organic compounds.

The unsaturated double bond and the acid anhydride group lead MA to a variety of chemical reactions.

For instance, MA gives Diels-Alder reaction with butadiene, to yield tetrahydrophthalic anhydride; the latter, after a hydrogenation reaction, is transformed into esahydrophthalic anhydride (Figure 1.2).

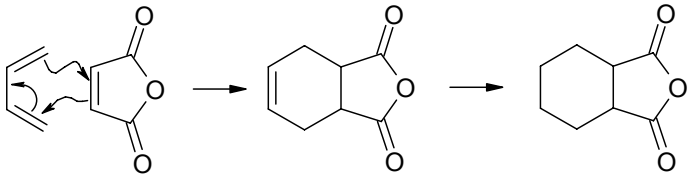

Figure 1.2: MA and butadiene yield tetrahydrophthalic anhydride.

Moreover, MA and isoprene react to give methyl-esahydrophthalic anhydride, which is used (with esahydrophthalic anhydride) as vulcanizer agent and in the production of epoxy resins.

MA also finds application in the food industry, as precursor of maleic acid and fumaric acid (Figure 1.3), both used as additives to adjust the acid flavour.

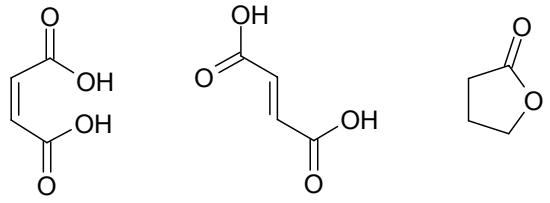

maleic acid fumaric acid GBL

Figure 1.3: Structures of maleic acid, fumaric acid and γ-butyrolactone.

By selective hydrogenation, MA can be transformed into succinic anhydride, which is hydrolyzed to succinic acid, that is the starting molecule for the synthesis of γ-butyrolactone (GBL), tetrahydrofurane (THF) and 1,4-butandiol (BDO).
Finally, in the fine chemistry industry, MA is used for the production of aspartic acid, which is an intermediate in the production of aspartame.

1.1.2 Maleic anhydride production

MA can be produced either by selective oxidation of *n*-butane or by selective oxidation of benzene.
Selective oxidation of benzene is the older process for MA production, industrially used since 1933. The reaction is carried out in the gas phase, at 400-450°C, in a multi tubular plug flow reactor. To have an efficient removal of the reaction heat, the catalyst (a V/Mo mixed oxide) is deposed on an inert and high-conductive support (i.e. Steatite).
Benzene conversion is almost total (about 96%), selectivity to MA can be as high as 73%. Although the unreacted benzene amount is low, it must be either adsorbed and recycled, or burned. Benzene emissions in the atmosphere cannot be higher than 5μg/m^3 due to environmental regulations [4].

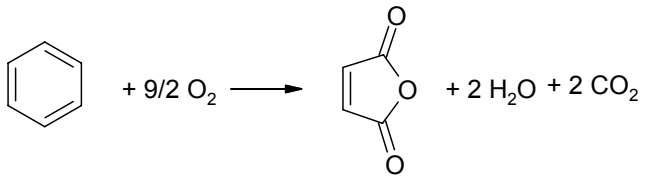

Figure 1.4: Selective oxidation of benzene to MA.

Figure 1.5 shows the simplified flow sheet of a process using benzene as feedstock. In the case of Polynt's process the so-called High-Load-Technology is used, which allows operation up to 210 g/h/tube (2% mol concentration) of benzene. The reaction gases are cooled down by means of gas coolers and crude MA is partially recovered by condensation and partially as maleic acid solution in a water scrubber. Off gases leaving the scrubber are sent to a catalytic incinerator. Pure MA is obtained in a distillation column operated batch wise [5].

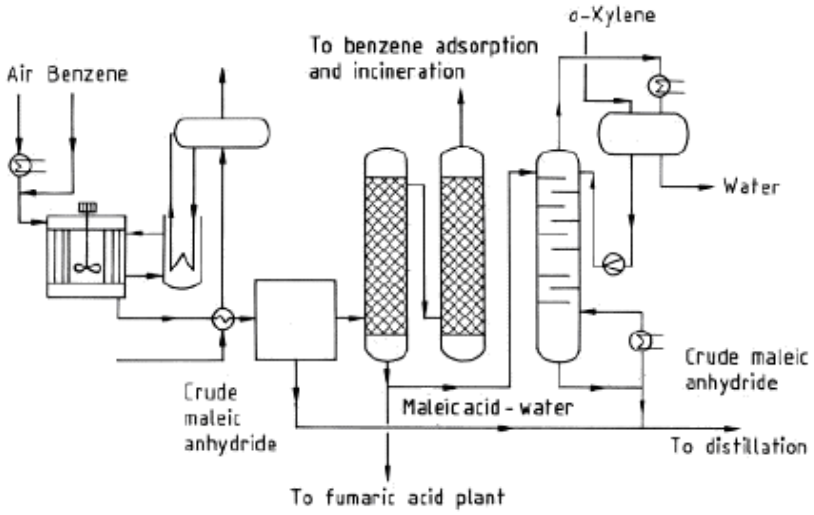

Figure 1.5: Process for producing MA from benzene [elaborated from 1].

Since 1974, *n*-butane is successfully used as feed for MA production; the reaction is carried out at 400°C in the gas phase; the catalyst is a Vanadium and Phosphorus mixed oxide, used in bulk phase.

Depending on the employed technologies (fixed or fluidized bed) the *n*-butane conversion varies from 53 to 65% and MA selectivity is not higher than 86%.

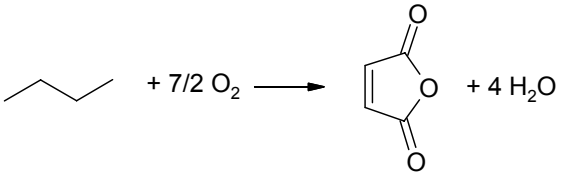

Figure 1.6: Selective oxidation of *n*-butane to MA.

The use of *n*-butane instead of benzene leads to many advantages:

1. the lower cost of the alkane, as compared to the aromatic: *n*-butane is present in natural gas and it is also produced by steam cracking of oil;
2. better safety and lower environmental impact: benzene is a proven carcinogenic compound;
3. better atom economy: in benzene oxidation two of the six C atoms are transformed to CO_2 ;

4. lower costs of MA separation and purification; starting from benzene some heavy compounds (such as benzoquinone and phthalic anhydride) are by-produced.

Nowadays, approximately 80% of MA is produced from *n*-butane, the remaining 20% is produced starting from benzene [3]; nevertheless, it is worth noting that in recent years, because of a decreased price gap between chemicals derived from oil and those from natural gas, and of an increased awareness of environmental problems and hence of the considerable steps forward done in the field of ambient monitoring of pollutants and of contaminants abatement from tail streams, some companies are reconsidering the use of benzene.

Currently, the selective oxidation of *n*-butane is the only successful example of the use of an alkane as the reactant for the synthesis of a bulk chemical. The discovery of an active and selective catalyst, the vanadyl pyrophosphate, made possible the development of this technology. However, notwithstanding the good catalytic performance, the results from *n*-butane are worse than those obtained from benzene. This is due to the following problems, which limit the performance in the alkane oxidation:

1. by-production of high amount of CO and CO_2 through parallel and consecutive reactions of *n*-butane and MA combustion. CO and CO_2 are kinetically and thermodynamically favoured at the temperature of reaction; due to this, *n*-butane conversion can not be higher than 80%;
2. high exothermicity of the reaction: a very important issue is the control of the heat-removal to avoid the run-away of the reaction;
3. process safety: flammable mixtures could form due to the concomitant presence of a fuel and an oxidant; so, in each plant zone (except inside the reactor) the gas composition has to be kept far from the explosion limits [3].

MA is produced from *n*-butane by different technologies: (i) fixed-bed (Scientific Design, Huntsman, BASF, Pantochim) or (ii) fluidised-bed (Polynt, BP, Mitsubishi); the transported-bed technology developed by DuPont has been recently abandoned.

Table 1.2 summarizes the possible process technologies, which are distinguished by type of reactor, recover method of crude MA, gas phase composition (from

1.8% of *n*-butane in air in the case of fixed bed, to 5% in the fluidized bed), catalyst (synthesis, activation step, presence of promoters and regeneration).

Table 1.2: Industrial technologies for MA production from *n*-butane [6, 7].

Process	Type of reactor	Recover method
ALMA	Fluidized bed	Anhydrous
Mitsubishi	Fluidized bed	Aqueous
Sohio-UCB	Fluidized bed	Aqueous
Monsanto	Fixed bed	Anhydrous
Scientific Design	Fixed bed	Aqueous
DuPont	Transported bed (CFBR)	Aqueous

Fixed bed technology.

The reaction is carried out in a multi tubular reactor; the catalyst is loaded in pellets. The concentration of *n*-butane in feed has to be less than 1.85% mol (the lower explosion limit). The gas mixture is recovered from the reactor in two different ways:

(i) absorption in water: MA reacts with water to form the maleic acid, which is dehydrated at temperature below 130°C, to minimize the isomerization to fumaric acid. Finally, crude MA is purified by distillation under vacuum.

(ii) absorption in an organic solvent (i.e. o-xylene): in such way about 98% of the MA produced is recovered, without any fumaric acid formation.

In Figure 1.7 the simplified flow-sheet of the Denka-Scientific Design process is shown. 1.7% *n*-butane in air is fed to the fixed bed reactor, working at 390-400°C. The *n*-butane conversion is about 83%, with MA yield of 54%.

The crude MA is recovered by adsorption in water; the formed maleic acid is distilled by means of azeotropic distillation in o-xylene, to obtain pure MA.

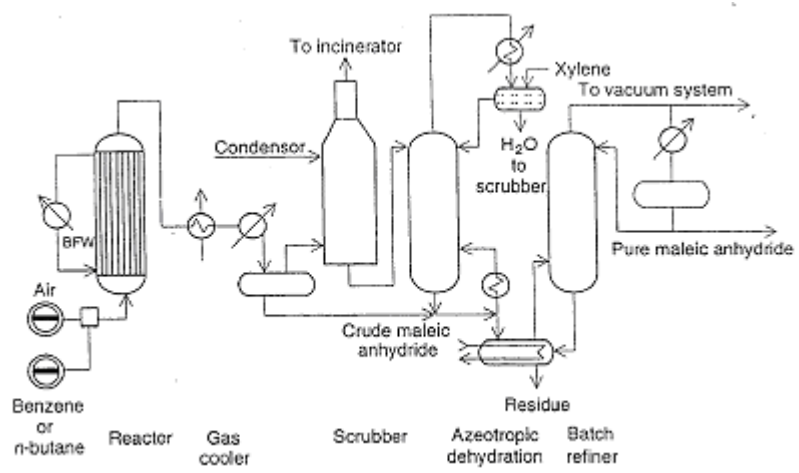

Figure 1.7: Flow sheet of Denka-Scientific Design process [elaborated from 8]

Fluidized bed technology.

The most important advantages in the use of fluidized bed technology are:

1. no temperature hot-spot and no heat-removal problems, because of an uniform thermal profile, guaranteed by an optimal dissipation of the reaction heat.
2. high productivity, due to the possibility of operating at high inlet concentration of *n*-butane (inside the explosion limits).

Some drawbacks are:

- feed back-mixing, responsible for a decrease of MA selectivity;
- high mechanical stress on the catalyst, and abrasion phenomena.

To limit the abrasion of bulk catalyst particles, different techniques can be employed:

- impregnation of the active components on an inert support characterized by good fluidization properties and high attrition resistance;
- addition of additives to the precursor, to improve the mechanical resistance;
- encapsulation of the active phase in a silica structure.

One of the most advanced fluidized bed technology is the ALMA (Alusuisse Italia-Lummus Crest) process. The bulk VPO catalyst is spray-dried with a low amount of additives, to improve the mechanical resistance. The *n*-butane concentration in

the feed is about 4% mol; conversion is typically 80-85%, with a molar yield to MA over 50%. [9].

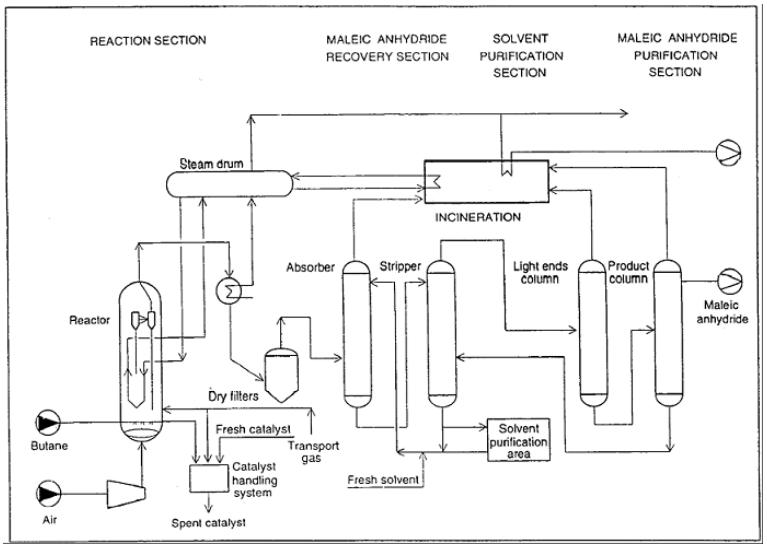

Figure 1.8: Flow sheet of ALMA Process [elabotated from 9].

Figure 1.8. reports the scheme of the ALMA process: *n*-butane and air are fed to a fluidized bed catalytic reactor to produce MA. Cooling coils are merged in the bed to generate high-pressure steam. In the recovery section, an organic solvent is used to remove the MA from the reaction effluent gas; a conventional absorption/stripping scheme is used. Crude MA is refined by continuous distillation to separate light and heavy impurities. Tail gas is sent to an incinerator that converts the residual hydrocarbon (and CO) to extra steam [5].

Transported bed process.

The transported fluidized bed was developed by Monsanto and Du-Pont; it was working from 1996 to 2004, for tetrahydrofuran (THF) production. In 2005, the plant was shut down.

Figure 1.9 shows the flow sheet of the Du-Pont process. In the riser reactor only *n*-butane is fed (eventually diluted with an inert gas); the *n*-butane is transformed to MA by the catalyst, which releases oxygen and reduces; the outlet stream contains both the reduced catalyst and the mixture of *n*-butane, CO_x and MA. The catalyst is recovered by a cyclone and transported to the regenerator reactor; in this reactor only air is fed, to restore the oxidation state of the catalyst.

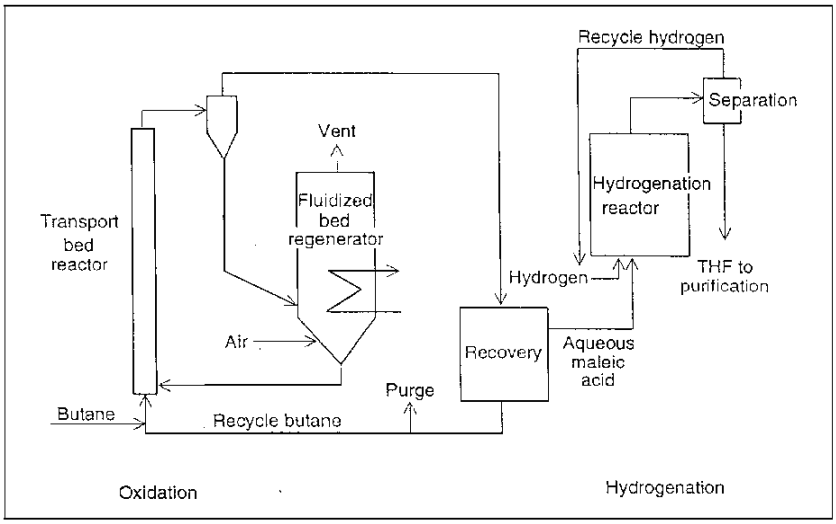

Figure 1.9: Flow sheet of Du Pont process for THF synthesis [elaborated from 9].

MA is recovered using water; after the hydrolysis, aqueous MA and maleic acid are reduced to tetrahydrofuran in a hydrogenation reactor. The peculiarity of this process is that it works in complete absence of oxygen in the feed; the oxygen used for the reaction is the lattice oxygen of the catalyst, the vanadyl pyrophosphate. The absence of oxygen in the feed allows avoiding the formation of flammable mixtures and working at very high concentration of *n*-butane (from 1 to 50%wt). The *n*-butane conversion is about 50% and the MA yield is normally about 37%. This technology has been operating with a new generation of catalyst, highly resistant to the attrition in the riser. The catalyst was coated by silica, which gives a very high mechanical resistance and does not cause any selectivity decreasing.

The energy use of the process for the synthesis of MA by *n*-butane oxidation is shown in Figure 1.10, for the fluidized bed and the fixed-bed process, also including the feedstock energy consumed by the process (i.e., the difference between the heating values of the product and the feedstock), and in an optimum heat exchange network constructed using the pinch analysis [10].

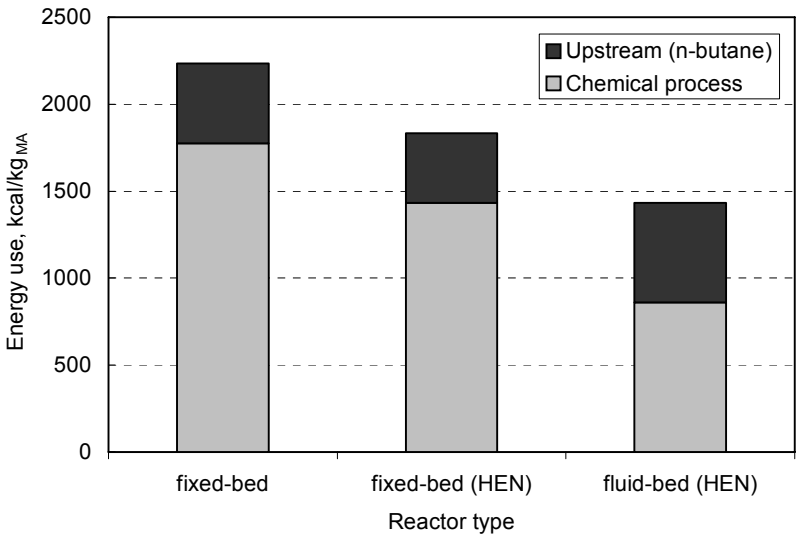

Figure 1.10: Comparison of energy use among reactor alternatives for *n*-butane oxidation to MA. HEN=optimum heat-exchange-network

The fluidized bed consumes more of the *n*-butane feedstock, because of the lower selectivity to MA due to back-mixing phenomena, that favours the consecutive combustion of MA. Nevertheless, because of the more efficient technology for heat recovery (that also allows production of high-pressure steam), the energy consumption is lower. In overall, the fluidized bed technology still consumes less energy than the fixed bed; moreover, operation inside the flammable area, with *n*-butane-richer conditions (up to 5 molar % in feed) is possible. This also contributes to a slightly lower selectivity to MA, but on the other hand it improves productivity and lowers the cost of post-reactor treatment, because of the more concentrated streams.

1.2 CATALYTIC SYSTEM

1.2.1 Synthesis of vanadyl pyrophosphate

The only industrially used catalyst for the selective oxidation of *n*-butane to maleic anhydride is a Vanadium/Phosphorus mixed oxide, with a particular crystalline structure, the vanadyl pyrophosphate $(VO)_2P_2O_7$ [9, 11-13]. Different preparation methods (inorganic or organic) are described in literature; however, the final active phase is obtained by some similar steps:

1. synthesis of the vanadyl pyrophosphate precursor: $VOHPO_4 \cdot 0.5H_2O$;

2. thermal decomposition of hemihydrate vanadyl acid orthophosphate, with total or partial loss of crystallization water: during this step new phases can frm and impurities present on the precursor surface, such as chlorine or organic compounds, are eliminated;
3. catalyst forming to reach the suitable morphology and the required mechanical resistance in function of the reactor type (either fixed or fluidized bed);
4. catalyst activation to obtain stable catalytic performances. During this step, different transformations take place, in particular recrystallization, and creation or elimination of structural defects.

Synthesis of the precursor: $VOHPO_4.0.5H_2O$

The structure of the hemihydrate vanadyl acid orthophosphate is reported in Figure 1.11.

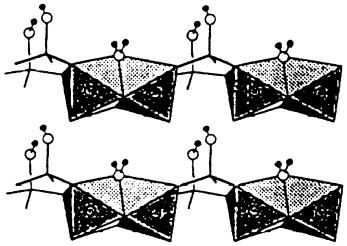

Figure 1.11: Structure of $VOHPO_4 \cdot 0.5H_2O$ [14].

The precursor is obtained by the reduction of a V^{5+} compound (normally V_2O_5) to V^{4+}, followed by addition of H_3PO_4. The reduction occurs both in water and in an organic solvent; in the first case the reducing agents is either HCl or hydrazine; in the second case a mixture of alcohols (or a single alcohol) is employed both as the solvent and the reducing agent.

The main differences between the precursor synthesized by the organic method and that prepared with the aqueous procedure are observed in the crystallinity; in particular, the precursor prepared in the aqueous medium is more crystalline. In the case of the organic synthesis, a precursor with structural defects is obtained, due to the presence of alcohol molecules trapped between the crystalline layers of $VOHPO_4 \cdot 0.5H_2O$ (which has a lamellar morphology) [15]. Moreover, catalysts prepared in the organic medium finally yield a catalyst which shows higher

activity, due not only to the higher surface area, but also to the higher density of active sites [6]. For this reason, all the industrial preparations are done using the organic method to have more active and selective catalysts.

The synthesis in the aqueous medium involves the following steps:

- reduction of V_2O_5 to V^{4+}, that is solubilized by HCl or hydrazine;
- addition of H_3PO_4 (the strong acid conditions do not allow the precursor precipitation);
- formation of $VOHPO_4 \cdot 0.5H_2O$ and of other amorphous phases, due to the total evaporation of the solvent;
- crystallization of $VOHPO_4 \cdot 0.5H_2O$ by water addition (when the solution viscosity is sufficiently high) or by germination (in hydrothermal conditions) [11, 16,17].

The preparation with the organic route involves the following steps:

- solubilization of V^{5+} through the formation of vanadyl alcoholates or of $VOCl_3$ (when HCl is used as reducing agent [18]);
- reduction of the V alcholate into solid V_2O_4, by the organic compounds (normally the solvent), or due to the presence of an inorganic reducing agent, such as HCl;
- surface reaction of V_2O_4 with H_3PO_4, followed by the formation of $VOHPO_4 \cdot 0.5H_2O$ at the liquid-solid interface;
- separation of the precursor by filtering, centrifugation, decantation or evaporation; then the precursor is recovered by drying.

Thermal treatment of the precusor

Hemihydrate vanadyl acid orthophosphate is thermally treated to trasnform into the real active phase, $(VO)_2P_2O_7$. During this transformation, two water molecules are lost [16]:

$$\mathbf{2\ VOHPO_4 \cdot 0{,}5H_2O \rightarrow 2\ VOHPO_4 + H_2O}$$

$$\mathbf{2\ VOHPO_4 \rightarrow (VO)_2P_2O_7 + H_2O}$$

The first dehydration leads to an amorphous or microcrystalline compound, in which still the typical functional groups of hemihydrate vanadyl acid orthophosphate are present. The second dehydration corresponds to the condensation of the orthophosphate to pyrophosphate groups.

Normally the thermal treatment is carried out using a multi-step procedure:

1. drying of the precursor at temperature lower than 300°C, to avoid dehydration, but to eliminate organic or chlorinated compounds.
2. dehydration of the precursor to vanadyl pyrophosphate; this step can be carried out using different methods, such as:
   (i) dehydration inside the reactor, starting from relative low temperature (about 280°C) under reaction mixture at low residence time and increasing temperature and residence time too. Normally about one day is necessary to conclude the dehydration.
   (ii) Dehydration under oxygen-free atmosphere at temperature above 400°C, and then under reaction mixture. After the feeding of *n*-butane and oxygen $(VO)_2P_2O_7$ could be oxidized to a V^{5+} phase [19,20].
   (iii) Calcination under air at temperature above 400°C and then introduction of the reaction mixture [21, 22]
   (iv) Hydrothermal treatment, which consists in a treatment at 280°C under air and water and a second treatment under nitrogen at 390°C.

The structure of vanadyl pyrophosphate is shown in Figure 1.12.

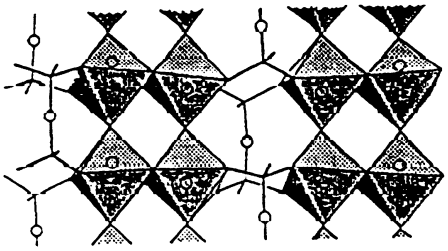

Figure 1.12: Structure of $(VO)_2P_2O_7$ [14].

In the literature, different hypotheses have been proposed for the mechanism of transformation of the precursor into vanadyl pyrophosphate. One of the most recognized hypothesis was proposed by Bordes [23], and is supported by TEM and SEM analysis. A topotactic transformation of $VOHPO_4 \cdot 0.5H_2O$ to $(VO)_2P_2O_7$ is proposed. This transformation consists in a structural conversion, in which V-O and P-O bonds remain unaltered, while weak V-H_2O, e P-H_2O are broken: HPO_4 group condenses into pyrophosphate units. After the dehydration of the precursor, a rearrangement of the structure takes place, and finally layers of precursor condense to obtain the structure of the vanadyl pyrophosphate.

Different parameters could influence the transformation, in particular:

- temperature, time and atmosphere of treatment;
- precursor morphology;
- P/V ratio;
- presence of additives;
- presence of structural defects.

One of the most important catalyst characteristics, at the end of the thermal treatment, is the V oxidation state. Even though vanadium is present as V^{4+} in stoichiometric vanadyl pyrophosphate, the V/P/O obtained by thermal treatment of the crystalline precursor $VOHPO_4 \cdot 0.5H_2O$, could contain crystalline and amorphous vanadium phosphates other than $(VO)_2P_2O_7$ [24, 25]. These additional or spurious phases may contain V^{5+} or even V^{3+}, and the relative amount of each compound is a function of (i) the procedure employed for the preparation of the precursor, and (ii) the thermal treatment adopted for the transformation of the precursor. Furthermore, the VPP itself may host V ions other than V^{4+} as defects, without undergoing substantial structural changes; specifically, the possible development of either V^{3+} or of V^{5+}, even in considerable amounts, has been demonstrated [26-28]. Outer surface layers of V^{5+} phosphates may develop in the reaction environment, and play active roles in the catalytic cycle.

Activation under reaction mixture

Activation (or equilibration) of the catalyst is obtained leaving the sample under reaction mixture at 400°C for several hours. During this period changes not only in

the catalytic performance, but also in the catalyst chemical-physical features, take place.

A "fresh catalyst" is a "non-equilibrated" one; a catalyst can be defined "equilibrated" only when its catalytic performances are constant for more than 50 hours. Normally for a "reduced" catalyst containing only V^{4+} the equilibration time does not exceed 200-300h, while in the case of an oxidized sample containing also V^{5+} at least 500 hours are necessary to complete the transformation and obtain the vanadyl pyrophosphate.

In an equilibrated catalyst the average oxidation state of vanadium is 4.00-4.04, the specific surface area is about 16-25 m^2/g and the P/V ratio is higher than 1.0 [6]. During the activation step, the catalytic activity decreases, while the yield to MA increases, due to the increase of selectivity. The fresh catalyst is normally more active than the equilibrated one, because the V^{4+} easily oxidizes to V^{5+} in the final part of catalytic bed, in which the *n*-butane concentration is low, but the oxygen concentration is still high [29].

1.2.2 The P/V ratio

The optimal catalytic performance of vanadyl pyrophosphate is obtained when the catalyst contains a slight excess of phosphorus (instead of the stoichiometric P/V 1/1 ratio in the compound), which limits the oxidation of V^{4+} in $(VO)_2P_2O_7$. Generally, on the catalyst surface, the P/V ratio is higher than in the bulk.

A low P/V ratio leads to a catalyst active but not selective [6]; the different performances can be attributed to the oxidation state of V. In fact, it has been demonstrated that in catalysts having a lack of phosphorus (P/V=0.95) the oxidation takes place easier than in samples with a P/V ratio higher than 1.0.

1.2.3 The role of the different V species

The oxidation state of V in VPP under working conditions, and the role of V species having different oxidation states, have been debated for several years. The importance of having a defined amount of V^{5+} in order to obtain better selectivity has been pointed out by Volta and co-workers, with the optimal V^{5+}/V^{4+} ratio being equal to 0.25 [30-34]. Evidences of the V^{5+} role have been reported by other authors as well [24, 35-36]. Isolated V^{5+} sites in strong interaction with the VPP provide the optimal surface concentration of sites in charge for the alkane

activation and for O-insertion sites, while the formation of bulk $VOPO_4$ is detrimental for selectivity.

More controversial is the role of V^{3+}. While it is clear that the generation of V^{3+}/P/O compounds is negative for selectivity, the generation of a discrete number of these species in the lattice of the VPP, and the associated anionic vacancies, have been proposed to play a positive role on catalytic activity [37-38]. V^{3+} defects are generated during the thermal treatment of the precursor, and the number of them is function of the amount of organics retained in the precursor, and of the nature of the heat treatment carried out for the transformation of the precursor into the active catalyst [40].

The oxidation state of V in VPP under working conditions is function of reaction conditions and, more specifically, of the gas-phase composition. Mallada et al. [41] investigated the effect of reducing (hydrocarbon-rich) and oxidizing (hydrocarbon-lean) conditions on the oxidation level of the catalyst. In the latter case, V^{3+}/P/O surface phases developed, which are detrimental for the selectivity to MA. At the same time, substantial amounts of C deposits are accumulated on the catalyst, in the fraction of catalytic bed, which was operating under low oxygen partial pressure. The same conclusions were reached by Volta et al., [42]: the reduction of V^{5+} and the formation of C deposits are responsible for the decrease of the selectivity to MA. The deactivation is not so rapid when the catalyst is pre-oxidized at mild temperature. One way to overcome these limitations is to add promoters, which helps to maintain a higher V oxidation degree, probably through the formation of specific compounds, or through a mediation of V re-oxidation in the redox mechanism. Also the catalyst morphology was found to be an important parameter under hydrocarbon-rich conditions, more than under leaner conditions [43]. The rose-petals-like morphology gives the most active and selective catalyst, thanks to the higher V reducibility and re-oxidability as compared to VPP having a different morphology.

1.2.4 Supported systems

To improve the catalytic performances of vanadyl pyrophosphate it is necessary to avoid the consecutive side reaction of maleic anhydride to CO and CO_2, which decreases the selectivity at high *n*-butane conversion. One of the most studied methods to obtain such condition is the supportation of the active phase on an

oxide surface. In the case of vanadyl pyrophosphate, the support should have some features:

1. good mechanical properties, to improve attrition resistance of the catalyst;
2. high thermal conductivity, to avoid temperature hot spots which favour total oxidation reactions;
3. not very high specific surface area, to avoid high residence time of reactants inside catalyst pores;
4. chemical inertia not only to *n*-butane and oxygen, but also to the active phase, to avoid changes in its morphology.

The first studied supports for VPO were the "classic" oxides such as SiO_2, TiO_2, Al_2O_3; recently, also new kind of materials (such as SiC) have been investigated. Following are summarized the main characteristics of supported VPO catalysts [44].

VPO supported on TiO_2

The precipitated VPO phase was amorphous and well-dispersed over the surface of the support; the surface of P/V 1.1 supported catalysts resulted enriched in phosphorus (P/V=1.2-3) similar to the bulk VPO catalyst (typically, P/V=1.1-1.7). The supported VPO showed activity and selectivity in *n*-butane oxidation at temperatures 100°C lower than commercial VPO catalysts. Overbeek at al. [45,46] shows that the activity of titania-supported VPO catalysts is related to several characteristics:

- high surface area,
- strong interaction of the VPO component with the titania support,
- different reducibility of VPO on TiO_2,
- different average oxidation state of vanadium ions on the surface.

Ruitenbeek et al. [47] observed no changes in average vanadium oxidation state during equilibration, since they concluded that the lattice VPO oxygen species was not involved in *n*-butane oxidation and the reaction does not follow the Mars van Krevelen mechanism.

VPO supported on SiO_2

The VPO component in the silica-supported catalysts was well dispersed, but interacted weakly with the support surface as compared to the titania-supported system. In contrast to the titania-supported VPO system, the silica-supported VPO catalysts were less active, but more selective to MA. The lower catalytic activity of the silica-supported system was attributed to the non-reducible nature of silica support. However, the higher surface P/V ratios found in the silica-supported catalysts as compared to the titania-supported systems, may also be responsible for lower activity in *n*-butane oxidation and higher selectivity to maleic anhydride at high conversion in these catalysts [46].

VPO supported on Al_2O_3

The high affinity between Al and P limited the dispersion of VPO phase on the support; catalysts obtained showed poor catalytic performances [48].

VPO supported on $AlPO_4$

The most used type of $AlPO_4$ was trydimite; in this case the main VPO phase is present as vanadyl pyrophosphate. The supportation of VPO on $AlPO_4$ improves both catalytic performances and activation time of the catalyst. Very high conversion (90%) and MA selectivity (42%) are reached and the activation time is lower (20h instead of the classical 100h, necessary for the bulk VPO) [49-51].

Highly-heat-conducting supports

Ledoux et al. studied the use of heat-conducting supports (β-SiC, thermal conductivity 14-270 W m^{-1} K^{-1}, Si_3N_4, 6 W m^{-1} K^{-1}, and BN, 31 W m^{-1} K^{-1}) for the VPP [52,53]. The peculiarity of these materials is the relatively high surface area (e.g., for β-SiC, >20 m^2/g, prepared via the "shape memory synthesis"), which makes them useful as supports for exothermal oxidation reactions [54]. In fact, because of the better control of the catalyst surface temperature, these systems allows a significant gain in MA yield. Moreover, the chemical inertness of the support did not modify the reactivity properties of the precursor and of VPP, which instead is what happens with conventional supports [55]. In the case of the β-SiC-supported VPO (30 wt.% of active phase), the selectivity to MA at high *n*-butane conversion was higher than that obtained with the unsupported catalyst. An even more

relevant result was reported under *n*-butane-rich conditions (e.g., O_2/n-butane feed ratio 3.2, with 11 mol.% *n*-butane), with 72% alkane conversion and 54% MA yield at 485°C. This represents the best result ever reported in *n*-butane oxidation under hydrocarbon-rich conditions.

1.2.5 Recent developments to improve the catalytic system

Best catalytic performances reported in literature range from 53 to 65% molar yield to MA [6, 11, 56-59], with a conversion of *n*-butane not higher than 85-86%. The best performance for a fixed-bed reactor does not exceed 65% per-pass yield, while that in a fluidised-bed is typically lower due to back-mixing phenomena.
It is known that the maximum yield to MA is limited by two factors:

a) The presence of parallel reactions of *n*-butane combustion and of oxidative degradation to acetic and acrylic acids
b) The presence of consecutive reactions of combustion, which lower the selectivity to MA when the alkane conversion is increased over 70-80% . This has been attributed to the development of local catalyst overheating, due to the high reaction exothermicity, and to the poor heat-transfer properties of the catalytic material.

To overcome these problems, different options have been proposed:

1. Addition of specific dopants to modify the redox and acid-base properties of the active phase or the development of new procedures for the preparation of the catalyst that allow a modification of the chemical-physical or morphological features of the precursor.
2. Use of highly heat-conductive supports for VPO, in order to better distribute the reaction heat and develop more homogeneous particle temperatures (Chapter 1.2.4).
3. Development of new catalytic systems.

Addition of specific dopants

Despite it seemed that in the 80's all the possible dopants for this catalyst had been already investigated [60-63], the numbers of scientific papers dealing the study of promoters for VPO has been growing in recent years. In fact, a more profound knowledge of the chemical physical properties of the VPP has made

possible a better comprehension of the role of some known dopants (such as Co, Fe and Bi [64-72]). Moreover, also new dopants, such as Nb, have been found [73-77]. Results on several dopants recently published, are summarized in Table 1.3

Table 1.3: C= conversion, S = selectivity of non doped catalyst → doped catalyst in standard reaction conditions [78]

Dopant, optimal amount	Promotional effect	Reasons for promotion
Co, Co/V 0.77%	C: 15 → 25% S: 0 → 11% under hydrocarbon-rich conditions	Control of the optimal V^{5+}/V^{4+} surface ratio; stabilization of an amorphous Co/V/P/O compound
Co, Co/V 13%	C: 55 → 79% S: 43 → 35% at 653K	Optimal surface Lewis acidity
Ce+Fe	C: 44 → 60% S: 63 → 66% in absence of O_2	Improvement of redox properties
Fe, Fe/V 0.08	Increase of catalytic activity	Fe replaces V^{4+} in $(VO)_2P_2O_7$ Re-oxidation rate is increased
Ga, Ga/V 0.10	C: 22 → 73% S: 55 → 51%	Increase of surface area + increase of intrinsic activity (electronic effect)
Nb, 0.25 wt%	C: 20 → 17% S: 35 → 53%	Increase of surface acidity promotes desorption of MA
Nb, Nb/V 0.01	C: 58 → 75% S: 70 →70%	Nb concentrates at the surface, where defects are generated. Nb acts a n-type dope; development of a more oxidized surface

Modifications of VPP chemical-physical properties

One way to improve catalytic performances is the development of different synthetic methods, in order to modify the VPP properties. Methods to modify the preparation procedure recently published include:

a) Preparation of the precursor in the presence of glycols (1,2-etandiol, 1,3-propandiol, 1,4-butandiol). This method affects the morphology of the precursor [15,79] because the molecules can be trapped in the interlayer spacing of the precursor, in agreement with literature data obtained using other types of alcohols [80,71]. A relationship exists between the organics content in the precursor and the "aspect ratio" of the crystal; increasing

amounts of retained organic compounds disturb the stacking of crystallographic planes along the c direction, and only [hk0] reflections remain sharp for the higher C contents. Correspondingly, the aspect ratio changes considerably, indicating the development of crystals having different morphology, as also confirmed by SEM micrographs. The thermal treatment is a crucial step to determine the morphology of the VPP [82]. It was also found that for defined ranges of organics amount retained in the precursor, it is possible to infer a controlled defectivity to the final VPP [15], with a limited number of V^{3+} species. These catalysts were more active than those obtained from the precursor prepared in the absence of glycols [79].

b) Tribomechanical (ball-milling) activation of the precursor or of the VPP. The idea was first reported by Horowitz et al. [83], and later applied by other authors [84,85]. Ball milling of the precursor is carried out with the aim of increasing the surface area by reducing particle size; this results in higher catalyst activity [86]. However, as a consequence of the high energy used for milling, lattice imperfections are introduced; these defects are transferred to the VPP during transformation of the precursor, and finally affect the catalytic performance [687]. This leads to an improvement of the activity and selectivity.

c) Intercalation of layered $VOPO_4 \cdot 2H_2O$ with various compounds (e.g., alcohols, amines,..), followed by exfoliation in polar solvents into delaminated sheets; finally, impregnation of silica with the solution containing the delaminated layers [88-90]. The same procedure can be adopted to reduce the $VOPO_4 \cdot 2H_2O$ into $VOHPO_4 \cdot 0.5H_2O$ [91,92], to obtain a high-surface-area precursor, and finally a VPP that is more active and selective than that one prepared by conventional procedures (60% conversion, 78% selectivity at 390°C) [90]. Dispersion of VPP inside or over high-surface-area silica was also tried by other researchers, but in general this procedure did not lead to active catalysts [93-95].

d) Preparation of an amorphous, microspheroidal VPO catalyst using supercritical CO_2 as an antisolvent [96,97]. The amorphous compound was claimed to be intrinsically more active than crystalline VPP, and did not require extensive activation periods to reach stable performance. However, a maximum yield to MA of only 7% was reported.

e) Preparation of mesostructured VPO phases and of VPO/surfactant composites [98-103]. Guliants et al. described the preparation of microporous mesostructured VPO, with surfactants as structure-directing agents, and optimised the thermal treatment and template removal, obtaining systems characterized by high surface area. These systems were however not stable under reaction conditions, and transformed into various VPO dense phases. The selectivity to MA was fairly good at low *n*-butane conversion, but fell for increasing hydrocarbon conversions.

New catalysts for *n*-butane oxidation

Recently it has been reported that the pyridine salt of Nb-exchanged molydo(vanado)phosphoric acid is the precursor of a catalyst, mostly consisting of amorphous molybdenum oxide, which is active and selective in the oxidation of propane to acrylic acid and of *n*-butane to maleic anhydride [104-106]. The authors found that key-properties to achieve good catalytic performance are (i) the development of reduced Mo^{5+} and Nb^{4+} species, that are stable when hydrocarbon-rich reaction conditions are used, and (ii) the contemporaneous presence of P, Nb and pyridine in the polyoxometalate (pyridine acts as the reductant for Mo^{6+} during the thermal treatment). Catalysts are active under both *n*-butane-rich and *n*-butane-lean conditions. The best performance reported is 90% selectivity at 15% conversion at 380°C, under n-butane-rich conditions (with total oxygen conversion), and 62% conversion with 46% selectivity at 340°C, under hydrocarbon-lean conditions (2% *n*-butane in feed)

1.3 REACTION SCHEME AND MECHANISM

1.3.1 Reaction scheme

The study of the reaction mechanism is quite difficult, due to the absence of by-products, which can give information about reaction intermediates. However the most proposed scheme for the selective oxidation of *n*-butane to maleic anhydride is represented in Figure 1.13, *n*-butane is transformed into MA through sequential steps of oxydehydrogenation, oxidation and oxygen insertion [6,11,107]:

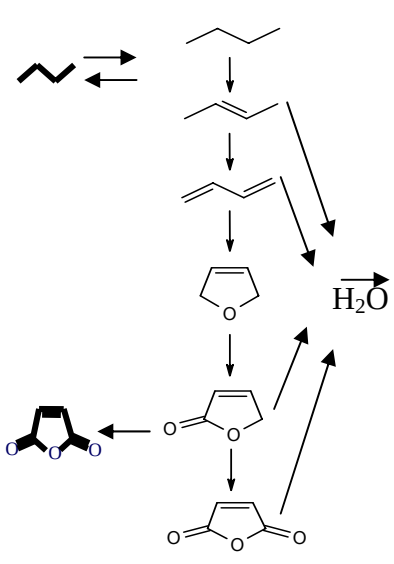

1) *n*-butane + 1/2 O_2 → butenes + H_2O
(oxidative dehydrogenation)

2) butenes + 1/2 O_2 → butadienes + H_2O
(allylic H extraction)

3) butadienes + 1/2 O_2 → 2,5-dihydrofurane
(1,4-oxygen insertion)

4) 2,5-dihydrofurane +2 O_2 → AM + 2 H_2O
(o-allylic insertion lactone mediated)

4a) 2,5-dihydrofurane + 1/2 O_2 → furan + H_2O
(allylic extraction)

5) furan + 3/2 O_2 → AM + H_2O
(electrophilic oxygen insertion)

Figure 1.13: Reaction scheme.

The proposed mechanism was confirmed by isolation of some intermediates at unusual reaction conditions (such as under high hydrocarbon to oxygen ratio or at low residence time) [108-110]. Moreover *n*-butene, butadiene and furan were identified by Kubias et al. [35] under vacuum conditions.

It is also known, that olefinic intermediates are the first products in all C_3-C_5 alkane oxidation reactions to the corresponding oxidized compounds [109]. The slowest state, kinetically determinant, is the oxidative deydrogenation of *n*-butane to butenes. To obtain high MA selectivity, the rate of the oxidative dehydrogenation reaction has to be higher than the one of oxygen insertion; in fact, the olefinic intermediate has to be transformed into a dienic compound and not into another, more reactive molecules, such as crotonaldehyde, methylvinylketone, that are precursors of CO_X.

New recent information are obtained by *in-situ* IR measurements; studying the molecules adsorbed on the catalytic surface during the reaction [111]. Different molecules were fed (1-butene, 1,3-butadiene, furan, maleic anhydride) and the adsorbed species on VPO were studied. It was found that at low T (lower than 100°C) *n*-butane is activated by VPO and forms unsaturated compounds, such as butenes and 1,3-butadiene.

The proposed reaction scheme is shown in Figure 1.14.

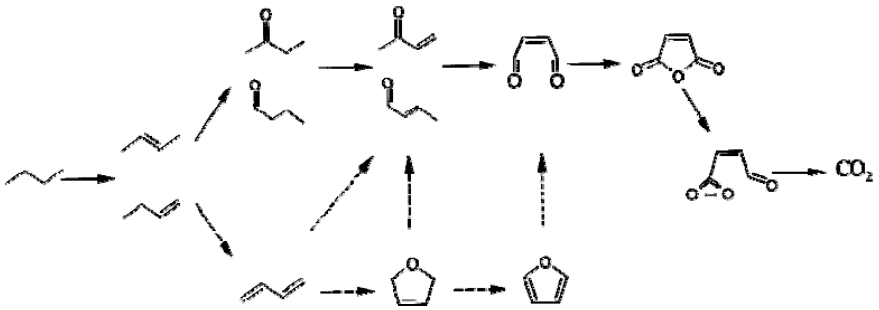

Figure 1.14: Reaction scheme of maleic anhydride formation through carbonylic intermediates [111].

On the contrary with recent computational calculations it was found that 1-butene is not interacting with VPO and could not be a reaction intermediate [112-115].

1.3.2 Reaction mechanism

The selective oxidation of butane follows the Mars Van Krevelen mechanism; in this case, *n*-butane is transformed into MA by the lattice oxygen of VPO and not by the fed molecular oxygen. In particular, the catalytic cycle could be separated in two steps: during the "reduction" step, the lattice oxygen atoms of the catalysts are involved in the oxidation of *n*-butane; in this step the V^{4+} ions of vanadyl pyrophosphate are reduced to V^{3+}. During this step the catalyst give 7 O^{2-} ions; four are used to co-produce water, the remaining 3 are inserted in the *n*-butane molecule to form AM. During the "oxidation" step the fed oxygen oxides V^{3+} ions to V^{4+} and forms O^{2-} ions, which are incorporated in the structural vacancies generated during the reduction step.

To summarize the catalytic cycle:

reduction: $R\text{-}CH + 2KO \rightarrow R\text{-}C\text{-}O + H_2O + 2K$

oxidation: $2K + O_2(gas) \rightarrow 2KO$

where R-CH e R-C-O are the reactant and the products, respectively, while KO e K are the oxidised and reduced form of the catalysts.

Recently, Hodnett and coworkers [112-115] have demonstrated, studying the electronical properties of VPO using the DFT method, that the superficial V is only

a chemisorption site, while the nucleophil oxygen atoms of terminal P-O are selective in the oxy-functionalization of *n*-butane.

1.3.3 Nature of active sites

As it is for all selective oxidation reaction of paraffins, also in the case of *n*-butane oxidation, the core problem is reaching high selectivity in the desired products; this issue is often difficult to obtain, for some aspects:

- the product is more reactive then the reactant (and the reaction proceeds to CO_x);
- paraffins are slow reactive and so the reaction conditions have to be drastic.

The use of active and selective catalysts is necessary to activate the C-H bound of the paraffin to make the multielectronic oxidation and oxygen insertion. Moreover the catalyst should have proper acid properties, so to be able to quickly desorb the product, to avoid over-oxidation reactions [18].

VPO catalyst shows all the necessary multifunction properties necessary to transform *n*-butane into MA, such as [116]:

- oxidative dehydrogenation sites;
- allylic oxidation sites;
- active sites which can insert oxygen in electron rich substrates;
- acid sites able to activate paraffins and desorb acid-products [117];

the presence of all these sites is guaranteed in $(VO)_2P_2O_7$ by the different oxidation state of V(V^{3+}, V^{4+} e V^{5+}) and different Lewis and Bröensted acid sites (Table 1.4).

Table 1.4: Active sites in vanadyl pyrophosphate.

Nature of active sites on $(VO)_2P_2O_7$ surface
Lewis acidic sites
Bröensted acidic sites
Redox couple with one electron: V^{5+}/V^{4+}, V^{4+}/V^{3+}
Redox couple with two electrons: V^{5+}/V^{3+}
Bridged oxygen in the groups V-O-V e V-O-P
Terminal oxygen in the groups $(V=O)^{3+}$, e $(V=O)^{2+}$
Adsorbed molecular oxygen: species η^1-peroxo e η^2-superperoxo

Acid Lewis sites: the Lewis acid sites are attributed to the presence of V ions coordinatively unsatured in the family plan (100) and are identified by FT-IR of basic probe molecules adsorbed on the VPO surface. The most part of acid sites are Lewis acid sites (quite twice respect to the Broensted ones). In the catalyst prepared by organic route, the Lewis acid sites are more active with respect to the one observed in the samples prepared in water.

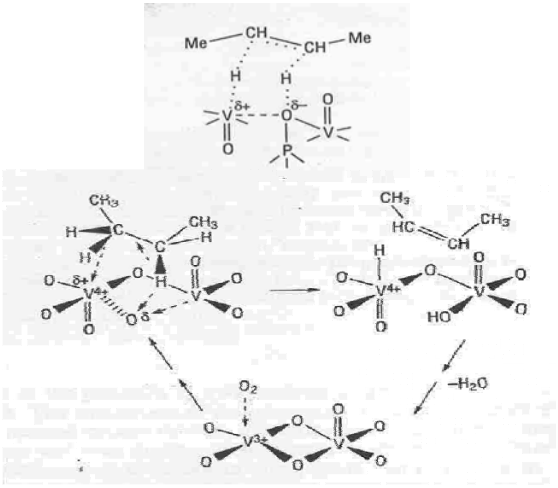

Figure 1.15: Mechanism of *n*-butane activation on $(VO)_2P_2O_7$ [6].

The Lewis acid sites play a role in the extraction of two hydrogen atoms from the $-CH_2-$ groups with basic oxygen through a concerted mechanism [6]. The so formed olefinic intermediate is rapidly oxidized to maleic anhydride by the near oxygen atoms.

Bröensted acid sites: they were identified by FT-IR spectroscopy and are the P-OH groups in the terminal position. These sites belong to P-O bonds broken in terminal position in the phosphorus tetrahedra.
The main functions of these surface P-OH groups are [6, 118]:

- facilitate the H removal, favouring the H shift toward the H_2O formation and desorption sites;
- facilitate maleic anhydride desorption avoiding total oxidation;
- activate the C-H bonds.

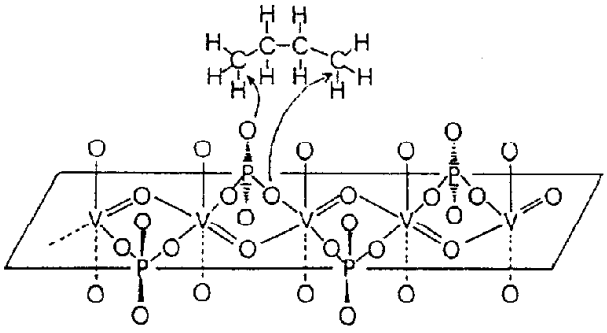

Figure 1.16: Acid Bröensted sites.

V^{5+}: notwithstanding the average oxidation state of V in the bulk phase is V^{4+}, a quite big amount of V^{5+} could be present at the surface. The amount of V^{5+} at the surface varies from 20 to 100%, depending on the preparation method (in particular on the thermal treatment), the presence of dopants or the reaction conditions. This specie is active in the oxygen insertion of activated paraffins, but also leads to the total oxidation to CO and CO_2. So a defined amount of V^{5+} is necessary to improve activity, but an excess of oxidized V is detrimental for selectivity. Volta e al. have demonstrated that the best performances are obtained when the V^{5+}/V^{4+} ratio is about 0,25 [29,31-34].

V^{4+}: this specie is responsible for butane activation. The specie $(V=O)^{2+}$, in correspondence of the cleavage of layer (100), is involved in the H extraction from paraffin and in the allylic oxidation [6]. Ebner and Thompson suggested that V^{4+} species are involved in the oxygen insertion reaction on butadiene with the formation of the 5 elements cyclic entity.

V^{3+}: the role of this specie is difficult to be clarified; so far it is clear that the formation of V^{3+}/P/O compounds is detrimental for the VPO selectivity, but the generation of small amount of V^{3+} (and its associated anionic vacancies) could be positive for the catalytic activity [26-28, 39]. The amount of V^{3+} depends on the thermal treatment and on the amount of organic compounds retained in the precursor.

V-O-P: are involved in the oxidative dehydrogenation of activated *n*-butane (and adsorbed butadienes) to butadiene, moreover they play a role in the oxygen insertion reaction on the 5-elements ring molecules.

Adsorbed molecular oxygen: the adsorbed molecular oxygen is a non-selective specie, because it forms nucleophilic species which normally over-oxide *n*-butane into CO and CO_2. Molecular oxygen is absorbed in two different ways: it could form the η^1-superoxo species and the η^2-peroxo species; these species can interact with the V=O group, and so the *n*-butane is activated [119].
In Figure 1.17 are summarized all the different active sites of $(VO)_2P_2O_7$

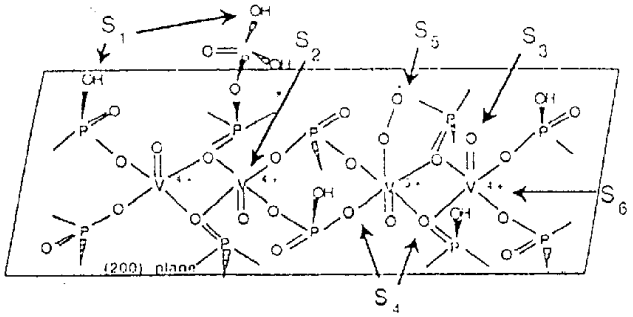

Figure 1.17: Active sites present on vanadyl pyrophosphate: (S_1) Bronsted acid sites; (S_2) Lewis acid sites; (S_3) terminal oxygen; (S_4) bridged oxygen; (S_5) η^2-superoxo sites or η^1-peroxo sites; (S_6) redox couples V^{5+}/V^{4+}.

1.4 REFERENCES

[1] Ulmann's Chemical Encyclopedia, Vol A16, page 54.

[2] MSDS of Maleic Anhydride.

[3] Tecnon Orbichem, London SW11 3TN, UK.

[4] For Italy: Decreto Ministeriale n°60, 2nd April 2002.

[5] www.polynt.com

[6] F. Cavani, F. Trifirò, Chem. Tech., 24 (1994) 18.

[7] G. Centi, F. Cavani, F. Trifirò, Selective Oxidation by Heterogeneous Catalysis, Kluwer Academic, 2001.

[8] Meyers, Handbook of chemicals production processes, McGraw-Hill

[9] P. Arpentier, F. Cavani, F. Trifirò, The Tecnology of Catalytic Oxidation, Technip, 2001.

[10] BRIDGES to Sustainability, "A Pilot Study of Energy performance Levels for the U.S. Chemical Industry", report ot the U.S. Department of Energy, June 2001. Available at http://www.bridgestos.org/Publications.htm

[11] G. Centi, F. Trifirò, J. R. Ebner and V. Franchetti, Chem. Rev., 88 (1988) 55.

[12] F. Cavani, F. Trifirò, Appl. Catal. A, 88 (1992) 115.

[13] R. M. Contractor, A. W. Sleight, Catal. Today, 3 (1988) 175.

[14] C. C. Torardi and J. C. Calabrese, Inorg. Chem., 23 (1984) 1308.

[15] S. Albonetti, F. Cavani, S. Ligi, F. Pierelli, F. Trifirò, F. Ghelfi, G. Mazzoni, Stud. Surf. Sci. Catal. 143, 963 (2002).

[16] F. Cavani, A. Colombo, F. Giuntoli, F. Trifirò, P.Vazquez, P. Venturoli, "Advanced Catalysis and Nanostructured Materials", W.R. Moser (Ed.), Academic Press, (1996), page 43.

[17] M. Meisel, G. U. Wolf, A. Bruckner, Proceed. DGMK Conference on "Selective Oxidations in Petrolchemistry", M. Boerus and J. Wertkamp (Eds.), Tagungsbericht, 1992, page 27.

[18] F. Cavani, F. Trifirò, 3rd World Congress on Oxidation Catalysis, R. K. Grasselli, S. T. Oyama, A. M. Gaffney and J. E. Lyons (Edt.), (1997) 19.

[19] J. W. Johnson, D. C. Johnston, A. J. Jacobson, J. F. Brody, J. Am. Chem. Soc., 106 (1984) 8123.

[20] M. R. Thompson, J. R. Ebner in P. Ruyiz, B. Delmon (Eds.) "New Developments in Selective Oxidation by Heterogeneous Catalysis", Elsevier, Amsterdam, 1992, page 353.

[21] L. M. Cornaglia, C. Caspani, E. A. Lombardo, Appl. Catal., 15 (1991) 74.

[22] R. M. Contractor, J. R. Ebner, M. J. Mummey in "New Developments in Selective Oxidations", G. Centi and F. Trifirò (Eds.), Elsevier Science, Amsterdam, 1990, page 553.

[23] E. Bordes, Catal. Today, 16 (1993) 27.

[24] S. Albonetti, F. Cavani, F. Trifirò, P. Venturoli, G. Calestani, M. Lopez Granados, J.L.G. Fierro, J. Catal., 160 (1996) 52.

[25] S. Albonetti, F. Budi, F. Cavani, S. Ligi, G. Mazzoni, F. Pierelli, F. Trifirò, Stud. Surf. Sci. Catal., 136 (2001) 141.

[26] P.L. Gai, K. Kourtakis, Science, 267 (1995) 661.

[27] F. Cavani, S. Ligi, T. Monti, F. Pierelli, F. Trifirò, S. Albonetti, G. Mazzoni, Catal. Today 61 (2000) 203.

[28] P.T. Nguyen, A.W. Sleight, N. Roberts, W.W. Warren, J. Solid State Chem. 122 (1996) 259.

[29] F. Cavani and F. Trifirò, In Preparation of Catalysis VI, G. Poncelet et al. edt (1995).

[30] G.J. Hutchings, A. Desmartin-Chomel, R. Olier, J.C. Volta, Nature, 368 (1994) 41.

[31] M. Abon, K. Béré, A. Tuel, P. Delichere, J. Catal., 156 (1995) 28.

[32] K. Ait-Lachgar, M. Abon, J.C. Volta, J. Catal., 171 (1997) 383.

[33] K. Ait-Lachgar, A. Tuel, M. Brun, J.M. Herrmann, J.M. Krafft, J.R. Martin, J.C. Volta, J. Catal., 177 (1998) 224.

[34] G.J. Hutchings, C.J. Kiely, M.T. Sananes-Schulz, A. Burrows, J.C. Volta, Catal. Today, 40 (1998) 273.

[35] U. Rodemerck, B. Kubias, H.W. Zanthoff, M. Baerns, Appl. Catal., 153 (1997) 203.

[36] U. Rodemerck, B. Kubias, H.W. Zanthoff, G.U. Wolf, M. Baerns, Appl. Catal., 153 (1997) 217.

[37] G.W. Coulston, S.R. Bare, H. Kung, K. Birkeland, G.K. Bethke, R. Harlow, N. Herron, P.L. Lee, Science, 275 (1997) 191.

[38] P.L. Gai, K. Kourtakis, D.R. Coulson, G.C. Sonnichsen, J. Phys. Chem. B, 101 (1997) 9916.

[39] P.L. Gai, Topics Catal., 8 (1999) 97.

[40] F. Cavani, F. Trifirò, in "Basic Principles in Applied Catalysis", M. Baerns (Ed.), Springer-Verlag, Berlin, (2004) 21.

[41] Mallada, S. Sajip, C.J. Kiely, M. Menendez, J. Santamaria, J. Catal., 196 (2000) 1.

[42] S. Mota, M. Abon, J.C. Volta, J.A. Dalmon, J. Catal., 193 (2000) 308.

[43] Y. Kamiya, E. Nishikawa, T. Okuhara, T. Hattori, Appl. Catal. A, 206 (2001) 103.

[44] V.V. Guliants, Catal. Today, 51 (1999) 255.

[45] R.A. Overbeek, P.A. Warringa, M.J.D. Crombag, L.M. Visser, A.J. van Dillen, J.W. Geus, Appl. Catal. A 135 (1996) 209.

[46] R.A. Overbeek, A.R.C.J. Pekelharing, A.J. van Dillen, J.W. Geus, Appl. Catal. A 135 (1996) 231.

[47] M. Ruitenbeek, R.A. Overbeek, A.J. van Dillen, D.C.Koningsberger, J.W. Geus, Recl. Trav. Chim. Pays-Bas 115 (1996) 519.

[48] M. Nakamura, K. Kawai, Y. Fujiwara, J. Catal. 34 (1974) 345.

[49] S. Holmes, L. Sartoni, A. Burrows , V. Martin , G.J. Hutchings , C. Kiely , J.C. Volta, Stud. Surf. Sci. Catal.,130 (2000) 1709.

[50] P.S. Kuo, B.L. Yang, J. Catal., 117 (1989) 301.

[51] L. Sartoni, J.K. Bartley, R.P.K. Wells, A. Delimitis, A. Burrows, C. Kiely , J.C. Volta, G.J. Hutchings , J. of Mater. Chem., 15(40) (2005) 4295.

[52] C. Bouchy, M.J. Ledoux, C. Crouzet, H. Baudouin, K. Kourtakis and J.J. Lerou, WO 62,925 (2000).

[53] M.J. Ledoux, C. Crouzet, C. Pham-Huu, V. Turines, K. Kourtakis, P. Mills and J.J. Lerou, J. Catal. 203 (2001) 495.

[54] M.J. Ledoux, S. Hantzer, C. Pham-Huu, J. Guille and M.P. Desanaux, J. Catal. 114 (1998) 176.

[55] R.A. Overbeek, P.A. Warringa, M.J.D. Crombag, L.M. Visser, A.J. van Dillen and J.W. Geus, Appl. Catal. A 135 (1996) 209.

[56] F. Cavani and F. Trifirò, Stud. Surf. Sci. Catal. 91 (1995) 1.

[57] J. Weiguny, S. Storck, M. Duda and C. Dobner, US Patent 222,436 (2005), assigned to BASF AG.

[58] I. Sawaki, Eur. Patent 1,359,138 (2003), assigned to Mitsubishi Chem Co.

[59] H. Hibst, R. Noe, M. Exner Kai and M. Duda, Eur Patent 1,417,194 (2004), assigned to BASF AG.

[60] G.J. Hutchings, Appl. Catal. 72 (1991) 1.

[61] F. Cavani and F. Trifirò, Catalysis 11 (1994) 246.

[62] B.K. Hodnett, Catal. Rev. Sci. Eng. 27 (1985) 373.

[63] G.J. Hutchings and R. Higgins, J. Catal. 162 (1996) 153.

[64] M. Abon, J.M. Herrmann and J.C. Volta, Catal. Today 71 (2001) 121.

[65] S. Mota, J.C. Volta, G. Vorbeck and J.A. Dalmon, J. Catal. 193 (2000) 319.

[66] S. Sajip, J.K. Bartley, A. Burrows, M.T. Sananes-Schulz, A. Tuel, J.C. Volta, C.J. Kiely and G.J. Hutchings, New J. Chem. 25 (2001) 125.

[67] S. Sajip, J.K. Bartley, A. Burrows, C. Rhodes, J.C. Volta, C.J. Kiely and G.J. Hutchings, Phys. Chem. Chem. Phys. 3 (2001) 2143.

[68] L. Cornaglia, S. Irusta, E.A. Lombardo, M.C. Durupty and J.C. Volta, Catal. Today 78 (2003) 291.

[69] L.M. Cornaglia, C.R. Carrara, J.O. Petunchi and E.A. Lombardo, Catal. Today 57 (2000) 313.

[70] L. Cornaglia, C. Carrara, J. Petunchi and E. Lombardo, Stud. Surf. Sci. Catal. 130 (2000) 1727.

[71] C. Carrara, S. Irusta, E. Lombardo and L. Cornaglia, Appl. Catal. A 217 (2001) 275.

[72] Y.H. Taufiq-Yap, K.P. Tan, K.C. Waugh, M.Z. Hussein, I. Ramli and M.B. Abdul Rahman, Catal. Lett. 89 (2003) 87.

[73] R. Higgins and G.J. Hutchings, US Patent 4,418,003 (1983), assigned to ICI.

[74] I. Matsuura, T. Ishimura, S. Hayakawa and N. Kimura, Catal. Today 28 (1996) 133.

[75] V.V. Guliants, J.B. Benziger, S. Sundaresan and I.E. Wachs, Stud. Surf. Sci. Catal. 130 (2000) 1721.

[76] A.M. Duarte de Farias, W. De A. Gonzalez, P.G. Pris de Oliveira, J.G. Eon, J.M. Herrmann, M. Aouine, S. Loridant and J.C. Volta, J. Catal. 208 (2002) 238.

[77] P.G. Pries de Oliveira, J.G. Eon, M. Chavant, A.S. Riché, V. Martin, S. Caldarelli and J.C. Volta, Catal. Today 57 (2000) 177.

[78] F. Cavani, C. Cortelli, S. Ligi, F. Pierelli, F. Trifirò, DGMK Tagungsbericht, 2004-3 (2004) 87.

[79] S. Ligi, F. Cavani, S. Albonetti and G. Mazzoni, US Patent 6,734,135 (2004), assigned to Lonza SpA.

[80] C.J. Kiely, A. Burrows, S. Saijp, G.J. Hutchings, M.T. Sananes, A. Tuel and J.C. Volta, J. Catal. 162 (1996) 31.

[81] G.J. Hutchings, M.T. Sananes, S. Sajip, C.J. Kiely, A. Burrows, I.J. Ellison and J.C. Volta, Catal. Today 33 (1997) 161.

[82] N. Duvauchelle, E. Kesteman, F. Oudet and E. Bordes, J. Solid State Chem. 137 (1998) 311.

[83] H.S. Horowitz, C.M. Blackstone, A.W. Sleight and G. Teuref, Appl. Catal. 38 (1988) 193.

[84] V.A. Zazhigalov, J. Haber, J. Stoch, A.I. Kharlamov, L.V. Bogutskya, I.V. Bacherikova and A. Kowal, Stud. Surf. Sci. Catal. 110 (1997) 337.

[85] G.J. Hutchings and R. Higgins, Appl. Catal. A 154 (1997) 103.

[86] W. Ji, L. Xu, X. Wang, Z. Hu, Q. Yan and Y. Chen, Catal. Today 74 (2002) 101.

[87] M. Fait, B. Kubias, H.J. Eberle, M. Estenfelder, U. Steinike and M. Schneider, Catal. Lett. 68 (2000) 13.

[88] N. Hiyoshi, N. Yamamoto, N. Terao, T. Nakato and T. Okuhara, Stud. Surf. Sci. Catal. 130 (2000) 1715.

[89] N. Yamamoto, N. Hiyoshi and T. Okuhara, Chem. Mater. 14 (2002) 3882.

[90] N. Hiyoshi, N. Yamamoto, N. Ryumon, Y. Kamiya and T. Okuhara, J. Catal. 221 (2004) 225.

[91] G.J. Hutchings, M.T. Sananes, S. Sajip, C.J. Kiely, A. Burrows, I.J. Ellison and J.C. Volta, Catal. Today 33 (1997) 161.

[92] G.J. Hutchings, R. Olier, M.T. Sananes and J.C. Volta, Stud. Surf. Sci. Catal. 82 (1994) 213.

[93] K.E. Birkeland, S.M. Babitz, G.K. Bethke, H. Kung, G.W. Coulson and S.R. Bare, J. Phys. Chem. B 101 (1997) 6895.

[94] N. Herron, D.L.Thorn, R.L. Harlow and G.W. Coulston, J. Amer. Chem. Soc. 119 (1997) 7149.

[95] Z.Q. Zhou, H.Y. Xu, W.J. Ji and Y. Chen, Catal. Lett. 96 (2004) 221.

[96] G.J. Hutchings, J.K. Bartley, J.M. Webster, J.A. Lopez-Sanchez, D. Gilbert, C.J. Kiely, A.F. Carley, S.M. Howdle, S. Sajip, S. Caldarelli, C. Rhodes, J.C. Volta and M. Polyakoff, J. Catal. 197 (2001) 232.

[97] G.J. Hutchings, J.A. Lopez-Sanchez, J.K. Bartley, J.M. Webster, A. Burrows, C.J. Kiely, A.F. Carley, C. Rhodes, M. Hävecker, A. Knop-Gericke, R.W. Mayer, R. Schlögl, J.C. Volta and M. Polyakoff, J. Catal. 208 (2002) 197.

[98] N. Mizuno, H. Hatayama, S. Uccida and A. Taguchi, Chem. Mater. 13 (2001) 179.

[99] M.A. Carreon and V.V. Guliants, Chem. Commun. (2001) 1438.

[100] M.A. Carreon and V.V. Guliants, Microp. Mesop. Mat. 55 (2002) 297.

[101] M.A. Carreon and V.V. Guliants, Catal. Today 78 (2003) 303.

[102] M.A. Carreon, V.V. Guliants, M.O. Guerrero-Perez and M.A. Bañares, Microp. Mesop. Mat. 71 (2004) 57.

[103] M.A. Carreon, V.V. Guliants, F. Pierelli and F. Cavani, Catal. Lett. 92 (2004) 11.

[104] J.H. Holles, C.J. Dillon, J.A. Labinger and M.E. Davis, J. Catal. 218 (2003) 42.

[105] C.J. Dillon, J.H. Holles, R.J. Davis, J.A. Labinger and M.E. Davis, J. Catal. 218 (2003) 54.

[106] C.J. Dillon, J.H. Holles, M.E. Davis and J.A. Labinger, Catal. Today 81 (2003) 189.

[107] F. Trifirò, Catal. Today, 16 (1993) 91.

[108] G. Centi, G. Fornasari and F. Trifirò, J. Catal. , 89 (1984) 44.

[109] S. Albonetti, F. Cavani and F. Trifirò, Catal. Rev.-Sci. Eng., (1996) 413.

[110] G. Centi and F. Trifirò, Catal. Today, 3 (1988) 151.

[111] Z.Y. Xue, G.L. Schrader, J. Catal, 184 (1999) 87.

[112] D.J. Thompson, I.M. Ciobîca, B.K. Hodnett, R.A. van Santen, M.O. Fanning, Surface Science, 547 (2003) 438.

[113] D.J. Thompson, M.O. Fanning, B.K. Hodnett, J. Molec. Catal A, 198 (2003) 125.

[114] D.J. Thompson, M.O. Fanning, B.K. Hodnett, J. Molec. Catal A, 206 (2003) 435.

[115] D.J. Thompson, I.M. Ciobîca, B.K. Hodnett, R.A. van Santen, M.O. Fanning, Catal. Today, 91 (2004) 177.

[116] F. Cavani, F. Trifirò, Appl. Catal., 157 (1997) 195.

[117] G. Busca, E. Finocchio, G. Ramis, G. Ricchiaroli, Catal. Today, 32 (1996) 1330.

[118] V. A. Zazhigalov, J. Haber, J. Stoch, V. M. Belousov, Appl. Catal., 96 (1993) 135.

[119] P. A. Agaskar, L. De Caul, R. K. Grasselli, Catal. Lett., 23 (1994) 339.

2

EXPERIMENTAL

2.1 CATALYSTS SYNTHESIS

2.1.1 Synthesis of vanadyl pyrophosphate, $(VO)_2P_2O_7$

Catalysts were prepared by the "organic procedure"; $VOHPO_4 \cdot 0.5H_2O$, precursor of vanadyl pyrophosphate, was synthetized suspending the desired amounts of V_2O_5 and H_3PO_4 in isobutanol.

The precipitation of hemihydrate acid vanadyl orthophosphate occurred through the reduction of vanadium (V) oxide to VO^{2+} ions by isobutanol; in presence of H_3PO_4 the precursor precipitated:

$V_2O_5 + C_4H_9OH + 2\ H^+ \rightarrow 2\ VO^{2+} + C_4H_8O + 2\ H_2O$

$VO^{2+} + H_3PO_4 + 0.5\ H_2O \rightarrow VOHPO_4 \cdot 0.5H_2O + 2H^+$

By-products of isobutanol oxidation were isobutyric aldheyde and other oxidation products (such as: acetaldehyde, acetic acid, formic acid, etc.); moreover water was co-produced.

The mixture was heated at reflux temperature (120°C) for 6 hours. The colour varied from the typical dark orange of V_2O_5, to an intense light blue, characteristics of $VOHPO_4 \cdot 0.5H_2O$. After filtration, the obtained precipitate was thermally treated according to the following procedure:

(a) drying at 120°C for 12 h, in static air, to obtain the so called Precursor;

(b) pre-calcination step in flowing air (130 ml/min), with temperature gradient from room temperature up to 300°C; then isothermal step at 300°C in air for 6 h;

$2\ (VO)HPO_4 0.5H_2O \rightarrow 2\ (VO)HPO_4 + H_2O$

(c) thermal treatment in flowing N_2 (20 ml/min), with temperature gradient up to 550°C, and final isothermal step at the latter temperature for 6 h.
$2\ (VO)HPO_4 \rightarrow (VO)_2P_2O_7 + H_2O$

2.1.2 Synthesis of supported catalysts

Catalysts were prepared by the wet impregnation technique: an aqueous solution containing the desired amount of NH_4VO_3 and H_3PO_4 (85 wt%) was added to the support (monoclinic ZrO_2, with specific surface area 14 m^2/g). Water was evaporated under vacuum at 70°C; the solid obtained, precursor of the final catalyst, was thermally treated according one of the following procedures:

(a) calcination in static air, heating with gradient 10°C/min up to 150°C for 3h and then up to 450°C, final isotherm of 5h;
(b) thermal treatment in flowing 10 mol% steam in air, sample was heated up to 150°C in air, then steam was added and sample was heated up to 450°C for 5 hours (τ=0.9 s);
(c) treatment under steam/helium, following the same protocol described in (b).

2.2 SAMPLES CHARACTERIZATION

FT-IR Spectroscopy

The IR-spectra were recorded using a FT-IR Perkin-Elmer spectrometer, with the KBr method, with a resolution of 4 cm^{-1}, using 10 scansions, between 4000 and 400 cm^{-1}.

UV-VIS Spectroscopy

UV-Vis spectra were recorded in diffuse reflectance using a Perkin-Elmer UV/VIS/NIR Lambda 19 instrument, equipped with an integrating sphere, between 190 and 1500 nm, with a scansion rate of 480 nm/min. After recording, spectra were transformed in F(R) by the Kubelka-Munch law.

RAMAN Spectroscopy

Raman studies were performed using a Renishaw 1000 instrument, equipped with a Leica DMLM microscope, laser source Argon ion (514 nm) with power <25

mW. Generally for all samples different spectra were recorded. "*In-situ*" analysis were performed using a commercial Raman cell (Linkam Instruments TS1500).

Specific surface area

The specific surface area was determined by N_2 adsorption at 77K (the boiling T of nitrogen), with a Sorpty 1700 Instrument (Carlo Erba). The sample was heated at 100°C under vacuum, to eliminate water and other molecules eventually adsorbed on the surface. After this pre-treatment, sample was maintained at 77K in a liquid nitrogen bath, while the instrument slowly sent gaseous N_2, which was adsorbed on the surface. By BET equation it was possible to calculate the volume of monostrate and finally the sample surface area.

X-Ray Diffraction

The XRD measurements were carried out using a Philips PW 1710 apparatus, with Cu Kα (λ = 1.5406 Å) as radiation source in the range of $10°<2\theta<50°$, with steps of 0.05 grade and acquiring the signal for 3 seconds for each step.
Reflects attribution was done by the Bragg law, using the d value. ($2d\ sen\theta = n\lambda$)

SEM-EDX analysis

SEM-EDX analyses were carried out with a Zeiss EVO 50 electronic microscope, equipped with a INCA probe (Oxford Instrument) for quantitative analysis. No pretreatment of samples was necessary.

2.3 CATALYTIC TESTS

2.3.1 Bench-scale plant

Catalytic tests were carried out in a continuous-flow, fixed bed, quartz reactor. Different parameters could be varied, such as the feed composition, residence time and temperature inside the reactor. The laboratory plant is schematized in Figure 2.1 (page 45)and could be divided in three main different parts:

1) "feed"
2) "reaction"
3) "downstream"

1) Feed:

Three different gases could be simultaneously fed: *n*-butane, air and helium; their composition could be varied using three mass-flow meters (1). The Helium pipe was independent, while *n*-butane and air were mixed together before entering in a three-ways valve (3) that was used to switch the feed inside the reactor or in a bubble flow meter, used to check the real entrance flux (5). After the three-ways valve a four-ways commutation valve was present (6), using this valve the mixture of *n*-butane and air could be fed in the reactor or analyzed by GC (on-line sampling in the FID). During the sampling it was possible to feed Helium in the reactor, using the four ways valve.

2) Reaction:

The fixed bed reactor (8) was constituted by a quartz tube, operating at ambient pressure. In the reactor head a porous septum allowed to sample the fed gas through a syringe. In the middle of the reactor a second quartz tube allowed to place a thermocouple (10), with which the real temperature inside the bed was controlled. With the aim of minimize dispersions and equalize temperature on the axial direction, the reactor was wrapped in a copper block (9) surrounded by a resistance, to regulate the temperature through a regulator with an inside thermocouple. At the reactor exit a heater string maintained at 200°C avoided any crystallization of the products on the inner walls.

3) Downstream:

After the heating string at the reactor exit, a gas split was placed: opening the micro valve (4) a part of flow was sent to the gascromatograph and by a sampling valve (15) it was possible to make directly the analysis of the organic products from the reaction and of the unconverted butane on the FID column. The second part of the gas outing from the reactor was collected in a crystallizer (12). From the crystallizer exit it was possible to sample by a syringe all the incondensable gases such as CO_x. To collect the fraction not condensed, at the crystallizer exit a glass bubbler filled with acetone (13) was placed; linked to the bubbler a second bubble flow meter to measure the exiting gas flow was present.

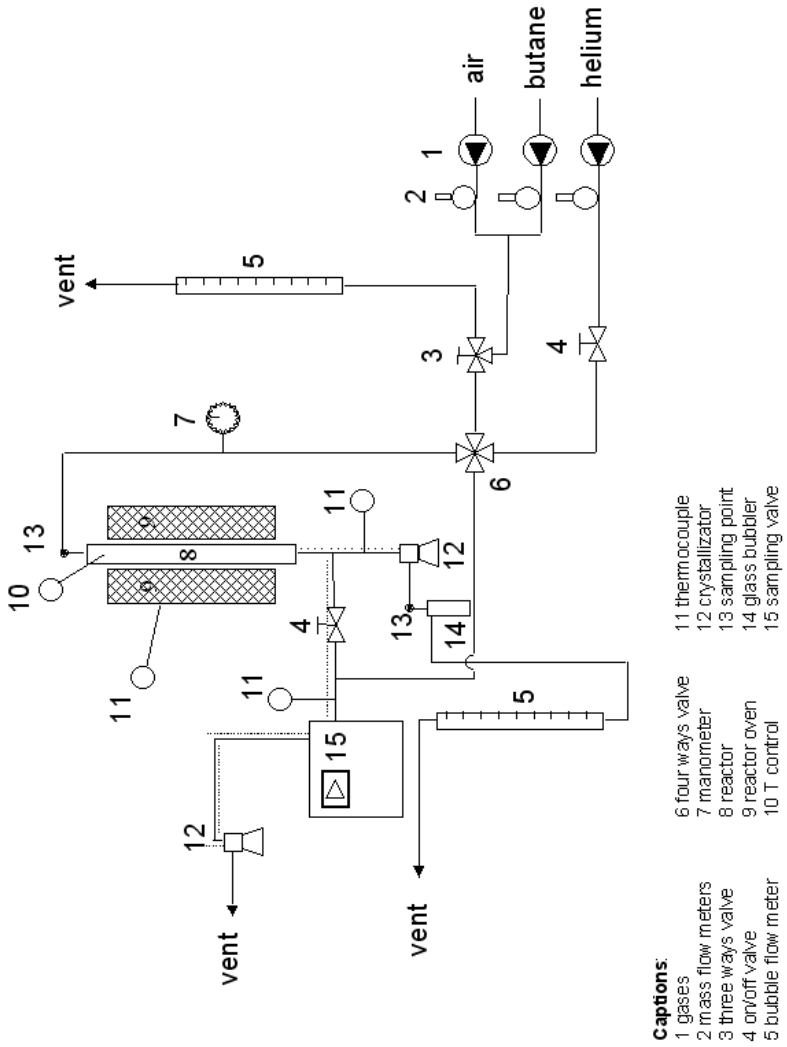

Figure 2.1: Scheme of the bench scale plant.

2.3.2 Analytical system

By gascromatography were analyzed reactants and products. In the Varian GC two different columns were loaded:

1) Semicapillar HP1 column, of 30 m length, with an internal diameter of 0.53 mm and a stationary phase of dimethylpolysiloxane with a thickness of 3.00 μm. By this column are separated maleic anhydride, by-products (acetic acid, acrylic acid and other light by-products) and also *n*-butane (in and out) is analyzed: The detector was a FID.

2) Packed Carbosieve SII column, of 2 m length, with a stationary phase formed by active carbons (mesh between 80 and 100). In this column CO, CO_2, H_2O, O_2 and N_2 are separated and detected by a TCD.

For both columns Helium was employed as carrier gas.

The temperature program of the oven was: 7 minutes at 40°C, heating up to 220°C (heating rate of 30°C/min), final isothermal step at 220°C for 10 minutes.

In the FID column was used an on-line sampling which allowed the direct determination of the amount of maleic anhydride present in the gas mixture and also the analysis of a constant volume of off-gas. The sampling valve, having a loop of 560 µl volume, was maintained at 200°C to avoid any maleic anhydride condensation inside.

The incondensable by-products (CO, CO_2, and non converted air) were sampled with a gas syringe (volume: 500 µl) through the porous septum positioned in the crystallizer; these were injected in the packed column linked to the TCD.

The analysis of in *n*-butane was carried out by the on-line sampling, while in-oxygen was determined by sampling in the porous septum at the inlet of reactor.

2.3.3 Elaboration of catalytic data

From the gascromathography analysis the values of yield, conversion and selectivity were determined, by the following equation:

$$Conversion = \frac{n^\circ mols\ of\ converted\ reactant}{n^\circ mols\ of\ fed\ reactant} \times 100$$

$$Yield = \frac{n^\circ mols\ of\ product/stoichiometric\ coeff.}{n^\circ mols\ of\ fed\ reactant/stoichiometric\ coeff.} \times 100$$

$$Selectivity = \frac{Yield}{Conversion} \times 100$$

$$C\ balance = \frac{\sum Yields}{Conversion} \approx 100$$

3

SURFACE DYNAMICS OF V/P/O CATALYST

3.1 INTRODUCTION

The problem of the real nature of the active surface of vanadyl pyrophosphate (VPP) has been investigated by several authors, often with the use of *in-situ* techniques [1-10]. Several articles discuss the role of different crystalline and/or amorphous compounds in VPO, not only in VPP, but also in other vanadium phosphates, in the complex transformation of the alkane to MA [11-17]. In general two different hypotheses were formulated; while bulk VPP is in all cases assumed to constitute the core of the active phase, differences concerns the nature of the first atomic layers, those that are in direct contact with the gas phase. It is well known that surface reconstruction, especially in the presence of reactive gases, may substantially alter the surface arrangement of atoms as compared to the bulk. However, due to the difficulties in the characterization of the catalytically active surface under reaction conditions, the alternative hypothesis either indicate the development of surface amorphous layers which play a direct role in the reaction [18-22], or are based on the crystallographic models of the VPP, assuming that specific planes contribute to the reaction pattern [2,11,23-29], and that the redox process occurs reversibly between VPP and $VOPO_4$ [1,30]. An excellent discussion of the scientific literature dealing with the working state of the active surface in VPP has been published by Schlögl and co-workers [6]. The discussion is supported by *in-situ* measurements of the structure of the active compound and of the composition of the active surface [7,8]. HRTEM images of basal and prism edges of the VPP made possible the identification of non-crystalline adlayer, about 1 nm thick, on the surface of equilibrated VPO catalysts

[6]. By application of *in-situ* X-ray absorption spectroscopy (XAS) and *in-situ* XPS, it was concluded that the working surface is a two-dimensional structure containing more O than that present in the VPP; it is originated *in-situ* by hydrolysis of the VPP, which is metastable under reaction conditions [9]. The authors viewed this surface layer as being constituted of a binary V_xO_y, the growth of which is hindered by phosphate groups [6,8]. In contrast with this hypothesis are the results reported by Guliants et al. [10]; the authors found, by means of *in-situ* Raman and XRD techniques, that a disordered layer about 2 nm thick, covering the surface (100) planes of fresh VPP, disappeared during equilibration yielding a solid with steady and optimal catalytic performance. Therefore, it is evident that despite the many *in-situ* techniques employed for the investigation of VPP, it is not possible to draw a general picture concerning the nature of the active phase in VPP under working conditions. One possible explanation, is that the nature of the active layer is a function of the reaction conditions, and of the main features of VPO catalysts. Among the latter, the P/V atomic ratio used for catalyst preparation is known to be a very important factor that governs the catalytic performance of VPP. In fact, it is generally accepted that an excess of P with respect to the stoichiometric requirement (P/V= 1.0) is necessary in order to have a good selectivity to MA [23]. With the aim of finding whether this parameter may affect the nature of the transformations occurring at the surface of VPP, the surface transformations occurring in two catalysts, prepared with P/V ratio of 1.0 and 1.2, during variations of gas-phase composition were investigated by means of *in-situ* Raman spectroscopy and reactivity tests under unsteady-state conditions.

3.2 EXPERIMENTAL

Catalysts were prepared by the "organic procedure", as described in Chapter 2.1.1. Two samples, with different P/V ratio, were synthesized (Table 3.1).

Table 3.1: Prepared samples.

Sample	P/V theor	P/V (SEM-EDX)	P/V (XRF)	P/V (ICP-MS)
PV1.0, precursor	1.0	0.99±0.02		1.02±0.02
PV1.2, precursor	1.2	1.08±0.02	1.04±0.02	
PV1.0, calcined	1.0			
PV1.2, calcined	1.2	1.05±0.02		

Catalytic tests were carried out in the laboratory plant described in Chapter 2.2; the feed was composed of 1.7% *n*-butane, 17% O_2 and rest helium.

For Raman analysis a continuous flow of air or N_2 was sent into the cell; a saturator connected to the system allowed to feed also steam, varying the temperature of the saturator different amounts of water vapour could be obtained (3-10%). *In-situ* spectra were recorded for "equilibrated" catalysts, i.e., samples that had been preliminary treated in the reactive phase at 400°C for 100h reaction time.

X-ray photoelectron spectra (XPS) were recorded with a VG ESCALAB 220 XL spectrometer equipped with a monochromatic Al Kα (E = 1486.6 eV) X-ray source, and using as reference C1s peak (285.0 eV). The spectra were collected with a pass energy of 40 eV, using the electromagnetic lens mode low-energy electron flood gun (6 eV) for charge compensation effect; O1s/V2p, C1s and P2p core levels have been recorded.

3.3 RESULTS AND DISCUSSION

3.3.1 *In-situ* calcination

With the aim of understanding the role of P/V ratio on the formation of vanadyl pyrophosphate, the modifications occurring during the thermal treatment of precursor were investigated by means of *in-situ* X-ray diffraction and X-ray photoelectron spectroscopy. Analysis were performed at UCCS (Unité de Catalyse et de Chimie du Solide), during a three month stage I spent in Lille for the project "Investigation of the surface and reactivity properties of catalysts of selective oxidation of *n*-butane".

XRD profiles were recorded using a Bruker D8 diffractometer equipped with a Cu Kα (λ= 0.154 nm) radiation. The calcination procedure was reproduced in the XRD chamber. A first analysis at room temperature was performed, then samples were heated up to 300°C in air (heating rate: 1°C/min, air flow 5 l/h) and maintained at this temperature for 6 hours. The samples were cooled at room temperature and heated again under flow of nitrogen up to 550°C (heating rate: 1°C/min, N_2 flow: 4 l/h, isothermal step: 6h). Diffraction patterns have been recorded at increasing temperatures and during isothermal steps.

Figure 3.1 shows the evolution of the precursors having P/V ratio 1.0 and 1.2 during the first step of thermal treatment.

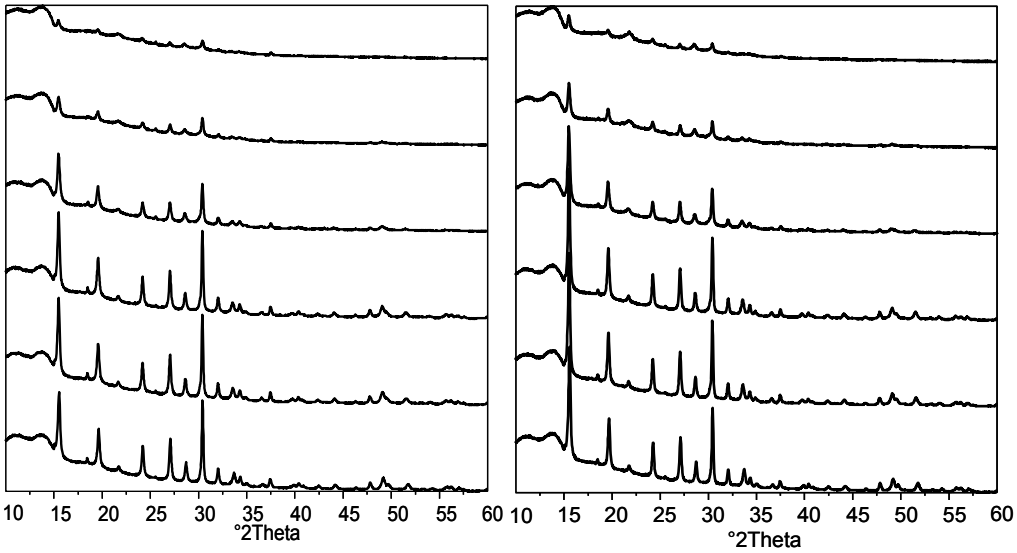

Figure 3.1: X-Ray diffraction patterns of precursors collected during calcination in air. Samples: PV1.0 (left), PV1.2 (right).

No great differences between the two samples can be noticed: at room temperature the XRD patterns of precursors were typical of $(VO)HPO_4.0.5H_2O$ (JCPDS 37-0269), increasing temperature in air the intensity of all reflections decreased but not totally disappeared neither after 6 hours at 300°C.

Under N_2, samples showed a slightly different behaviour. For catalyst PV1.0 the reflections of precursor progressively decreased in intensity and finally disappeared, at 350°C the sample was completely amorphous. At 400°C the reflections of $(VO)_2P_2O_7$ (JCPDS 34-1381) appeared, together with a mixture of V^{5+} phases, ω-$VOPO_4$ (JCPDS 37-0809) and δ-$VOPO_4$ (JCPDS 47-0951). At high temperature (450-550°C) the main and more narrow reflections were attributable to ω-$VOPO_4$. Nevertheless, this compound is not stable at low temperature; at room temperature XRD-diffraction pattern showed the presence of vanadyl pyrophosphate, δ-$VOPO_4$ and traces of β-$VOPO_4$.

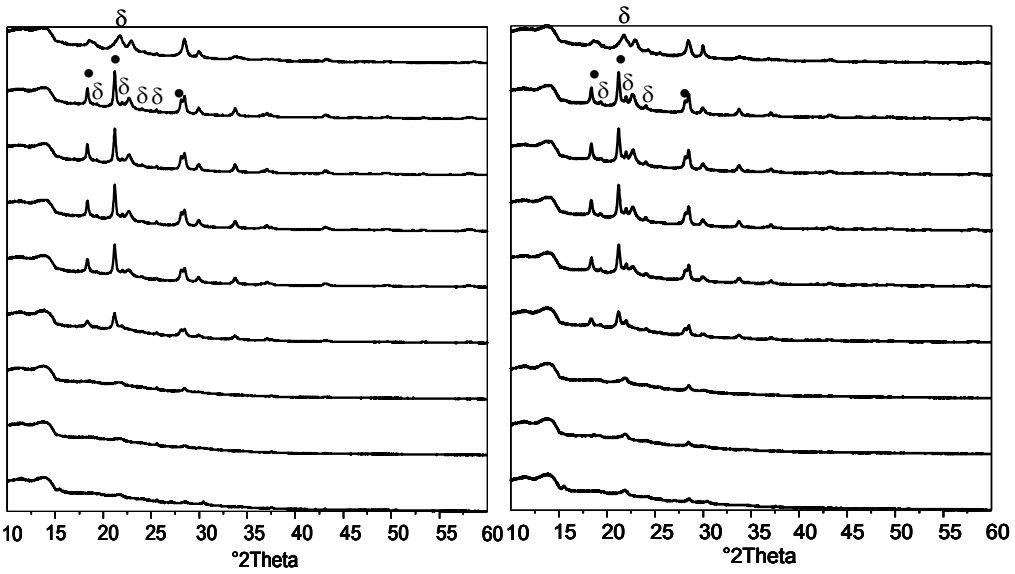

Figure 3.2: X-Ray diffraction patterns of precursors collected during calcination in nitrogen. Samples: PV1.0 (left), PV1.2 (right).

Sample having P/V ratio 1.2 showed a similar behaviour but, compared with the sample PV1.0, it seemed to be more crystalline at all temperature levels. At 350°C under N_2, the sample 1.0 was almost totally amorphous, while in the case of PV 1.2 weak reflections of VPP could be noticed. Also in this case, at temperature higher than 400°C ω-$VOPO_4$ formed. Another difference concerns the relative intensities of ω-$VOPO_4$ and VPP reflections. Comparing reflections at 28.1 °2θ (ω-$VOPO_4$) and 28.5 °2θ (VPP), it can be observed that for sample PV1.2 vanadyl pyrophosphate showed more intense reflections in the temperature range 450-550°C. At room temperature beside vanadyl pyrophosphate, also δ-$VOPO_4$ was present. Data indicates that, despite the second step of thermal treatment was carried out in non-oxidizing atmosphere, i.e. nitrogen, samples were gradually oxidized and ω-$VOPO_4$ formed. With sample PV1.2 the crystallization of vanadyl pyrophosphate occurs at lower temperature and it is favoured respect to the formation of ω-$VOPO_4$.

To confirm the importance of the excess of P to prevent oxidation of vanadium, XPS measurements were performed. Calcination has been carried out in a pre-treatment chamber: temperature was increased up to 300°C under air (heating rate: 1°C/min, air flow: 50 ml/min) and maintained in isotherm for about 10 hours, then the sample was heated under flow of nitrogen up to 500°C for 6 hours

(heating rate: 1°C/min, flow: 20 ml/min). The catalyst was transferred to the analysis chamber and XP spectra were recorded. Results are summarized in Table 3.2.

Table 3.2: XPS results

Sample	BE O1s	BE $V2p_{3/2}$	BE P2p	P/V	V_{OX}
PV1.0, calcined	532.80	518.70	134.80	1.61	4.23
PV1.2, calcined	532.80	518.60	135.00	1.71	4.16

For both samples surface P/V ratio is higher than the theoretical value, a surface enrichment in phosphorus is not unusual for this system. Many groups, studying the VPO catalysts, reported a surface P/V ratio significantly higher than the bulk value [31-34]. The excess of P has been explained by the presence of an amorphous layer of $VO(PO_3)_2$ [27] or pendent pyrophosphate groups [35].
The average vanadium oxidation state (V_{OX}) has been calculated using the method proposed by Coulston [36]. Oxidation state of vanadium is related to the splitting between the O1s and $V2p_{3/2}$ binding energies and can be calculated according to the following equation:

$$V_{OX} = 13.82 - 0.68\,[O1s - V2p_{3/2}]$$

After *in-situ* calcination both catalysts were partially oxidized, in accordance with XRD data which showed the presence of V^{5+} phosphate in calcined samples. In the sample PV1.0 the average vanadium oxidation state was slightly higher than in sample PV1.2. This confirm the importance of phosphorus for avoiding the oxidation of vanadium in VPO catalysts.

3.3.2 Ex-situ characterization

Both calcined and used (equilibrated) catalysts were characterized by means of XRD, Raman and UV-Vis spectroscopy.
Figure 3.3 shows the room-temperature XRD patterns of PV1.0 and PV1.2 catalysts. In XRD patterns of calcined samples, besides the reflections of VPP (JPCDS 34-1381), also those attributable to V(V) phosphates were present. In particular, in the PV1.0 pattern, reflections are attributable to δ-$VOPO_4$ and to an hydrated oxidized phase (JCPDS 47-0967); in the case of PV1.2, the very intense reflection at 2Θ 21.7 is due to δ-$VOPO_4$. In the case of equilibrated samples, XRD

patterns show only reflections attributable to VPP; however, traces of δ-$VOPO_4$ are likely present in PV1.0, as inferred from the very weak reflection at 2θ 21.7.

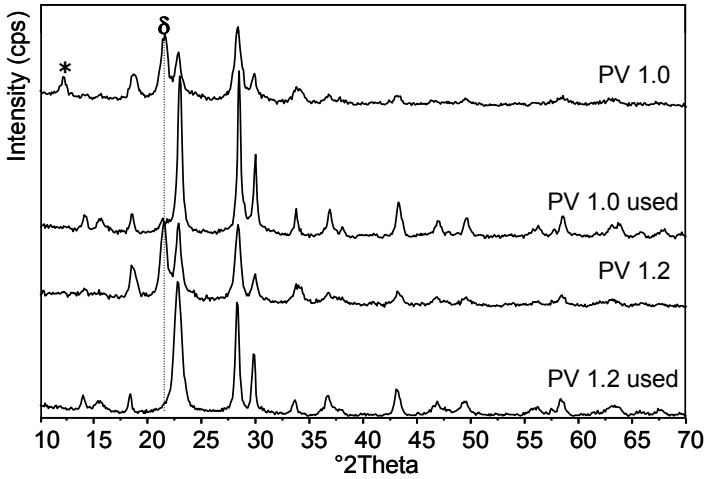

Figure 3.3: XRD patterns recorded ex-situ at room temperature of PV1.0 and PV1.2, calcined and used. Symbols: δ δ-$VOPO_4$ (JCPDS 47-0951), * $H_4V_3P_3O_{16.5}$ ·xH_2O (JCPDS 47-0967)

Also in Raman spectra (Figure 3.4), both calcined samples showed bands attributable to V(V) phosphates, but differences are seen between the spectra, that indicate the presence of different oxidized compounds in the two samples. In the case of PV1.0, bands can be attributed to γ-$VOPO_4$ and α_I-$VOPO_4$, whereas for P1.2, δ and γ-$VOPO_4$ are the predominant V(V) phosphates.

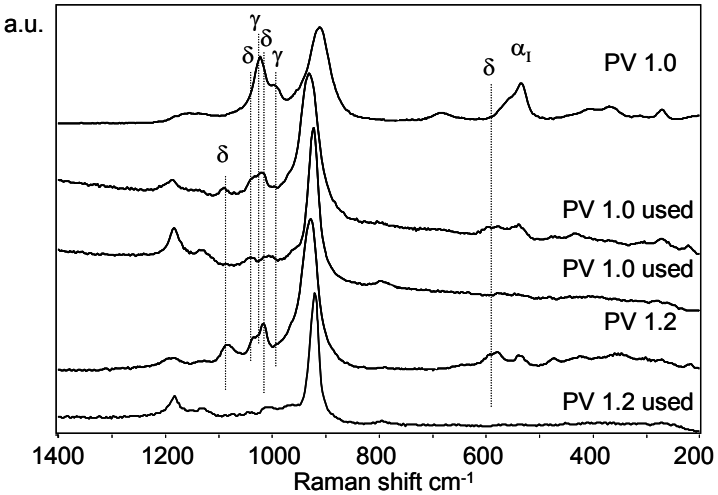

Figure 3.4: Raman spectra recorded ex-situ at room temperature of PV1.0 and PV1.2, calcined and used. Symbols: δ δ-$VOPO_4$, γ γ-$VOPO_4$, α_I α_I-$VOPO_4$

Some discrepancies between XRD patterns and Raman spectra are attributable to the formation of different V(V) phosphates at the surface and in the bulk of

samples. Concerning equilibrated samples, Raman spectra of PV1.2 recorded by focussing the beam on several different particles, did show exclusively the Raman features of VPP, with no trace of any V(V) phosphate. Sample PV1.0, on the contrary, was less homogeneous; for most of particles, corresponding spectra did show the presence of only VPP, but with some of them, also the band attributable to δ-$VOPO_4$ was seen.

UV-Vis DR spectroscopy confirm the presence of V(V) in both calcined samples: the strong band at around 400–450 nm is attributable to a CT band of V^{5+} [37]. Spectra of used samples confirmed that in average equilibrated PV1.0 was still slightly oxidized; on the contrary, equilibrated PV1.2 spectrum did not show any evidence for the presence of V^{5+}.

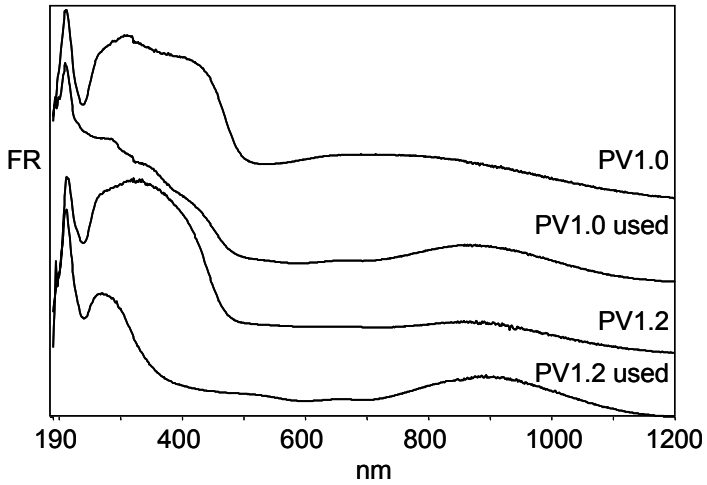

Figure 3.5: UV-Vis DR spectra recorded ex-situ at room temperature of PV1.0 and PV1.2, calcined and used.

It is known that equilibration leads to various transformations in calcined V/P/O catalysts, including (i) the crystallization of amorphous components, if any were present in fresh catalysts, to VPP, (ii) the reduction of bulk $VOPO_4$ phases to VPP, (iii) the oxidation of V(III) phosphates into VPP and (iv) the increase of crystallinity of VPP [38,39]. Indeed, during equilibration the catalyst performance may vary considerably, and a period of time between a few hours and almost 100 h may be necessary to complete bulk transformations and finally develop a catalyst that in bulk is made of well crystallized VPP. In the case of PV1.0, 100 h reaction time were evidently not enough to develop the fully "equilibrated", VPP.

3.3.3. "*In-situ*" Raman spectroscopy

All *in-situ* Raman measurements were performed on equilibrated samples. In the case of PV1.0, particles showing the only presence of VPP were chosen for experiments.

Analysis at different temperatures under flow of dry air, nitrogen and 10% steam in air were performed. In all experiments a small amount of catalyst was loaded into the ceramic crucible of the cell and a first spectrum at room temperature was recorded, then the temperature was increased up to the desired value (heating rate 50°/min) while recording spectra at intermediate temperatures, and finally maintained at isothermal conditions for a few hours at the final temperature.

Figure 3.6 shows the Raman spectra recorded while flowing dry air, at different temperatures.

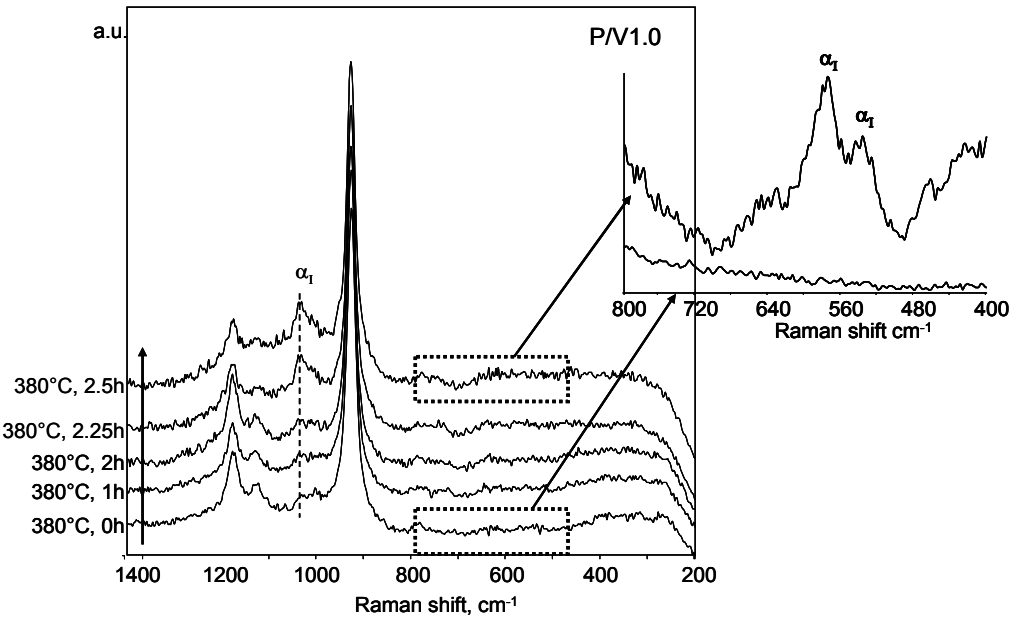

Figure 3.6: Raman spectra recorded *in-situ* in dry air flow at 380°C at increasing time-on-stream. Sample: PV1.0. Symbols: α_I α_I-$VOPO_4$

In the case of PV1.0, the spectrum did not show any change during heating-up the sample from room temperature to 380°C. However, during the isothermal step at 380°C, after 0.5h bands attributable to α_I-$VOPO_4$ developed (1036 cm^{-1}, and less intense at 540 and 575 cm^{-1}). Thereafter, the intensity of bands attributed to α_I-$VOPO_4$ did not increase any more during the 2h of isothermal step at 380°C. However, when the temperature was raised again from 380°C to 440°C, α_I-$VOPO_4$

transformed into δ-$VOPO_4$ (Figure 3.7); in fact, the band at 1036 cm^{-1} disappeared, and bands attributable to δ-$VOPO_4$ (1080, 1015, 588 cm^{-1}) developed.

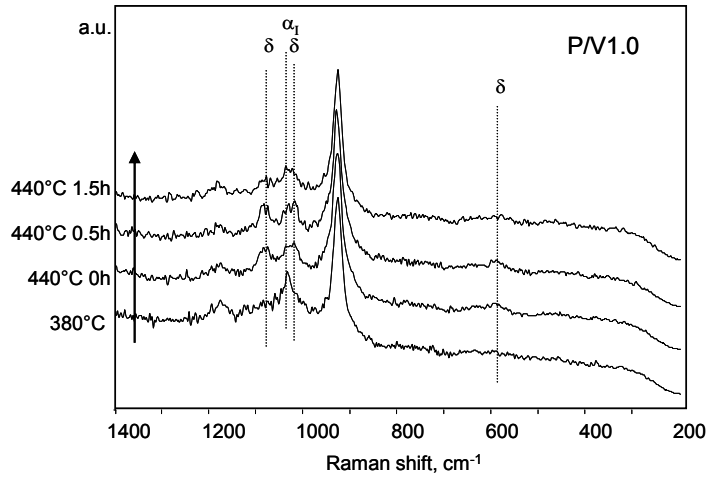

Figure 3.7: Raman spectra recorded *in-situ* in dry air flow at increasing temperature and time-on-stream. Sample: PV1.0. Symbols: δ δ-$VOPO_4$, α_I α_I-$VOPO_4$

With PV1.2, on the contrary, there was no modification of the spectrum up to 500°C (Figure 3.8); only at above 500°C the VPP was oxidized to δ-$VOPO_4$. These experiments clearly demonstrate that the VPP in the two samples shows a different oxidizability in dry air. It is worth noting that when the spectra were recorded in N_2 flow (not reported), neither PV1.0 nor PV1.2 spectra did show any modification with respect to the initial spectrum; VPP was the only compound stable under these conditions.

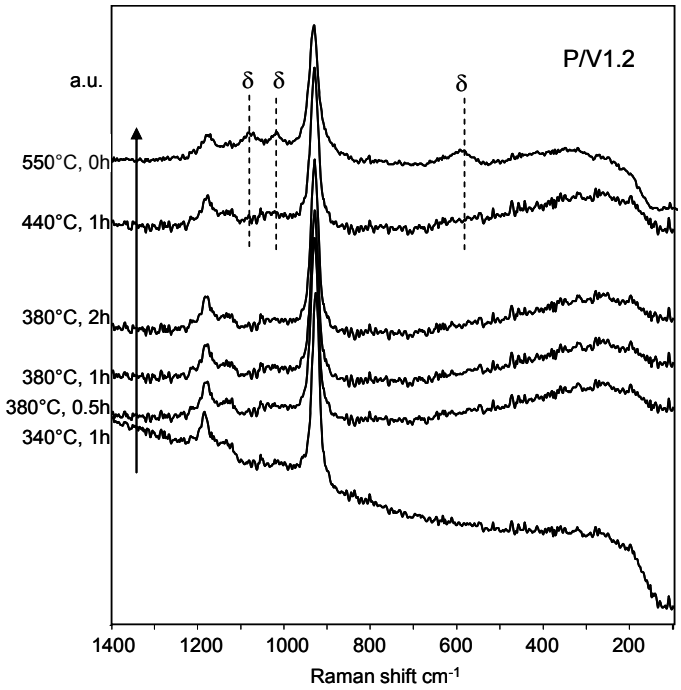

Figure 3.8: Raman spectra recorded *in-situ* in dry air flow at increasing temperature and time-on-stream. Sample: PV1.2. Symbols: δ δ-$VOPO_4$

Figure 3.9 and 3.10 report the evolution of sample PV 1.0 and PV 1.2 under flow of 10% steam in air at 380°C. In both cases, the first spectrum recorded at 380°C showed only the bands attributable to vanadyl pyrophosphate. In the case of PV1.2 (Figure 3.9), after 1 h at 380°C, a new band at Raman shift 1039 cm^{-1} appeared, indicating the formation of a new compound, stable for more than 5 hours under the conditions used. Then, the band at 1039 cm^{-1} disappeared and bands at 1080, 1015, 588 cm^{-1} formed, all attributable to δ-$VOPO_4$. It is worth noting that if steam was removed from the feed, the transformation into δ-$VOPO_4$ was much quicker than in the presence of steam (spectra not reported). Bands of V-O-P stretching in V/P/O compounds are visible in the spectral range between 1000 and 1100 cm^{-1}, and indeed several compounds show Raman bands close to 1040 cm^{-1} [40-42]. However, when the experiment was carried out under flow of either dry air, or dry nitrogen or even wet nitrogen (10% H_2O), no changes of the Raman spectrum were observed; in other words, with PV1.2, at 380°C, VPP only transforms into another compound when a wet and oxidizing environment is used.

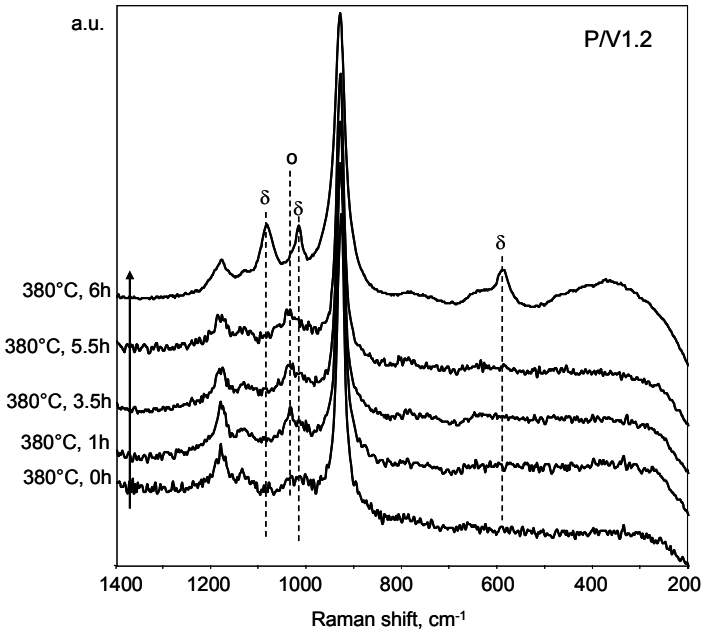

Figure 3.9: Raman spectra recorded *in-situ* at 380°C in flow of wet air (10 % steam). Sample: P/V 1.2. Symbols: δ δ-$VOPO_4$, ○ $VOPO_4 \cdot 2H_2O$

From these experiments, it can be inferred that the band at 1039 cm^{-1} is likely attributable to a V(V) hydrated phosphate. Notably, this band is one of the most intense one in $VOPO_4 \cdot 2H_2O$ (the most intense one being at 950 cm^{-1}, however hardly visible being a shoulder of the P-O stretching band in VPP) [42]. It can be concluded that the latter compound forms by oxidation of VPP in the presence of steam. However, after a few hours, i.e., after the transformation of VPP into $VOPO_4 \cdot 2H_2O$ had likely involved a few atomic layers, the hydrated compound dehydrated into δ-$VOPO_4$. The experiment was repeated from the beginning with equilibrated PV1.2, and the same phenomenon was observed again.

PV1.0 showed a completely different behaviour (Figure 3.10); in fact, this sample was more stable at the conditions used for this experiment. After 8 hours at 380°C in flow of air/steam, yet there was no evidence for the formation of any V(V) phosphate (Figure 3.10 (left)). However, a minor change in spectrum was the development of a weak band at 1020 cm^{-1}; the attribution of this band to any specific V/P/O compound is a difficult task. Raman band close to 1000 cm^{-1} are attributable to the stretching vibration of V=O in V/P/O compounds [40-42]; however, this band is never the most intense one in V/P/O spectra. In bulk vanadium oxides, the band of V=O stretching is at ~1000 cm^{-1}, while in the case of

supported vanadium oxide, especially in monolayer or submonolayer catalysts, this band is shifted towards wavenumbers slightly higher than 1000 cm^{-1}, the exact position being a function of the support type and the eventual presence of water molecules coordinated to the supported species [43-46]. Therefore, the formation of a VO_y compound is likely [6,8]; the presence of water can favour the partial hydrolysis of V-O-P in VPP leading to the formation of isolated or oligomerized VO_y (containing either V(IV) or V(V)) units surrounded by phosphate groups. This hypothesis is supported by evidences provided by Schrader et al [9], who reported that different $VOPO_4$ phases under flow of wet nitrogen finally transform into V_2O_5, and the first evidence for the formation of this new compound is the appearance of two bands at 995 and 1015 cm^{-1}.

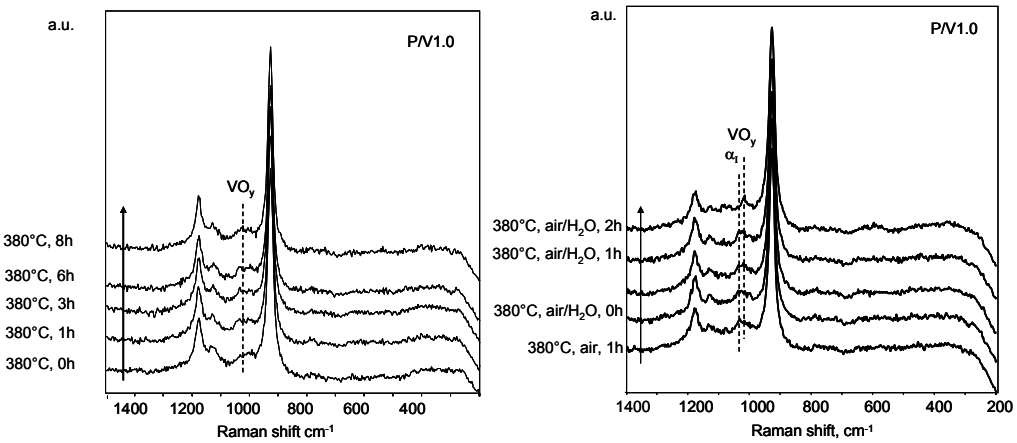

Figure 3.10: Raman spectra recorded *in-situ* at 380°C in flow of wet air (10 % steam). Sample: PV 1.0. Symbols: α_I α_I-$VOPO_4$

In another experiment (Figure 3.10(right)), water (10%) was added to the air flow after the formation of α_I-$VOPO_4$ at 380°C (shown in Figure 3.6). It is shown that in a few hours, α_I-$VOPO_4$ transformed into the [VO_y + $(PO_4)_n$]. This experiment shows that in the presence of steam, at 380°C, the stable compound at the surface of PV1.0 is not V(V) phosphate; at these conditions, both α_I-$VOPO_4$ and VPP are transformed into an hydrolysed, and likely oxidized, layer.

With both samples, at 440°C, in an air/water feed, VPP was quickly oxidized to δ-$VOPO_4$ (Figure 3.11); typical bands of this compound already appeared after 1.5 h, and their intensity increased during the isothermal step at 440°C.

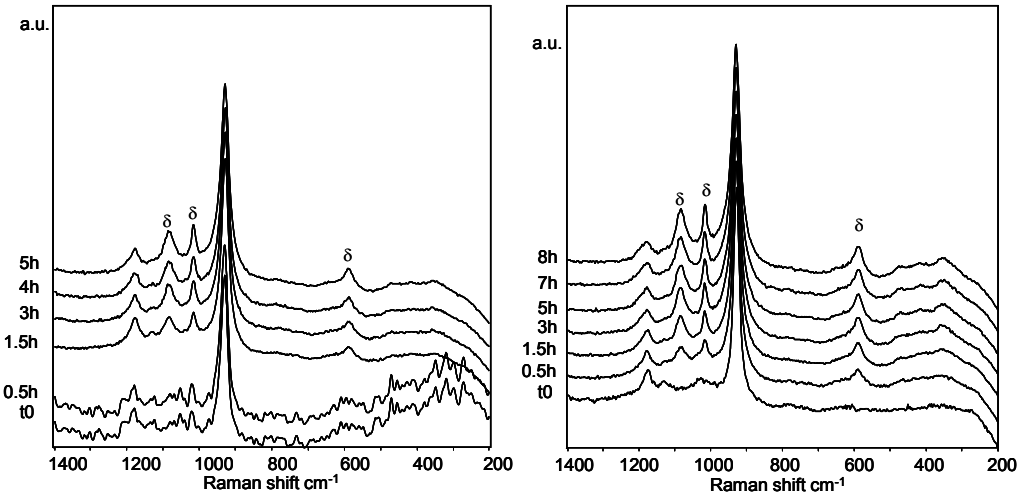

Figure 3.11: Raman spectra recorded *in-situ* at 380°C in a 10 vol% steam in air, at increasing times of exposure to the stream. Samples: PV 1.0 (left), PV1.2(right). Symbols: δ δ-$VOPO_4$

Even when PV1.0 was first oxidized in dry air at 380°C to α_I-$VOPO_4$, then brought to 440°C in air, and finally treated at the latter temperature with air/steam, the compound formed was δ-$VOPO_4$ (spectra not reported). Therefore, at high temperature, the stable compound is the latter one, regardless of the presence of either a dry or wet stream. Similarly, with PV1.2, the formation of δ-$VOPO_4$ at 440°C also occurred in the presence of steam, starting from $VOPO_4 \cdot 2H_2O$ (spectra not reported), the latter having been preformed at 380°C by treatment of VPP in the wet air stream.These tests demonstrate that the presence of steam in an oxidizing environment has a relevant effect on transformations occurring at the VPP surface, leading to different compounds, in function of the catalyst composition. With both samples, however, at high temperature δ-$VOPO_4$ is the preferred compound, regardless of the P/V ratio and the presence of steam. With PV1.0, the treatment with air leads to the direct transformation of VPP into α_I-$VOPO_4$, already at 380°C; on the contrary, VPP in PV1.2 is more stable in an oxidizing environment, and is transformed into δ-$VOPO_4$ only at very high temperature. This agrees with literature findings showing that an excess of P may stabilize the VPP and hinder its oxidation into V(V) phosphates [23]. It is worth noting that experiments carried out with either dry or wet nitrogen streams showed that samples did not undergo any transformation when treated in the absence of oxygen.

Reversibility of transformations

Figures 3.6 and 3.7 showed that in PV1.0, VPP is oxidized to α_I-$VOPO_4$ at 380°C in dry air, but finally transforms into δ-$VOPO_4$ when the temperature is increased to 440°C. When however the temperature was decreased again down to 380°C, δ-$VOPO_4$ transformed back again to α_I-$VOPO_4$ (Figure 3.12).

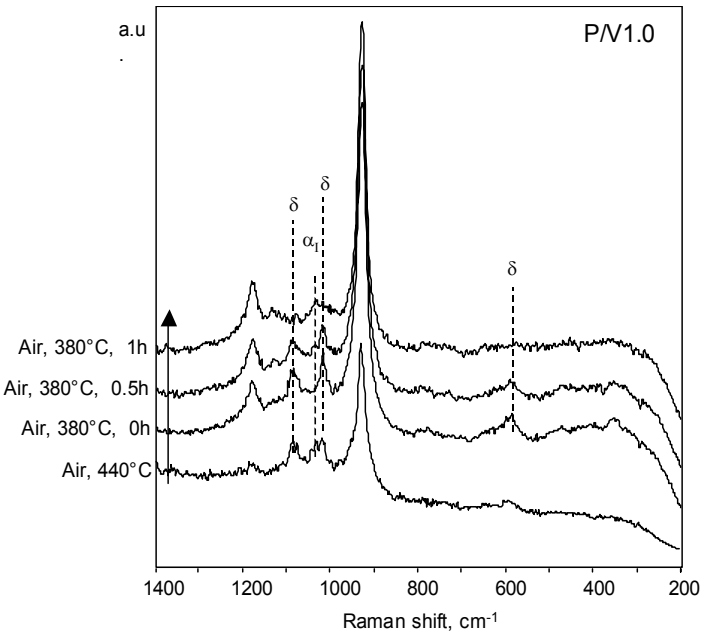

Figure 3.12: Raman spectra recorded *in-situ* by cooling from 440°C to 380°C in dry air. Sample: PV 1.0. Symbols: δ δ-$VOPO_4$, α_I α_I-$VOPO_4$

Therefore, the two V(V) phosphates interconvert, and the nature of the dominant compound is a function of temperature. The same interconversion was observed also in the presence of the wet air stream, with the difference that at 380°C α_I-$VOPO_4$ (formed by transformation of δ-$VOPO_4$) gradually transformed into the $[VO_y + (PO_4)_n]$ layer.

In the case of PV1.2, when the sample was cooled down from 440°C to 380°C in the wet air stream (i.e., starting from conditions at which the stable compound at the surface of VPP is δ-$VOPO_4$), the hydrated phase $VOPO_4 \cdot 2H_2O$ did not reform (Figure 3.13). Therefore, the transformation of $VOPO_4 \cdot 2H_2O$ into δ-$VOPO_4$ is not reversible. This also agrees with spectra reported in Figure 3.9; in fact, experiments at 380°C showed that $VOPO_4 \cdot 2H_2O$ finally transformed into δ-$VOPO_4$ after a prolonged exposure to the wet air flow. Moreover, when the treatment

was carried out by flowing dry air at 380°C, transformation of $VOPO_4 \cdot 2H_2O$ into δ-$VOPO_4$ was quicker than that one occurring in the wet air stream. It can be concluded that $VOPO_4 \cdot 2H_2O$ is not a stable compound, and is dehydrated to δ-$VOPO_4$ at both 380°C and 440°C, even in the presence of steam.

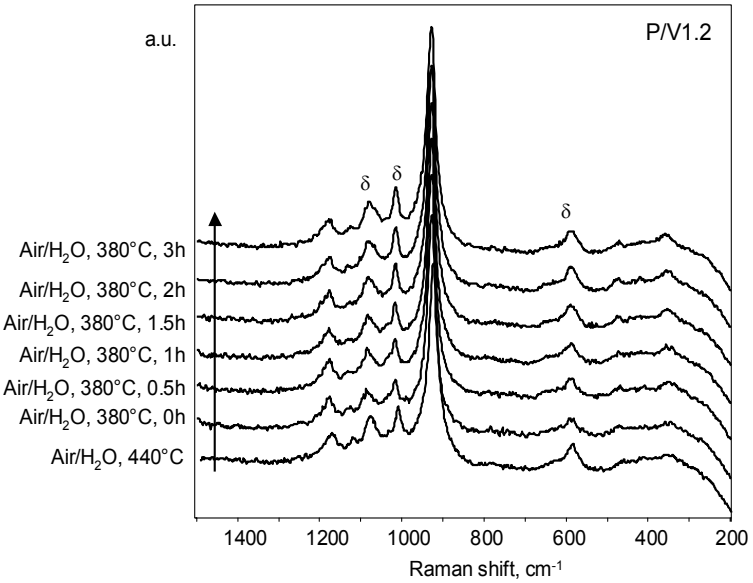

Figure 3.13: Raman spectra recorded *in-situ* by cooling from 440°C to 380°C in wet air (10% steam). Sample: PV 1.2. Symbols: δ δ-$VOPO_4$

Hydration of different $VOPO_4$ phases and their successive dehydration was studied by Volta et al. [40,41] by means of Raman spectroscopy. Hydration was carried out at room temperature submitting pure reference compounds (β, α_I, α_{II}, γ and δ-$VOPO_4$) to a flow of air saturated in water and it was found that, except for β–$VOPO_4$, all $VOPO_4$ phases undergo hydration to form $VOPO_4 \cdot 2H_2O$ more or less rapidly depending on the starting compound. Moreover, it was reported that successive dehydration of $VOPO_4 \cdot 2H_2O$ formed by hydration of α_I, α_{II}, γ and δ-$VOPO_4$, always led to α_I-$VOPO_4$. In our case several tests confirm the dehydration of $VOPO_4 \cdot 2H_2O$ to δ-$VOPO_4$. This difference is likely due to a different composition of our catalysts. Once more, P/V ratio seems to play a fundamental role; not only a slight excess of P with respect to the stoichiometric P/V ratio 1.0 was necessary for the formation of $VOPO_4 \cdot 2H_2O$ but also had an effect on its successive evolution, leading to dehydration to a different compound.

Finally, sample PV1.2 was first treated in air at increasing temperature until δ-$VOPO_4$ formed, the sample was then cooled in nitrogen from 550°C down to room temperature, and spectra were recorded during cooling (Figure 3.14); the bands relative to δ-$VOPO_4$ gradually disappeared, and finally the Raman spectrum was the same as that one of the starting sample (which did not contain δ-$VOPO_4$). This suggests that an equilibrium develops between VPP and δ-$VOPO_4$, and that the latter compound, formed at high temperature, is not stable and self-reduces spontaneously when the temperature is decreased under nitrogen stream.

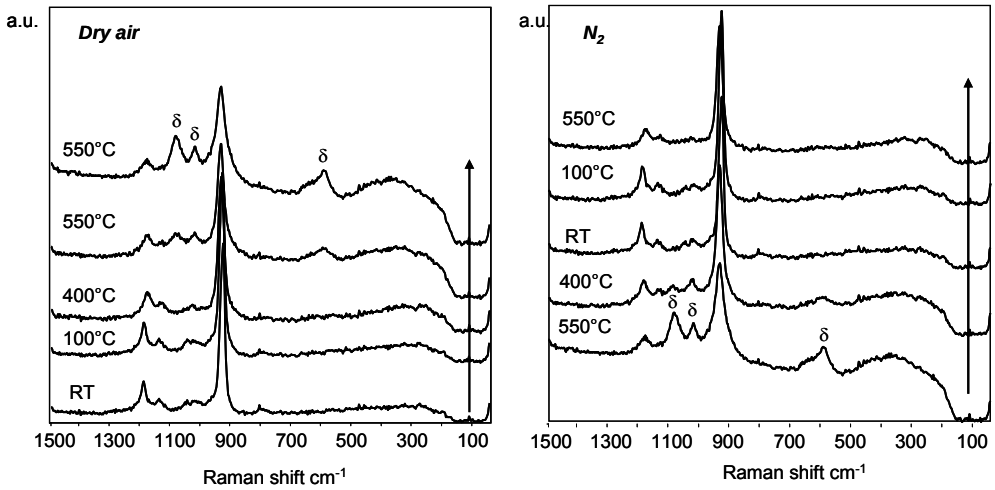

Figure 3.14: Raman spectra recorded *in-situ* heating up to 550°C under flow of air (left), and then changing temperature under flow of nitrogen. Sample: PV 1.2. Symbols: δ δ-$VOPO_4$

In-situ Raman experiments show that:

a) With PV1.2, the VPP is stable; it is not oxidized by air at mild temperature, and it transforms into δ-$VOPO_4$ only at T > 500°C. However, in the presence of steam, VPP transforms into δ-$VOPO_4$ at both 380°C and 440°C, through the intermediate formation of $VOPO_4 \cdot 2H_2O$. Therefore, δ-$VOPO_4$ is the stable V phosphate that forms at the surface of VPP over the entire range of temperature, from 380 to 550°C, under an atmosphere containing both oxygen and steam.

b) With PV1.0, VPP is more easily oxidizable, and even at 380°C it transforms into α_I-$VOPO_4$, that however readily converts into VO_y + $(PO_4)_n$ in the presence of steam; the latter is directly obtained from VPP at 380°C by heating it the presence of both oxygen and steam. At 440°C, the stable compound, both in the presence and in the absence of steam, is δ-$VOPO_4$.

Remarkably, if the temperature is lowered again from 440 down to 380°C, and steam is removed, δ-$VOPO_4$ gives back α_I-$VOPO_4$.

3.3.4 Steady state reactivity

Figure 3.15 shows the catalytic performance at steady state of equilibrated catalysts.

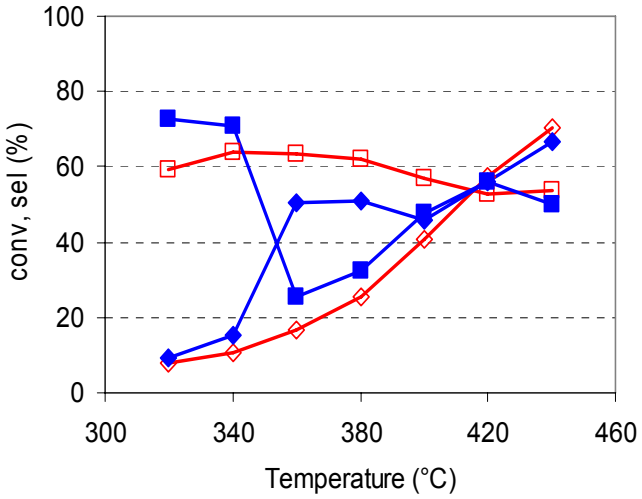

Figure 3.15: *n*-Butane conversion (◆◇) and selectivity to MA (■ □) as functions of temperature, for PV1.0 (full symbols) and PV1.2 (open symbols).

The two samples gave quite different behaviours. PV1.2 showed the expected increase of *n*-butane conversion when the reaction temperature was increased, and a slight decline of selectivity to MA. PV1.0 showed instead an anomalous behavior; in fact, the conversion rapidly increased in the 340-to-360°C temperature range, then remained approximately constant (~ 50%) up to 400°C, and finally increased again. Correspondingly, the selectivity to MA showed a dramatic fall at 340°C, reaching a minimum value of 27% at 360°C, and then increased again up to 68%, the maximum value being obtained at 440°C.The following considerations are worth of mention:

a) This behavior was totally reproduced when the temperature of reaction was increased and then decreased several times; in other words, the observed phenomena were not due to some effect attributable to irreversible changes of catalyst characteristics.

b) The two samples showed very similar performance in the temperature ranges of 320-340°C and 400-440°C, but they gave quite different performance in the intermediate temperature range, 340-400°C.
c) The fall of selectivity to MA shown by PV1.0 at above 340°C was not simply due to the anomalous raise of conversion. In fact, it has to be noted that a selectivity of 25% is too low to be solely attributed to the enhanced contribution of consecutive combustions.

All these evidences suggest that the behavior of PV1.0 is related to a modification of the surface characteristics under reaction conditions; in the intermediate temperature range, a very active but poorly selective active layer develops, different from that one forming at either low or high temperature (selective and moderately active), and also different from that one that develops with PV1.2 in the intermediate temperature range. On the other hand, the active layers of the two catalysts are likely similar, or at least offer similar performance, in the low-T and high-T intervals.
In order to confirm this hypothesis, reactivity tests under non-steady-state conditions were carried out.

3.3.5 Non-steady-state reactivity tests

Two kinds of tests were performed in order to investigate the response of samples to the application of conditions different from those which the catalyst underwent under reaction. Specifically, the reaction temperature was varied in He flow with the aim to observe how the active surface stable in specific conditions adapts itself to the new situation. If no changes of catalytic performances were notice it can be concluded that the active layer had not undergone modifications; in other words the active surface stable at the temperatures studied was likely the same. Moreover, specific treatment of oxidation and/or hydrolysis were applied and reactivity during the transition of catalyst from the forced situation to the stable active surface was followed.

Figure 3.16 shows the results of reactivity tests carried out with PV1.0 (left) and PV1.2 (right), obtained in response to modifications of the reaction temperature. The reaction was first carried out at 440°C; then the reaction stream was interrupted, and the catalyst was cooled down to 380°C in helium flow; finally, the

reaction stream was fed again. It is reported the conversion of *n*-butane and the selectivity to the main products, MA and CO_2, as functions of time-on-stream after the start-up of the reaction feed. This test was aimed at checking whether the active layer that develops in the reaction environment at 440°C is the same that develops at 380°C; if the active layer is the same, and no major changes occur in its characteristics when the reaction temperature is changed, the catalyst should show no change of catalytic performance when the reaction is started again at 380°C. If, instead, the active layer at the two temperatures is not the same, the active layer that had formerly developed at 440°C is modified when the feed stream is fed again at 380°C; in fact, a new composition for the active layer develops, in equilibrium with the gas phase at those specific conditions. Therefore, a progressive change of reactivity is expected in concomitance with the shift from the former active layer to the new one.

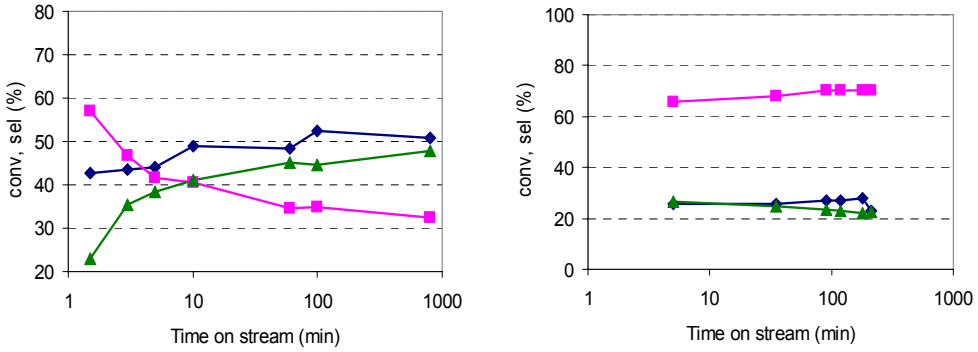

Figure 3.16: Conversion of *n*-butane (◆), selectivity to MA (■), and CO_x (▲), as a function of time-on-stream at 380°C after (i) reaction at 440°C, (ii) cooling in He down to 380°C, and (iii) feed of the reaction stream again. PV1.0 (left), PV1.2 (right).

Figure 3.16 shows that indeed this was the case for catalyst PV1.0. The catalyst took several hours to reach the new steady performance after the start-up of the reaction feed at 380°C. This means that the active layer that develops in the reaction environment at 380°C is different from that one formerly formed at 440°C, and that the latter is intrinsically less active but remarkably more selective than the former one. The opposite was shown when the reverse operation was done, i.e., increase of temperature in helium from 380 to 440°C, and start of the feed again. These results confirm that the behaviour shown in Figure 3.15 was due to the change of the active layer characteristics in the reaction environment that occurred when the reaction temperature was changed. Worth of mention, the

time needed to reach the steady performance, a few hours, is compatible with changes recorded by means of in-situ Raman experiments.
On the opposite, in the case of PV1.2 the catalytic performance showed only minor changes when the temperature was changed; this indicates that for this catalyst the nature of the active layer is similar at 380 and 440°C.

Changes in the stable active surface were induced by applying either oxidizing treatments (feed of dry air), or hydrolyzing treatments (feed of 4% steam in He), or both. Then, the reaction mixture was fed again, and variations of catalytic performance that occurred along with time-on-stream were followed during the transition of catalyst from the forced situation to the stable active surface under those conditions (steady-state). In most cases, variations were slow enough to be followed along reasonable periods of time, e.g., ranging from a few minutes to 10 hours. When the treatment induced no variation in catalytic performance, it is possible to assume that either the active surface was stable towards that treatment, or that it was insensitive to it, because it was already in the state we were meant to induce by that specific treatment.
Figure 3.17 compares the unsteady performance of the two equilibrated catalysts after a treatment with air at 380°C for 1 hour.

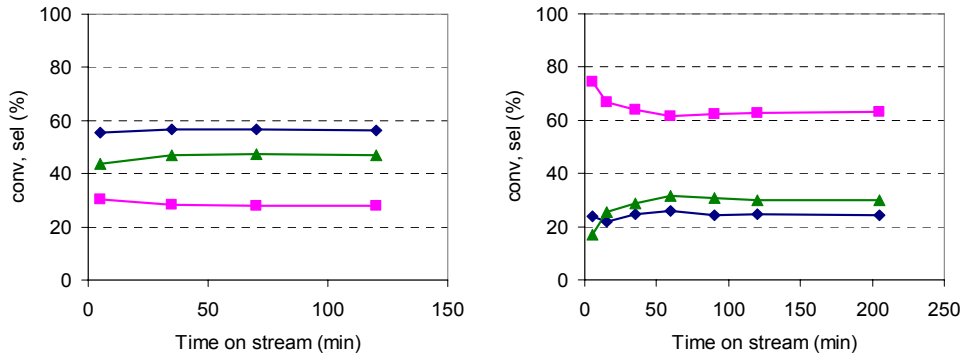

Figure 3.17: Conversion of *n*-butane (◆), selectivity to MA (■), and CO_x (▲), as a function of time-on-stream at 380°C after (i) reaction at 380°C, (ii) feed of air at 380°C for 1h, (iii) feed of the reaction stream again. PV1.0 (left), PV1.2 (right).

Dry air was used for the experiments; therefore, with respect to reaction conditions, during the treatment catalysts were submitted not only to a more oxidizing atmosphere (no butane was fed), but also to a less hydrolyzing stream

(no water was co-produced). This means that if changes of catalytic performances after treatment were observed, they could derive either to oxidation or dehydration of catalytic surface.

It is shown that the response of the two catalysts was quite different. At 380°C, catalyst PV 1.0 did not show any change of catalytic performance after the treatment with air (Figure 3.17 left); a few minutes after feeding of rthe eaction mixture, both *n*-butane conversion and selectivity to maleic anhydride were already typical of steady-state conditions (see Figure 3.15). On the contrary, the treatment with dry air modified the characteristics of catalyst PV 1.2. After the oxidizing treatment the catalyst was slightly less active but clearly more selective than it was before. Then, it took around 1 hour to restore the original steady state performance. This means that the treatment in air did not modify the catalytically active surface of the equilibrated catalyst PV 1.0, whereas it did alter the surface of the catalyst PV 1.2. It can be inferred that PV 1.0 was already in an oxidized and/or dehydrated state during reaction, or that it was insensitive to the treatment. On the opposite, the catalyst PV 1.2 was not stable under oxidizing condition. This could means that: (i) the active surface stable under reaction conditions is not completely oxidized, or (ii) it is partially hydrated and treatment with dry air causes its dehydration. Anyway, the ac tive surface stable at 380°Cwas less selective to MA and almost as active as the surface developing soon after treatment with air.

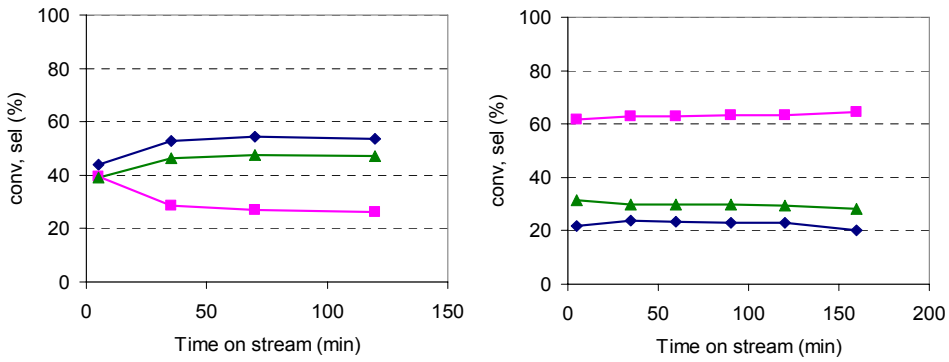

Figure 3.18: Conversion of *n*-butane (◆), selectivity to MA (■), and CO_x (▲), as a function of time-on-stream at 380°C after (i) reaction at 380°C, (ii) feed of 4% steam in He at 380°C for 1h, (iii) feed of the reaction stream again. PV1.0 (left), PV1.2 (right).

After the treatment of the two catalysts in the steam-containing stream, at 380°C (Figure 3.18), the sample PV 1.2 did not show any change of catalytic performance, whereas in the case of PV 1.0 the treatment rendered the catalyst less active but more selective than the sample equilibrated in the reactive atmosphere at 380°C. This means that with PV 1.0 the active layer is not fully hydrated under reaction conditions, and that a hydrolyzed surface is more selective than the active surface of the equilibrated PV 1.0 catalyst. On the contrary, the active surface of catalyst PV 1.2 was fully stable towards hydrolysis; this could mean that it is already hydrolyzed under reaction conditions, or the active layer is totally stable also in presence of water.

Both oxidizing and hydrolyzing treatments were performed also at 440°C. Figure 3.19 reports the unsteady performances of the two samples after exposure to dry air for 1 hour.

Samples showed a similar behaviour; no remarkable variations of catalytic performances were noticed after the air feed, to indicate this kind of treatment did not modify the surface layer of the catalysts. Therefore, regardless to P/V ratio of the catalysts, the active layer which develops in reaction mixture at 440°C was stable toward further oxidation.

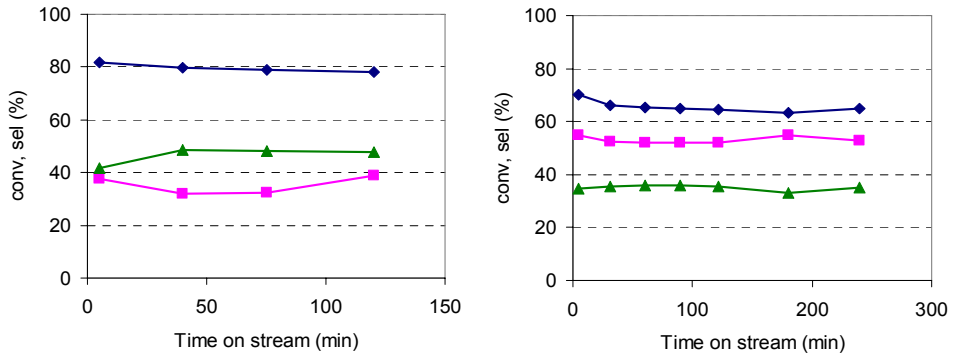

Figure 3.19: Conversion of *n*-butane (◆), selectivity to MA (■), and CO_2 (▲), as a function of time-on-stream at 440°C after (i) reaction at 440°C, (ii) feed of air at 440°C for 1h, (iii) feed of the reaction stream again. PV1.0 (left), PV1.2 (right).

Finally, in Figure 3.20 the response of the two samples to an hydrolyzing treatment at 440°C was reported. Also in this case samples responded similarly to the application of the treatment. The catalytic performances of catalysts did not undergo relevant changes after exposure to a flow of helium enriched with 4% of

steam. This suggests that the active layer present in reaction mixture at this temperature was stable to further hydration at 440°C.

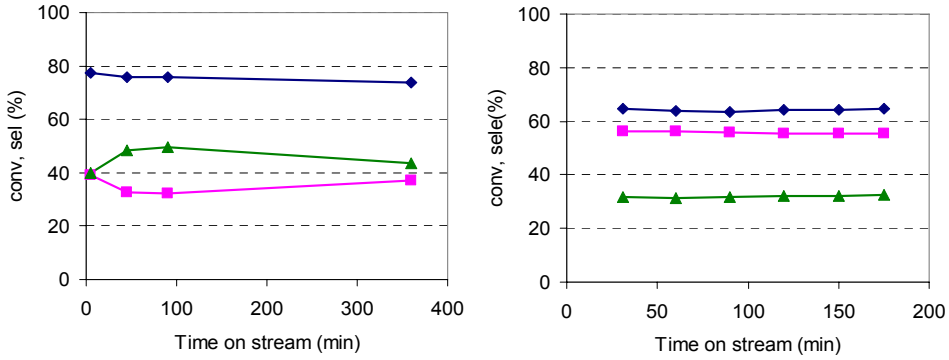

Figure 3.20: Conversion of *n*-butane (◆), selectivity to MA (■), and CO_x (▲), as a function of time-on-stream at 440°C after (i) reaction at 440°C, (ii) feed of 4% steam in He at 440°C for 1h, (iii) feed of the reaction stream again. PV1.0 (left), PV1.2 (right).

Catalytic tests demonstrated that:

1. at high temperature the active layers of the two catalysts are similar. The surface was quite stable under conditions different from the reaction ones, being insensitive to modifications induced varying the oxidizing/hydrolyzing strength of the gas-phase it is in contact with. At temperature higher than 400°C also the catalytic performances of samples were similar; the surface active layer which develops in these conditions is intrinsically both active and selective.
2. At temperature below 400°C, depending on P/V ratio, two different active layers develop:
   (i) if catalyst was prepared having P/V ratio close to 1.0 a very active but poorly selective active layer develops. This surface was sensitive to hydrolyzing treatment, by exposure to a steam containing stream a remarkable improvement of selectivity to MA can be obtained. On the contrary, oxidizing treatment did not modify catalytic performances. The active layer of the catalyst is likely in its higher oxidation state but it is not fully hydrolyzed.
   (ii) For samples having excess of P the active layer at 380°C was more similar to that one present at 440°C for both samples. Conversion of *n*-butane was lower than case (i) but MA selectivity still

maintained high values. Then, the phase constituting the surface layer is clearly less active but much more selective than the oxidized surface present in the sample having P/V close to 1.0. It was insensitive to hydrolyzing treatment, therefore it is probably partially hydrated, while forcing the dehydration by feeding dry air, selectivity to MA can be further improved.

3.3.6 Relationships between catalytic tests and in-situ Raman characterization

Reaction conditions are obviously different from those used for Raman experiments. In fact for Raman studies a flow of 10% steam in air was used; this means that the catalyst was submitted to a strong oxidizing and hydrolyzing environment. Also *n*-butane oxidation reaction is carried out with large excess of oxygen, and water was always present in the reaction atmosphere being a co-product of the reaction. The amount of water depends on the reaction temperature (that means on butane conversion) and on distribution of products but usually it is not higher than 5%. Moreover, the presence of butane and of oxidation products makes the reaction atmosphere on average less oxidant with respect to that used for Raman analysis. Nevertheless, comparing the results of in-situ Raman characterization and reactivity tests, a picture of the different active layers formed by VPP as a function of P/V ratio and reaction conditions can be drawn. Besides, also a few considerations about the intrinsic catalytic properties of each different surface can be inferred.

Both Raman characterization and reactivity tests demonstrated that regardless to P/V ratio, at high temperature samples develop the same active layer, which is active and selective to MA. In these conditions, the oxidation of VPP to δ-$VOPO_4$ is favoured; this compound is stable towards further modifications, also under conditions more oxidizing and hydrolyzing than the reaction mixture.

At 380°C different active layers form, depending on P/V ratio:

(i) P/V close to 1.0: a very active but not selective compound develops on the catalyst surface. This surface is stable to oxidation but an hydrolyzing treatment slightly improves its catalytic performances. In these conditions, if water content in gas phase is lower than 10% the catalyst surface is constituted by α_I-$VOPO_4$; increasing the amount of

steam, V-O-P bonds become weak and begin to be hydrolyzed to [VO_y + $(PO_4)_n$] which is slightly more selective to MA.

(ii) P/V>1.0: surface layer is similar to the active surface which is stable at 440°C and is clearly less active but much more selective than the compound formed at 380°C in the case (i). For this sample VPP was oxidized at first to $VOPO_4 \cdot 2H_2O$, and then to δ-$VOPO_4$; the dehydration of $VOPO_4 \cdot 2H_2O$ can be accelerate by exposing the catalyst to a flow of dry air. In this way also a slight improvement of MA selectivity can be obtained. Once δ-$VOPO_4$ was formed, no re-hydration to $VOPO_4 \cdot 2H_2O$ was possible.

The role of the excess of P is to improve selectivity to MA by favouring the formation of δ-$VOPO_4$ under reaction mixture already at 380°C and avoiding further transformations of this compound. If P/V ratio is close to 1.0, δ-$VOPO_4$ forms only at 440°C; at lower temperature the latter gradually transforms to α_I-$VOPO_4$ or [VO_y + $(PO_4)_n$], both compounds are poorly selective to MA.

3.3.7 *"In-situ"* modification of P/V ratio

Catalytic tests and Raman experiments highlight the importance of the P/V ratio in V/P/O catalysts, and indicate that small differences of this parameter may have profound effects on reactivity. In order to confirm the role of P, tests aimed to the *in-situ* removal of P from the catalyst surface, and then aimed to reintegrate the P formerly removed, were carried out. The catalytic performance of the sample was checked after P removal and reintegration.

Removal of P

In-situ removal of P was carried out applying an hydrolysis treatment, followed by feed of compounds able to form volatile phosphoric acid esters ("esterification"). The idea was to increase the "hydrolysis degree" of the surface feeding a relative high amount of water, breaking V-O-P bonds and so forcing the formation of P-OH groups in phosphate species. Subsequently, ethanol was fed to form ethylic esters of phosphoric acid; these compounds have a low boiling point (T_{eb} = 215 °C) and therefore are volatile at reaction temperature.

The procedure was the following:

1. equilibration in mixture of *n*-butane and air at 440°C for a few hours;

2. interruption of reagents stream and feeding of a flow constituted by 3 mol.% steam in He for 2 hours (hydrolysis);
3. cooling down to 380°C under He flow;
4. feeding of a mixture of 0.8 mol.% of ethanol in He for 1 hour (esterification).

The esterification treatment was carried out at lower temperature compared to the hydrolysis, i.e. 380°C, to avoid ethanol oxidation. Although no molecular oxygen was present in the feed stream, VPP could act as an oxidant toward the alcohol preventing the reaction with P-OH groups. In fact, it is known that the catalyst is able, according Mars-Van Krevelen mechanism, to give lattice oxygen atoms to organic substrate, reducing itself. However, analysis of the outlet stream during the esterification treatment at 380°C excluded the formation of CO_x by ethanol oxidation.

After esterification, butane/air mixture was fed again and catalytic tests were performed. Figure 3.21 compares the catalytic performance of the sample before and after the treatment of removal of phosphorus.

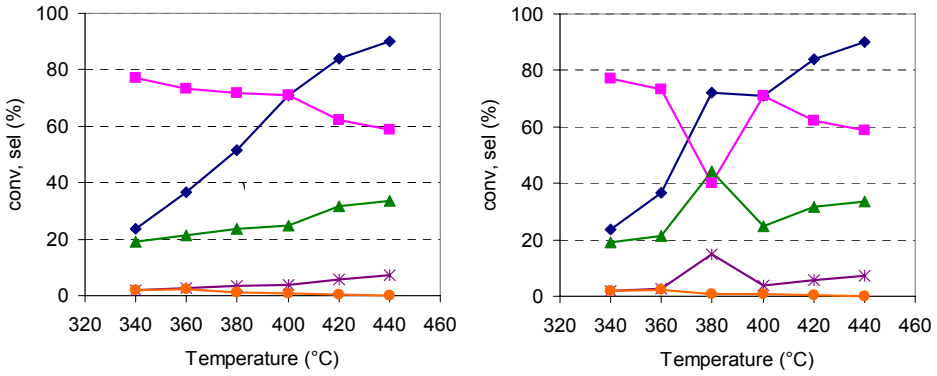

Figure 3.21: Conversion of *n*-butane (◆) and selectivity to maleic anhydride (■), $CO+CO_2$ (▲), formaldehyde (✳) and acetic acid+acrylic acid (●) as a function of temperature. Catalyst: PV 1.2., feed composition: 1.7% butane, 17% O_2. left: before esterification, right: after esterification.

It was found that the catalytic performances at low temperature and at temperature higher than 400°C were not affected by the treatment. On the contrary, at 380°C the selectivity to maleic anhydride fell down and *n*-butane conversion rapidly increased. This behaviour is clearly similar to the trends of conversion and MA selectivity obtained for the samples prepared with P/V ratio close to the stoichiometric 1.0 and suggested the decrease of P/V ratio due to

"esterification". To confirm the loss of surface phosphorus, after treatment of hydrolysis+esterification the sample was cooled down and SEM-EDX analysis were performed. Actually, P/V atomic ratio after the treatment was lower than the original one, to confirm the effective removal of part of P in excess as a consequence of esterification (P/V=1.14 vs P/V=1.24 for the sample before treatment). It is important to point out how a minimal variation of P/V surface ratio greatly affect the catalytic performances of the sample at intermediate temperatures. At 380°C, owing to treatment, the conversion increased of about 10%. Even more relevant was the effect of the treatment on MA selectivity that decreases of more than 25 point pre cent, while selectivity to CO_x increases of about 15%.

Restoring of P

Then it was tried to reintegrate the phosphorus previously removed, feeding a P-containing compound. The procedure was similar to the hydrolysis and esterification treatments:

1. equilibration in mixture of *n*-butane and air at 380°C;
2. interruption of reagents stream and feeding of a flow of P-containing organic compound in He for 20 minutes;
3. reaction mixture feed;
4. interruption of reagents stream and feeding of a flow of P-containing organic compound in He for 40 minutes;
5. reaction mixture feed;
6. etc..

Tests were performed at 380°C, exactly in the range in which the minimal selectivity to MA was observed. Figure 3.22 shows the trends of *n*-butane conversion and MA selectivity as a function of time of P treatment. Already after 20 minutes of P feed, the catalytic performance at 380°C improved; *n*-butane conversion slightly decreased and a recovery of MA selectivity of 7% was observed. After the second treatment, a further improvement can be noticed, although MA selectivity was still lower than that of the fresh sample.

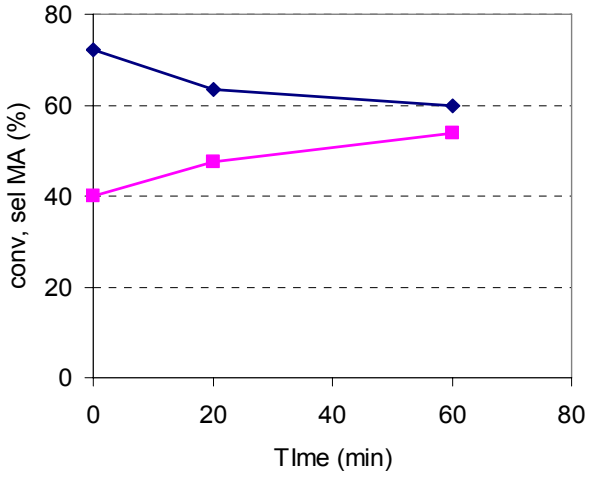

Figure 3.22: Conversion of *n*-butane (◆) and selectivity to maleic anhydride (■) as a function of time of exposure to P-containing compound. T=380°C, feed composition: 1.7% butane, 17% O_2. Catalyst: PV 1.2.

Tests suggested a gradual enrichment of P previously removed and consequently an improvement of the catalytic properties at "critical temperature", that is in condition in which the amount of P on the catalyst surface resulted a key parameter to avoid the formation of α_I-$VOPO_4$ and ensure high selectivity to MA. Also in this case SEM-EDX confirmed an increase of P/V ratio with respect to sample after the P removal treatment (P/V=1.28 vs P/V=1.14 for the sample after P removal treatment). Therefore, it was possible to modify in reversible way the P/V surface ratio, that means adjust it in order to control the catalytic properties and ensure good performances in terms of MA selectivity. Nevertheless, due to the extremely sensitive nature of VPP, a complete recovery of the P content is difficult to achieve and the feed of the P compound may be the reason for structural changes; in fact when the catalyst was submitted to prolonged exposure to the P-containing flow, it underwent irreversible modifications, with clear worsening of the catalytic properties in terms of both activity and MA selectivity.

3.4 CONCLUSIONS

The surface dynamic of VPO catalyst was investigate by means of in-situ Raman spectroscopy and reactivity tests. In particular, the effect of P/V atomic ratio on

the transformations that vanadyl pyrophosphate undergoes during reaction was studied. VPP showed to be a complex system, very sensitive to slight changes of catalyst composition and operative conditions. P/V ratio greatly affects the catalytic performance at intermediate reaction temperature (380°C). The phenomenon is due to reversible changes of the active layer under reaction mixture as a function of temperature and gas-phase composition, so that was necessary to study them by means of in-situ techniques. Figure 3.23 reports a scheme of transformations of VPP, as inferred by *in-situ* Raman experiments at 380 and 440°C.

The main difference between the two samples concerns the nature of the compound forming at the surface of VPP at 380°C, in the presence of air and steam. With PV1.0, the compound formed is α_I-$VOPO_4$, eventually hydrolyzed to [VO_y + $(PO_4)_n$]. With PV1.2, the stable compound on the VPP surface at 380°C is δ-$VOPO_4$. At high temperature, however, the two samples behave similarly, and the compound formed is δ-$VOPO_4$, by surface oxidation of VPP.

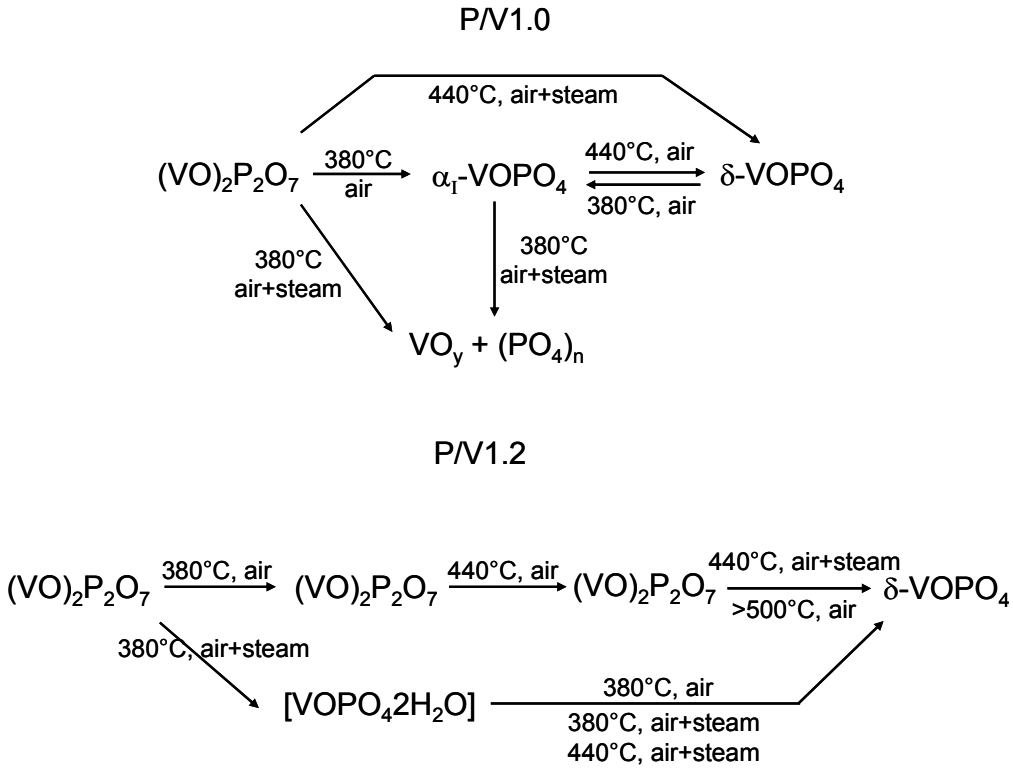

Figure 3.23: Scheme of transformations involving VPP as function of temperature and gas-phase composition. Samples: PV1.0 (top), PV1.2 (bottom).

Reactivity tests showed that the best catalytic performances were obtained when the surface layer contains δ-$VOPO_4$. For the catalyst having a slight excess of P, the oxidation to δ-$VOPO_4$ occurs at lower temperature and this ensure good catalytic performances in all the range of temperatures investigated. On the contrary, for samples prepared with stoichiometric P/V ratio, the formation of α_I-$VOPO_4$ or $[VO_y + (PO_4)_n]$ at intermediate temperature is responsible for the lower selectivity to MA. Therefore the excess of P favours the formation of δ-$VOPO_4$ and improves its stability under reaction mixture, ensuring high selectivity to MA.
For catalysts having low P/V ratio, improvements of the catalytic properties can be achieved increasing the P/V surface ratio with appropriate treatments. Nevertheless, due to the extremely sensitive nature of VPP, a proper control of each parameter is fundamental for obtain an active and selective catalyst.

3.5 REFERENCES

[1] I.E. Wachs, J.M. Jehng, G. Deo, B.M. Weckhuysen, V.V. Guliants and J.B. Benziger, Catal. Today 32 (1996) 47

[2] G. Koyano, T. Okuhara and M. Misono, J. Am. Chem. Soc. 120 (1998) 767

[3] F. Richter, H. Papp, T. Gotze, G.U. Wolf and B. Kubias, Surf. Interf. Anal. 26 (1998) 736

[4] P. Delichere, K.E. Bere, M. Abon, Appl. Catal A 172 (1998) 295

[5] L.M. Cornaglia and E.A. Lombardo, Appl. Catal A 127 (1995) 125

[6] H. Bluhm, M. Hävecker, E. Kleimenov, A. Knop-Gericke, A. Liskowski, R. Schlögl, D.S. Su, Topics Catal. 23 (2003) 99

[7] M. Hävecker, A. Knop-Gericke, H. Bluhm, E. Kleimenov, R.W. Mayer, M. Fait, R. Schlögl, Appl. Surf. Sci. 230 (2004) 272

[8] M. Hävecker, R.W. Mayer, A. Knop-Gericke, H. Bluhm, E. Kleimenov, A. Liskowski, D.S. Su, R. Follath, F.G. Requejo, D.F. Ogletree, M. Salmeron, J.A. Lopez-Sanchez, J.K. Bartley, G.J. Hutchings, R. Schlögl, J. Phys. Chem. B 107 (2003) 4587

[9] Z.Y. Xue, G.L. Schrader, J. Phys. Chem. B 103 (1999) 9459

[10] V.V. Guliants, S.A. Holmes, J.B. Benziger, P. Heaney, D. Yates, I.E. Wachs, J. Mol. Catal. 172 (2001) 265

[11] E. Bordes, C.R. Acad. Sci. Paris, Série IIc 3 (2000) 725

[12] E. Bordes, Topics Catal. 15 (2001) 131.

[13] P. Arpentinier, F. Cavani and F. Trifirò, The Technology of Catalytic Oxidations (Editions Technip, Paris, 2001)

[14] G. Centi, F. Cavani and F. Trifirò, Selective Oxidation by Heterogeneous Catalysis (Kluwer Academic/Plenum Publishers, New York, 2001)

[15] F. Cavani and F. Trifirò, Catalysis 11 (1994) 246

[16] J.C. Vedrine, Topics Catal. 11 (2000) 147

[17] J.C. Volta, Catal. Today 32 (1996) 29

[18] H. Berndt, K. Buker, A. Martin, A. Brückner and B. Lücke, J. Chem. Soc., Faraday Trans. 91 (1995) 725

[19] A. Brückner, A. Martin, N. Steinfeldt, G.U. Wolf and B. Lücke, J. Chem. Soc., Faraday Trans. 92 (1996) 4257

[20] A. Brückner, B. Kubias and B. Lücke, Catal. Today 32 (1996) 215

[21] M. Ruitenbeck, A.J. van Dillen, A. Barbon, E.E. van Fassen, D.C. Koningsberger and J.W. Geus, Catal. Lett. 55 (1998) 133

[22] A. Brückner, A. Martin, B. Kubias and B. Lücke, J. Chem. Soc., Faraday Trans. 94 (1998) 2221

[23] F. Cavani and F. Trifirò, Chemtech 24 (1994) 18

[24] J. Ziolkowski, E. Bordes and P. Courtine, J. Catal. 122 (1990) 126

[25] J. Ziolkowski and E. Bordes, J. Mol. Catal. 84 (1993) 307

[26] P.A. Agaskar, L. DeCaul and R.K. Grasselli, Catal. Lett. 23 (1994) 339

[27] R. Ebner and M.R. Thompson, Catal. Today 16 (1993) 51

[28] V.V. Guliants, J.B. Benziger, S. Sundaresan, N. Yao and I.E. Wachs, Catal. Lett. 32 (1995) 379

[29] V.V. Guliants, J.B. Benziger, S. Sundaresan, I.E. Wachs, J.M. Jehng and J.E. Roberts, Catal. Today 28 (1996) 275

[30] G. Koyano, T. Saito and M. Misono, J. Mol. Catal. A 155 (2000) 31

[31] G. Centi, F. Trifirò, J. R. Ebner and J. M. Franchetti, Chem. Rev., 88 (1988) 55

[32] G. Centi, Catal. Today, 1 (1993) 5

[33] N. Harrouch Batis, H. Batis, A. Ghorbel, J. C. Vedrine and J. C. Volta, J. Catal. 128 (1991) 248

[34] L. M. Cornaglia, C: Caspani and E. A. Lombardo, Appl. Catal. 74 (1991) 15

[35] T. P. Moser and G. L. Schrader, J. Catal. 104 (1987) 99

[36] G. W. Coulston, E. A. Thompson and N. Herron, Journal of Catalysis 163 (1996) 122

[37] E. Bordes and P. Courtine, J. Catal. 57 (1979) 236

[38] C. Cabello, F. Cavani, S. Ligi, F. Trifirò, Stud. Surf. Sci. Catal. 119 (1998) 925

[39] S. Albonetti, F. Cavani, F. Trifirò, P. Venturoli, G. Calestani, M. López Granados, J. L. G. Fierro, J. Catal. 160 (1996) 52

[40] F. Ben Abdelouahab, R. Olier, N. Guilhaume, F. Lefebvre, J. C. Volta, J. Catal. 134 (1992) 151

[41] F. Ben Abdelouahab, R. Olier, N. Guilhaume, F. Lefebvre, J. C. Volta, J. Catal. 148 (1994) 334

[42] V.V. Guliants, J.B. Benziger, S. Sundaresan, I.E. Wachs, J.M. Jehng, J.E. Roberts, Catal. Today 28 (1996) 275-295

[43] M. Bañares and I.E. Wachs, J. Raman Spectrosc. 33 (2002) 359

[44] I.E. Wachs, Catal. Today 27 (1996) 437

[45] G. Deo and I.E. Wachs, J. Catal. 129 (1991) 307

[46] G. Deo and I.E. Wachs, J. Catal. 146 (1994) 323

4

ZrO_2-SUPPORTED V/P/O CATALYSTS

4.1 INTRODUCTION

A great variety of V/P/O compounds exist which differ in the oxidation state of vanadium, the degree of phosphate groups condensation and the content of water molecules. It is known that the transformation of a compound into another one can be induced by means of thermal treatments. The atmosphere at which the treatment is carried out is a powerful tool for the control of such transformations [1,2]. The most well known V/P/O system is vanadyl pyrophosphate (VPP), the catalyst for *n*-butane oxidation [3]. Because of the tendency of these compounds to undergo changes as a consequence of slight variations of temperature or composition of the atmosphere of calcination, great attention has been given in the past to the study of modifications occurring during the thermal treatment of $VOHPO_4 \cdot 0.5H_2O$ (the precursor of VPP) [4,5] and of possible changes the VPP may undergo under reaction conditions [6,9]. As described in the previous section, the surface composition of VPP catalysts is affected by the reaction conditions [10] and during reaction a *dynamic equilibrium* is established at the catalyst surface between various V/P/O compounds. Therefore, under reaction conditions, catalyst could be seen as a core of VPP covered by a layer of the real active phase, a system quite similar to a supported catalyst.

In this section, I report about the attempt to build-up a V/P/O active layer on the surface of a zirconia support by thermal treatment of a precursor obtained by impregnation of a V^{5+} salt and of H_3PO_4. Raman spectra, recorded in-situ during

the thermal treatment, and reactivity measurements were used to characterize the catalyst surface, with the aim of finding the parameters that may influence the generation of the active phase.

4.2 EXPERIMENTAL

Catalysts were prepared by the wet impregnation technique using NH_4VO_3 and H_3PO_4 (85 wt%). As support monoclinic ZrO_2 (s.s.a. 14 m^2/g) was used. Precursor of the final catalyst contained 10 wt.% active phase (calculated hypothesizing the formation of $(VO)_2P_2O_7$), having P/V atomic ratio of 1.1 or 1.5.

Various procedures were used for the thermal treatment of the precursor:

(a) calcination in static air at 450°C for 5 hours;

(b) thermal treatment in flowing 10 mol.% steam in air at 450°C for 5 hours;

(c) treatment under steam/helium, following the same protocol described in (b).

Table 4.1 summarized the composition of prepared samples and the thermal treatment performed.

Table 4.1: Prepared samples.

Sample	P/V	Thermal treatment
PV1.1a	1.1	Air
PV1.1b	1.1	Steam/Air
PV1.1c	1.1	Steam/He
PV1.5a	1.5	Air
PV1.5b	1.5	Steam/Air
PV1.5c	1.5	Steam/He

Catalytic tests were carried out in a quartz continuous-flow reactor loading 0.8 g of catalyst (W/F=1.3 g s ml^{-1}) and feeding 1.7% *n*-butane and 17% oxygen (remainder N_2) or 1.7% *n*-butane, 4% (or 10%) steam, 17% oxygen (reminder N_2).

4.3 RESULTS AND DISCUSSION

4.3.1 Characterization of thermally treated samples

After calcination according to one of the procedures previously described, samples were characterized by means of Raman spectroscopy.

P/V 1.1

To examine the homogeneity and gain complete information about catalysts composition, several spectra were recorded in different areas of the same sample.

Figure 4.1 compares spectra obtained for sample having P/V 1.1 after different thermal treatments.

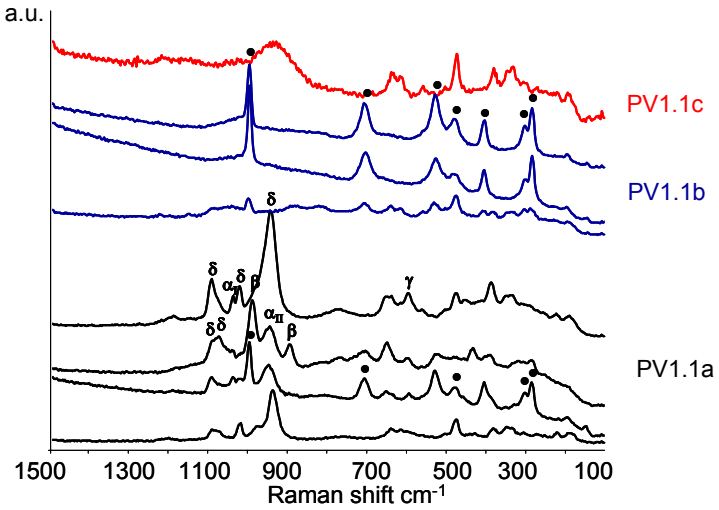

Figure 4.1: Raman spectra of calcined samples having P/V ratio 1.1. (PV1.1a: air, PV1.1b: 10%steam/air, PV1.1c: 10%steam/He). Symbols: ●= V_2O_5, α_I= α_I--$VOPO_4$, α_{II}= α_{II}--$VOPO_4$, δ= δ-$VOPO_4$, β= β-$VOPO_4$, γ= γ-$VOPO_4$.

All spectra showed the typical bands of the ZrO_2 support at Raman shift 190, 333, 347, 382, 476, 617 and 638 cm^{-1}; concerning the composition of the active phase, samples turned out to be very different from each other.

Catalyst calcined in static air (sample PV1.1a) was not homogeneous, being constituted of several compounds of V^{5+}. Different kinds of $VOPO_4$ were present on the surface: δ-$VOPO_4$ (bands at 1090, 1075, 1020, 936 cm^{-1}), β-$VOPO_4$ (968, 892 cm^{-1}), γ-$VOPO_4$ (656 cm^{-1}), α_I-$VOPO_4$ (1038 cm^{-1}) and α_{II}-$VOPO_4$ (945, 933 cm^{-1}).

Intensity of bands relative to these compounds was different depending on the area analyzed. In a few spectra also bands of vanadium oxide were observed (at 998, 705, 483, 305, 285 cm^{-1}).

The sample treated in steam and air (sample PV1.1b) was more homogeneous; also in this case vanadium was present as V^{5+}, but mostly as V_2O_5. Only in a few areas of the catalyst two bands at 884 and 820 cm^{-1} were recorded; the first one could be attributed to symmetric stretching of $P(OH)_2$ groups [11], while the band at lower Raman shift could indicate the presence of V-O-V bonds in dispersed polyvanadate species [12]. Sample calcined in steam and helium (sample PV1.1c) was homogeneous; in addition to the bands of zirconium oxide a broad band in the range 840-1000 cm^{-1} was present. In V/P/O systems the range 800-1000 cm^{-1} is distinctive of P-O bonds, moreover also V-O-V or V-O-Zr bonds (typical of supported vanadium oxide catalyst) show Raman bands in the same region [13-16]. The great variety of V/P/O compounds and the broadness of this band, did not allow an exact identification of surface species. Being the thermal treatment carried out at high temperature in non-oxidizing atmosphere, a partial or total reduction of vanadium to form an amorphous compound can not be excluded. In fact, previous studies on V/P/O catalysts for butane oxidation proved that δ-$VOPO_4$ under inert atmosphere gives spontaneous self-reduction, with release of oxygen and formation of vanadium(IV) phosphates also at temperature below 500°C (Chapter 3.3.3).

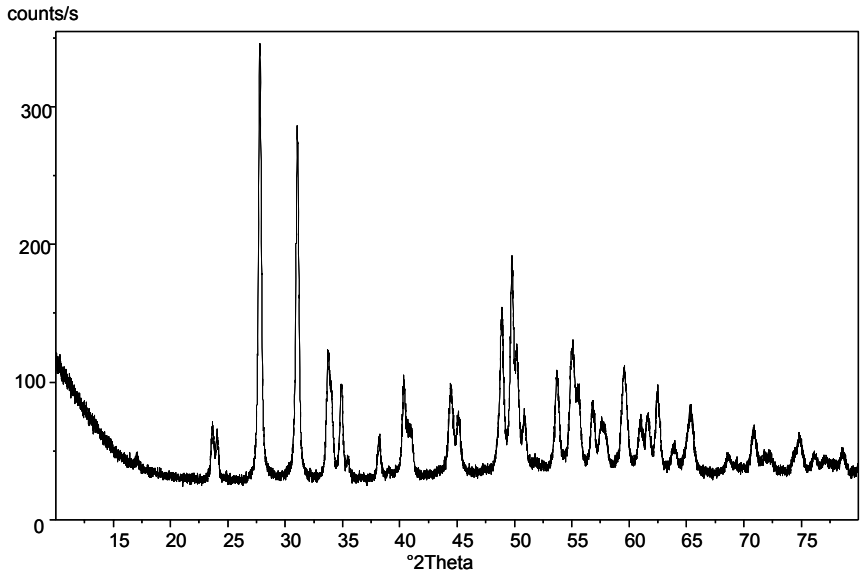

Figure 4.2: X-Ray diffraction pattern of sample PV1.1c (calcined in steam/He)

To confirm this hypothesis XRD and UV-Vis analysis were also performed. Actually, X-Ray diffraction pattern (Figure 4.2) did not show the presence of any reflections attributable to a phase containing V and P, all reflections were relative to monoclinic ZrO_2 used as the support. UV-Vis DR spectrum is showed in Figure 4.3; the bands at 200-250 nm are attributable to ZrO_2, while the band at 350 nm is relative to V(V) phosphates. In addition, a broad adsorption band can be noticed between 500 and 1000 nm, in the range of d-d transition in V^{4+} compounds; this confirms that when the termal tratment was carried out under non-oxidizing conditions, a partial reduction of vanadium occurs.

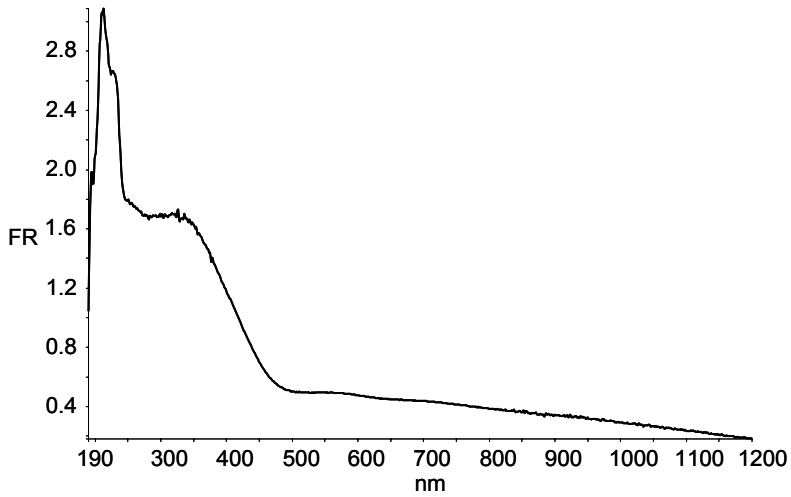

Figure 4.3: UV-Vis DR spectrum of sample PV1.1c (calcined in steam/He)

P/V 1.5

Figure 4.4 reports the Raman spectra of sample having P/V 1.5 after thermal treatment.

Depending on the kind of thermal treatment, different phases were formed by transformation of the precursor.

If calcination was carried out in air (sample PV1.5a) α_I-$VOPO_4$ (1036 cm^{-1}) and α_{II}-$VOPO_4$ (945, 993 cm^{-1}) formed, while when a stream of wet air (10% steam in air) was used, the active phase contained mostly $VOPO_4 \cdot 2H_2O$ and δ-$VOPO_4$. Also the presence of α_{II}-$VOPO_4$ (at 945 cm^{-1}) can not be excluded.

Spectra of sample calcined in steam and helium were similar to the ones obtained for sample PV1.1c having lower P/V atomic ratio. Therefore, also in this case the surface was likely made of an amorphous and partially reduced compound.

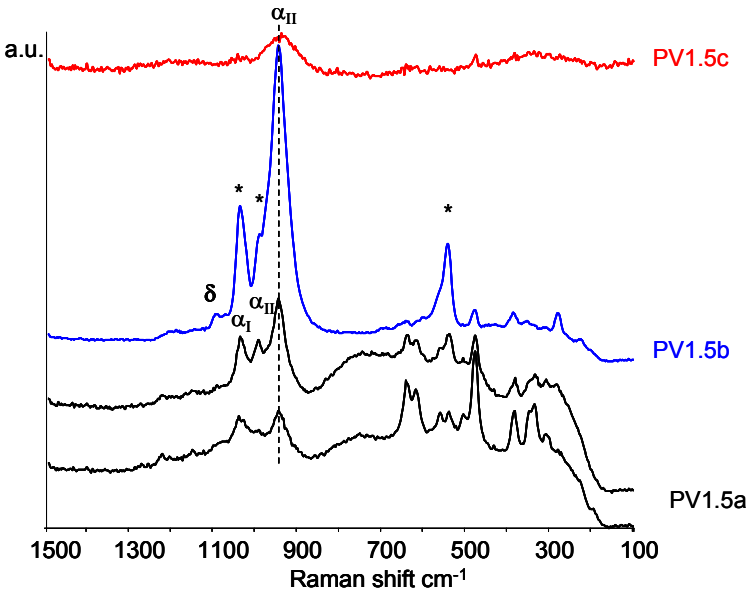

Figure 4.4: Raman Spectra of calcined samples having P/V 1.5 (PV1.5a: air, PV1.5b: 10%steam/air, PV1.5c: 10%steam/He). Symbols: α_I= α_I--$VOPO_4$, α_{II}= α_{II}--$VOPO_4$, δ= δ-$VOPO_4$, ∗= $VOPO_4 \cdot 2H_2O$.

Characterization of fresh samples showed that condition for thermal treatment greatly affected the composition of the catalysts, and in particular both the vanadium oxidation state and the "hydrolysis degree" of compounds which develop on the zirconia surface. For catalysts having P/V 1.1 the presence of steam avoids the formation of mixed compounds ($VOPO_4$), or favours hydrolysis of the latter to form V_2O_5. With higher amount of phosphorus (P/V 1.5), the formation of an hydrated mixed phase of vanadium and phosphorus ($VOPO_4 \cdot 2H_2O$) is favoured and vanadium oxide does not develop.

4.3.2 *"In-situ"* Raman analysis

The possible transformations of the precursor, occurring at increasing temperatures of thermal treatment, were studied by means of *in-situ* Raman spectroscopy.

P/V 1.1

In order to simulate the calcination in air, a flow of diluted oxygen (14.8% O_2 in nitrogen) was used. The precursor was heated up to 450°C and maintained at this temperature for 5 hours.

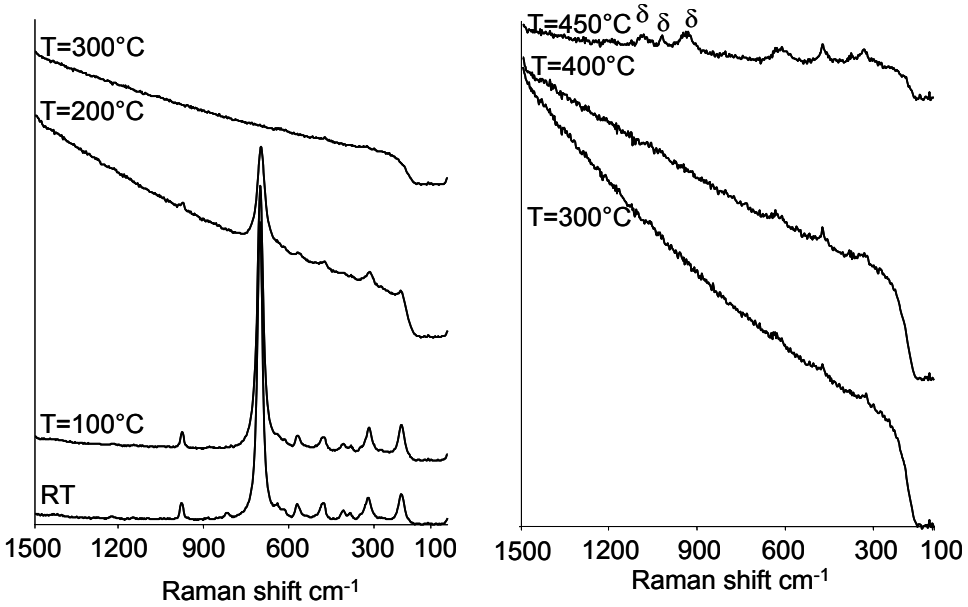

Figure 4.5: *In-situ* Raman spectra recordeded at increasing temperature under flow of 14.8% O_2 in N_2. Symbols: δ= δ-$VOPO_4$. Sample PV1.1.

Spectrum at room temperature showed bands resulting from the interaction between the reagents (NH_4VO_3 and H_3PO_4), used for the precursor synthesis, and the support; they gradually disappeared when the temperature was increased up to 300 and 400°C (Figure 4.5). In these conditions the decomposition of the precursor occurred, as also confirmed by thermogravimetric analysis that evidenced a weight loss of 3.5% at 300°C. At 450°C bands of δ-$VOPO_4$ appeared at Raman shift 936, 1020 e 1090 cm^{-1}.

Figure 4.6 reports spectra collected at 450°C during the isothermal step. Under these conditions δ-$VOPO_4$ was stable for about 2 hours; after 3 hours bands of this compound became less intense and the spectrum showed a broad band in the range 1000-1100 cm^{-1}. Also a new band attributable to V=O stretching mode in vanadium oxide appeared at 997 cm^{-1}.
At room temperature after calcination, the spectrum showed bands attributable to V_2O_5, δ, β and α_{II}-$VOPO_4$.

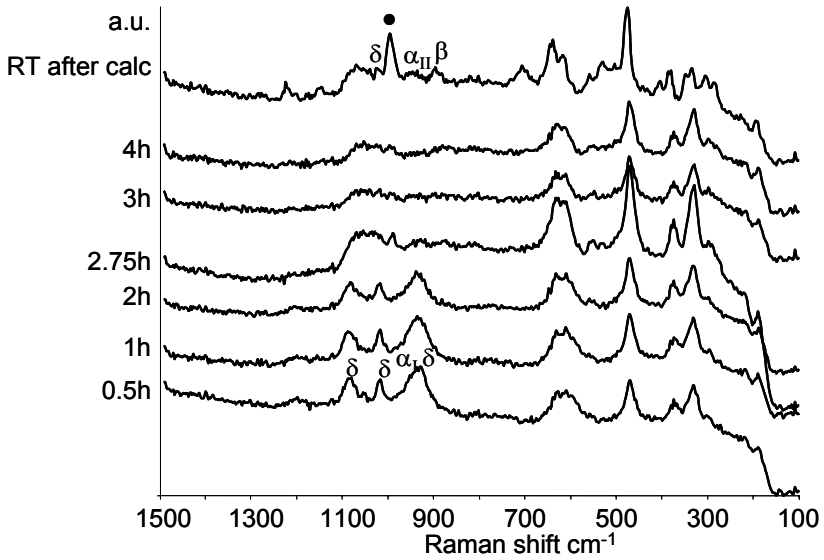

Figure 4.6: *In-situ* Raman spectra recorded at 450°C under flow of 14.8% O_2 in N_2. Symbols: ●= V_2O_5, α_{II}= α_{II}-$VOPO_4$, δ= δ-$VOPO_4$, β= β-$VOPO_4$. Sample PV1.1.

The same procedure was followed to simulate thermal treatments in the presence of steam. Wet stream was obtained saturating the flow of air or nitrogen by bubbling it in water at room temperature (approximately 3 vol.% steam).

Spectra recorded during the heating step (not reported) were very similar to those previously described for calcination in air; therefore, regardless the composition of the gas phase (either oxidizing and/or hydrolyzing) at 300°C precursor decomposes to form δ-$VOPO_4$.

Spectra obtained at 450°C under wet air are reported in Figure 4.7; also in this case δ-$VOPO_4$ was not stable and gradually transformed into V_2O_5. The presence of water seems to accelerate this transformation, in fact the bands of δ-$VOPO_4$ disappeared already after 2 hours when the broad band at 1000-1100 cm^{-1} appeared; at room temperature the sample contained mainly V_2O_5.

Additional tests carried out in Raman cell at 450°C confirmed that steam makes δ-$VOPO_4$ less stable and favours its transformation to V_2O_5. In fact, when the precursor was heated in dry air up to 450°C (temperature at which only δ-$VOPO_4$ formed) and then water was fed, bands of $VOPO_4$ disappeared already after 1 hour.

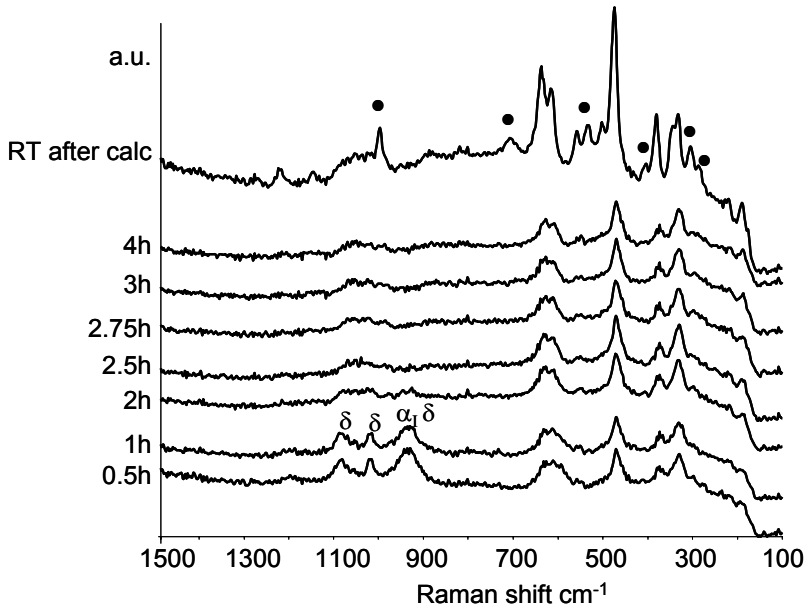

Figure 4.7: *In-situ* Raman spectra collected at 450°C under flow of 3vol.% steam in air. Symbols: ●=V_2O_5, α_I= α_I-$VOPO_4$, δ= δ-$VOPO_4$. Sample PV1.1.

The evolution of precursor at 450°C under wet nitrogen stream is shown in Figure 4.8.

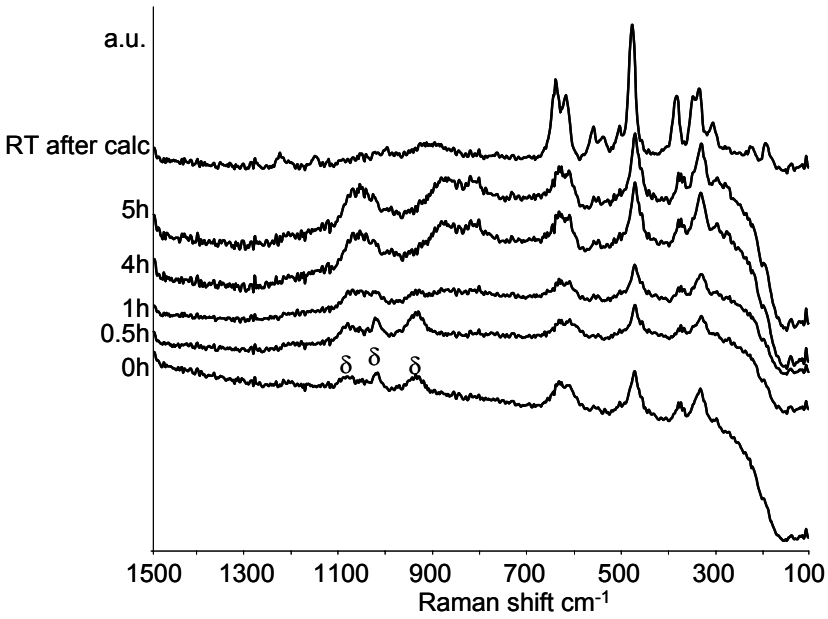

Figure 4.8: *In-situ* Raman spectra collected at 450°C under flow of 3vol.% steam in N_2. Symbols: δ=δ-$VOPO_4$. Sample PV1.1.

Also in presence of a non-oxidizing stream, the first compound formed was δ-$VOPO_4$; after 1 hour, the bands of this compound disappeared to form the band at 1000-1100 cm^{-1} previously observed under oxidizing atmosphere. After 4 hours, two bands at Raman shift 875 and 815 cm^{-1} appeared, attributable to P(OH) and V-O-V groups; after cooling at room temperature only one weak band centred at 910 cm^{-1} was present. This band was likely the result of two different contributions, P-O bonds stretching at 920 cm^{-1} and V-O-V groups at 820 cm^{-1}.
In-situ Raman measurements gave information on the dynamics of formation of the surface compound. The precursor decomposes to form δ-$VOPO_4$; under oxidizing atmosphere this compound gradually transform into V_2O_5, the rate of this transformation is increased by the presence of steam. Under non oxidizing atmosphere, the spreading of δ-$VOPO_4$ on the support occurs, and a disordered layer containing P-OH and V-O-V groups forms.

P/V 1.5

Raman spectra recorded at 450°C under flow of wet air for the precursor having P/V 1.5 are reported in Figure 4.9.

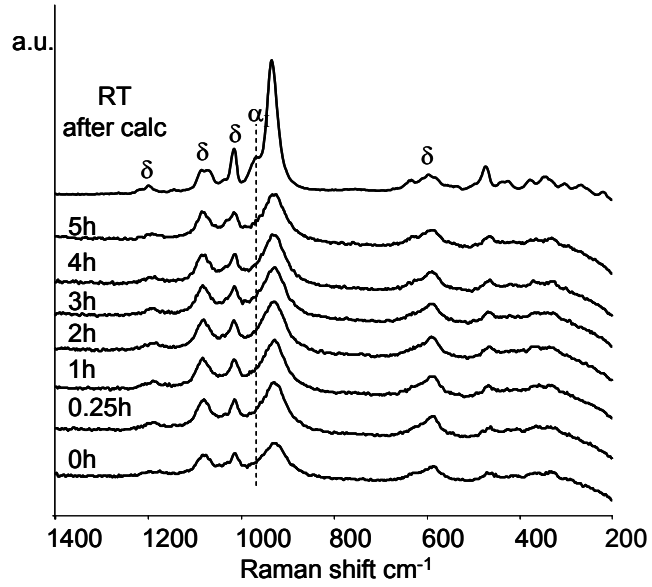

Figure 4.9: *In-situ* Raman spectra collected at 450°C under flow of 3vol.% steam in air. Symbols: α_I= α_I-$VOPO_4$, δ= δ-$VOPO_4$. Sample PV1.5.

Also in this case, the precursor decomposed to form δ-$VOPO_4$: the typical bands of this compound (at 590, 936, 1020 and 1090 cm^{-1}) remained quite intense and

well visible even after 5 hours of exposure to wet air. At room temperature, after the treatment, sample contained mainly δ-$VOPO_4$ (bands at 590, 936, 1020, 1075 and 1090 cm^{-1}). This suggests that an higher P/V ratio, improves the stability of δ-$VOPO_4$ and avoids the formation to V2O5, as compared to the sample having P/V 1.1.

Data are in agreement with the results from the study on the nature of the active phase in vanadyl pyrophosphate (Chapter 3).In fact, we demonstrated that the excess of phosphorus stabilizes δ-$VOPO_4$, avoiding its reversible change to α_I-$VOPO_4$, the first step for the formation of vanadium oxide.

4.3.3 Characterization of spent samples

Catalysts were characterized after catalytic tests under different reaction conditions for several hours, both feeding *n*-butane/air and steam-enriched *n*-butane/air (4% and/or 10% steam in air).

Catalytic tests were first carried out by feeding the usual reaction mixture for a few days, in order to understand if the compounds formed during calcination were stable or, on the contrary, the catalysts needed an "equilibration" before reaching the stable catalytic performances. All samples did not show variations of performance during more than 80 hours of exposure to the *n*-butane and air feed; therefore compounds formed during calcination were quite stable, or their transformation was so rapid that it was not possible to check variations of catalytic performances during the increasing reaction time.

P/V 1.1

Figures 4.10 and 4.11 compare Raman spectra of spent samples recorded at room temperature after working under different conditions.

After calcination in air sample PV1.1a (Figure 4.10 left) contained mainly δ-$VOPO_4$ but also smaller amounts of β, γ, α_I and α_{II}-$VOPO_4$ were present. These compounds were still present after reaction in *n*-butane/air, but the intensity of bands attributable to δ-$VOPO_4$ decreased while that of bands typical of α_I and α_{II} $VOPO_4$ increased. This effect was more evident in the sample downloaded after tests in the reaction mixture enriched with 10% of steam, moreover in this case also bands attributable to V_2O_5 became visible.

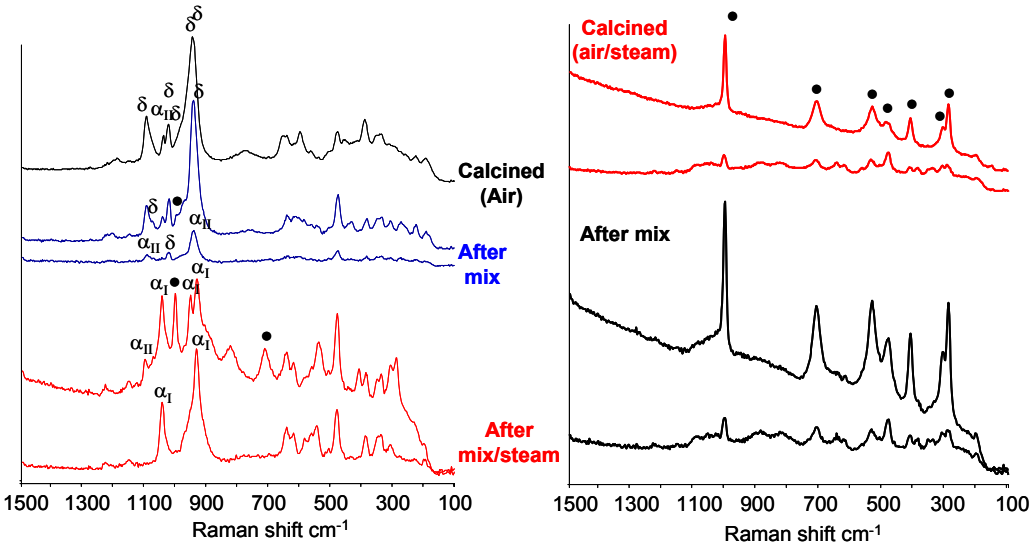

Figure 4.10: Comparison between calcined sample and corresponding spent catalyst. Symbols: ●=V_2O_5, α_I =α_I–$VOPO_4$, α_{II} =α_{II}-$VOPO_4$, δ =δ-$VOPO_4$. Samples: PV 1.1a (left), PV1.1b (right).

Sample PV1.1b (Figure 4.10 right) was calcined in steam and air; it contained mostly vanadium oxide; after reaction no great differences of composition were noticed. This confirms that the presence of relatively large amounts of steam in the reaction mixture reduce the stability of δ-$VOPO_4$ and favours its transformation into V_2O_5. The latter turned out to be stable both in presence and in the absence of steam and did not undergo relevant modifications.

Sample PV1.1c was treated in steam and helium; spectra of samples analyzed after reaction in mixture of *n*-butane/air, *n*-butane/air/4%steam and *n*-butane/air/10%steam are reported in Figure 4.11.

Great differences between the spectra were observed. Before catalytic tests, the sample surface was made of an amorphous layer containing P-OH and V-O-V groups, in which vanadium was reduced to V^{4+}, responsible for the broad band in the region 800-1000 cm^{-1}. After reactivity tests in *n*-butane/air several strong bands appeared, that are attributable to α_{II} and β $VOPO_4$. Also after reaction with steam the "disordered" surface layer was oxidized to V^{5+} compounds; the spectrum of the sample recorded after reaction with 4% of steam showed weak bands of V_2O_5, δ and β-$VOPO_4$, while after exposure to the reaction mixture enriched with 10% steam, bands attributable to V_2O_5, β and α_{II}-$VOPO_4$ were present.

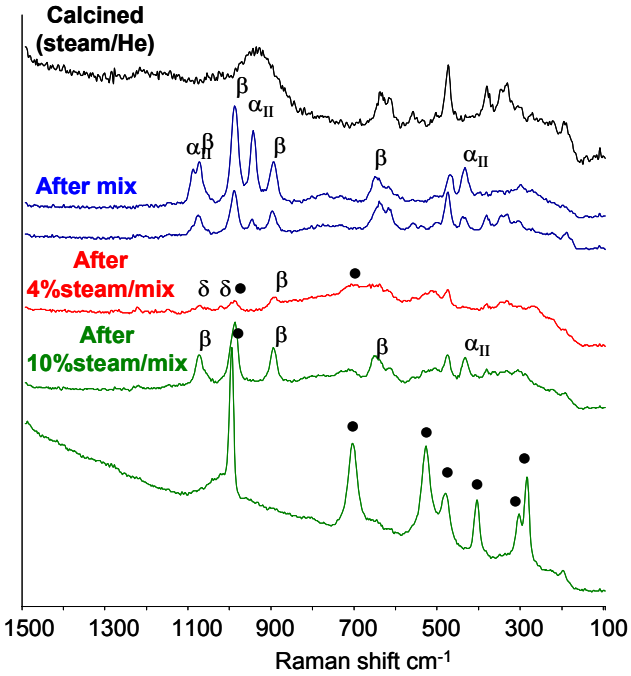

Figure 4.11: Comparison between calcined sample and corresponding spent catalyst. Symbols: ●=V_2O_5, β =β–$VOPO_4$, α_{II} =α_{II}-$VOPO_4$, δ =δ-$VOPO_4$. Sample PV 1.1c.

P/V 1.5

Figure 4.12 compares Raman spectra of the sample having P/V 1.5 after calcination in dry air and after reaction in *n*-butane and air.

Before reaction the catalyst contained α_I and α_{II}-$VOPO_4$; after catalytic tests bands of these compounds completely disappeared and the catalyst surface rturned out to contain δ-$VOPO_4$ and $VOPO_4 \cdot 2H_2O$. Hence, α_I and α_{II}-$VOPO_4$ are not stable in presence of steam and under working condition form δ-$VOPO_4$. $VOPO_4 \cdot 2H_2O$ could derive from the hydration of α-$VOPO_4$ or from the transformation of δ-$VOPO_4$. Nevertheless, the formation of $VOPO_4 \cdot 2H_2O$ and its further dehydration to δ-$VOPO_4$ is the most probable hypothesis. In fact, it is known the tendency of all $VOPO_4$ phases to undergo hydration to $VOPO_4 \cdot 2H_2O$ [17,18]; furthermore it was shown in the previous section that with the catalyst having excess of phosphorus, dehydration of $VOPO_4 \cdot 2H_2O$ to δ-$VOPO_4$ is favoured also in presence of steam.

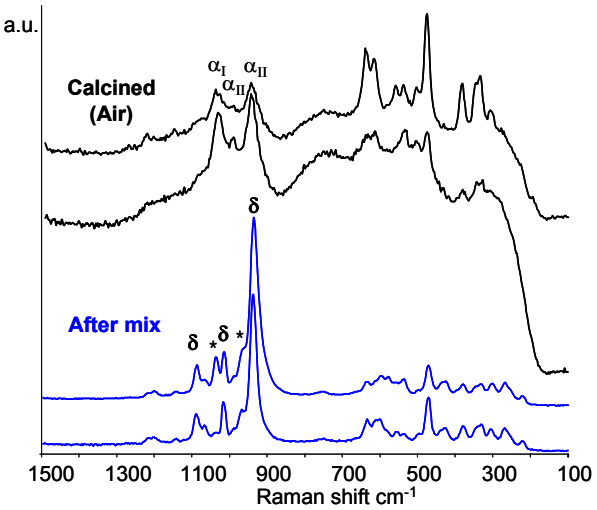

Figure 4.12: Comparison between calcined sample and corresponding spent catalyst. Symbols: ∗=$VOPO_4 \cdot 2H_2O$, α_{II} =α_{II}-$VOPO_4$, α_I =α_I-$VOPO_4$, δ =δ-$VOPO_4$. Sample PV1.5a.

Sample PV1.5b was prepared starting from the same precursor, but during the thermal treatment 10% of steam was added to the flow of air (Figure 4.13).

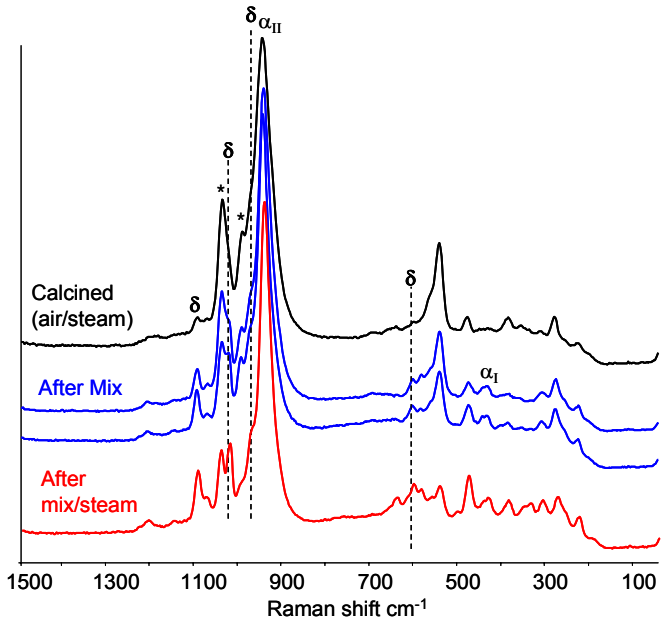

Figure 4.13: Comparison between calcined sample and corresponding spent catalysts. Symbols: ∗=$VOPO_4 \cdot 2H_2O$, α_{II} =α_{II}-$VOPO_4$, δ =δ-$VOPO_4$. Sample PV1.5b.

After calcination the sample contained mainly $VOPO_4 \cdot 2H_2O$. This compound was the main one also after reaction in *n*-butane/air mixture; however the intensity of

δ-$VOPO_4$ bands increased, especially after reaction in presence of steam. This confirms that $VOPO_4 \cdot 2H_2O$ is unstable, and under working conditions it tends to dehydrate and form δ-$VOPO_4$.

Characterization results confirmed the importance of the P/V ratio in the control of the composition of the final catalyst. It influences the nature of the different phases that form by thermal treatment, but it also affects the evolution of the active phase during reaction. When the catalyst surface is rich of phosphorus δ-$VOPO_4$ is the most stable phase. In the presence of steam (both during the thermal treatment and under working conditions), δ-$VOPO_4$ also forms by transformation of α_I and α_{II}-$VOPO_4$ to $VOPO_4 \cdot 2H_2O$ and its subsequent dehydration. On the contrary, when the catalyst has a P/V ratio closer to the stoichiometric values, δ-$VOPO_4$ is less stable and the presence of water favours its gradual transformation into other $VOPO_4$ phases, mainly α_I-$VOPO_4$. In this case, the latter is the precursor for V_2O_5 formation.

4.3.4 Reactivity tests

P/V 1.1

Results of catalytic tests are summarized in Table 4.2; all tests have been carried out at 400°C, in conditions similar to the industrial ones.

The reactivity of the support was also checked. ZrO_2 turned out to be slightly active but not selective to maleic anhydride. In the presence of either *n*-butane/air or *n*-butane/air/10% steam, conversion at 400°C was only 10%; carbon oxides and formaldehyde (traces) were the only detected products.

With all catalysts, regardless of feed composition, *n*-butane conversion ranged between 25 and 35%, higher than that of the bare support. Products were maleic anhydride, acetic acid, acrylic acid, formaldehyde, CO and CO_2 (named CO_x), all compounds obtained also using vanadyl pyrophosphate catalyst.

Low amount of 2,5-dihydrofuran and maleic acid were detected; these products have never been observed with the VPP.

Carbon oxides were the main products, with selectivity between 70 and 90%; selectivity to formaldehyde was always lower than 2%, while only traces of dihydrofuran and acids were detected. Selectivity to maleic anhydride was far below the values obtained using VPP; with the latter catalyst, for the same

conversion of the hydrocarbon, MA selectivity is typically 65% and CO_x only 25% . Therefore this kind of catalysts is poorly selective and total oxidation is favoured.

Table 4.2: Reactivity of samples having P/V 1.1 (T=400°C, W/F= 1.3 g·s/ml, Mix: 1.7 % *n*-butane in air).

Sample code		Conv (%)	Sel AM (%)	Sel form. (%)	Sel CO_x (%)	Sel maleic acid (%)
PV1.1a	Mix	30	15	2	83	nd
	Mix+4%H_2O	27	14	3	83	nd
	Mix+10%H_2O	25	7	2	81	0
	Mix dopo H_2O	37	8	1	79	6
PV1.1b	Mix	31	5	2	82	0.1
	Mix+10%H_2O	28	4	1	72	5
PV1.1c	Mix	34	5	1	89	6
	Mix+4%H_2O	31	4	1	70	6
	Mix+10%H_2O	32	4	1	56	12

The best catalytic performances in terms of MA selectivity were obtained with the PV1.1 sample calcined in air (PV1.1a) and feeding only butane/air; in this case, the catalyst surface was made of δ-$VOPO_4$ (see Chapter 4.3.3). Other $VOPO_4$ compounds were more stable under reaction conditions but less selective to MA. Sample PV1.1b and PV1.1c which mainly contained V_2O_5 formed the higher amount of CO_x and, if steam was co-fed, of maleic acid.

It is important to underline that the reaction mechanism reported in literature for the formation of maleic anhydride does not include the formation of maleic acid [19]. The latter could form from maleic anhydride by hydrolysis, or could be formed by a different reaction pathway; in fact, at high partial pressure of water a modification of active sites can not be excluded.

To investigate the reaction scheme tests were carried out varying the residence time; results are showed in Figure 4.14.

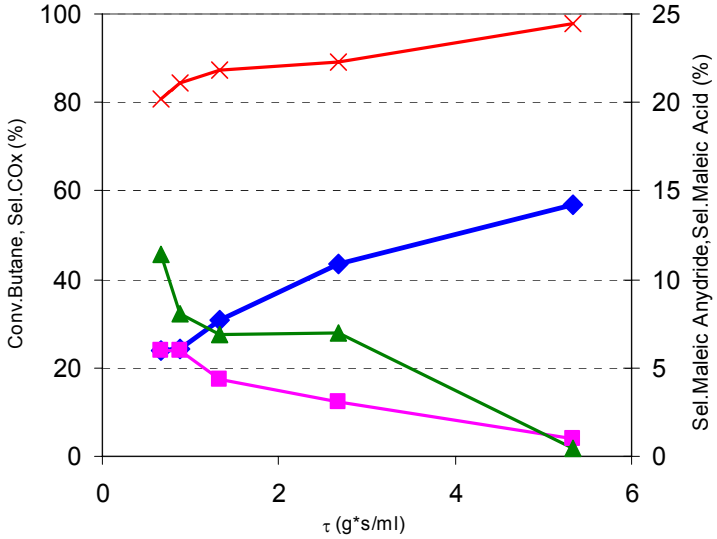

Figure 4.14: Conversion of *n*-butane (◆), selectivity to maleic anhydride AM (■), maleic acid (▲), COx (×) as a function of residence time. T=400°C, feed composition: 4% steam,1.7% butane, 17% O_2. Sample: PV1.1c.

On increasing the residence time, the conversion of *n*-butane and the selectivity to CO_x increased, whereas the selectivity to maleic acid and maleic anhydride decreased; at residence time 5.3 g·s/ml carbon oxides were the only products. Hence an increase of *n*-butane conversion favoured the consecutive reactions of total oxidation. Selectivities to maleic acid and maleic anhydride had parallel trends; this suggests that these products derive from the same intermediate, probably 2,5-dihydrofuran. The latter can be oxidized to maleic anhydride (via lactone) or undergo ring opening and then oxidation to maleic acid [20].

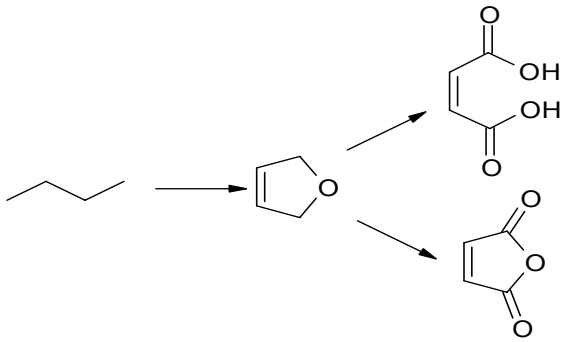

Figure 4.15 Reaction scheme for *n*-butane oxidation feeding 4% steam,1.7% butane, 17% O_2

P/V 1.5

Table 4.3 summarizes the results of catalytic tests on sample having P/V ratio 1.5. Data obtained at 400°C and at the temperature of 30% *n*-butane conversion are reported. In such a way it is possible to evaluate the effect of phosphorus on activity (by comparing *n*-butane conversion at 400°C), and on selectivity to maleic anhydride (comparing the MA selectivity at similar *n*- butane conversion).

Table 4.3: Reactivity of samples having P/V 1.5 (W/F= 1.3 g·s/ml, Mix: 1.7 % *n*-butane in air).

Sample code		T (°C)	Conv (%)	Sel AM (%)	Sel form. (%)	Sel CO_x (%)	Sel maleic acid (%)
PV1.5a	Mix	400	12	11	3	86	0
		440	32	14	3	84	0
PV1.5b	Mix	400	6	18	4	72	0
		440	25	14	3	53	0
	Mix+10%H_2O	400	24	5	1	18	15
		420	26	9	2	32	14

Concerning catalytic performances under *n*-butane/air mixture, both samples were less active than catalysts having P/V ratio 1.1. *n*-Butane conversion at 400°C was lower than 15%; nevertheless selectivity to maleic anhydride never reached 20% and carbon oxides were the major products. Sample PV1.5a, which after working in reaction mixture was mainly δ-$VOPO_4$, was slightly more active and less selective of sample PV1.5b that contained also other $VOPO_4$ phases. Selectivity to MA at 25-30% butane conversion was similar to that of sample PV1.1a, having lower P/V atomic ratio but containing the same surface compound, δ-$VOPO_4$. Therefore, the main effect of the excess of P was tht of a decrease of catalyst activity, that however did not lead to improvements of selectivity.

When the reaction was carried out in presence of steam, an higher conversion of butane was observed. Selectivity to maleic anhydride and CO_x decreased and maleic acid formed. In these conditions carbon balance was usually lower than 70% and the sample catalyzed the formation of heavy compounds. A first attempt of identifying these products by means of mass spectroscopy suggested that they could derive from Diels Alder reaction on maleic anhydride. Moreover, the presence of water could favour the formation of P-OH group on catalyst surface

and consequently increase the acidity. Therefore, we cannot exclude that the formation of heavy compounds was due to the higher acidity of the catalyst.

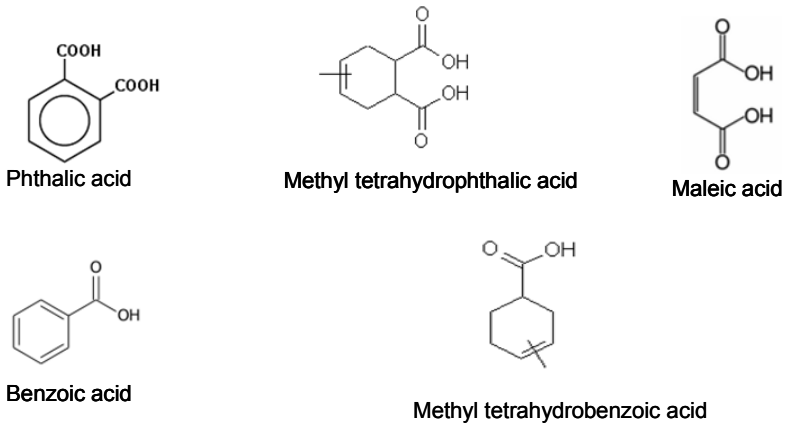

Figure 4.16: Some heavy compounds formed with Sample PV1.5

4.4 CONCLUSIONS

In-situ Raman spectroscopy was used to monitor the changes occurring on the surface of a ZrO_2-supported V/P/O catalyst during the calcination treatment, with the aim of understanding the phenomena that lead to the generation of the active phase. It was found that a proper control of the parameters during the thermal treatment is essential for the build-up of the desired active phase.

When the catalysts were prepared from V^{5+} and phosphoric acid, δ-$VOPO_4$ formed. Nevertheless, the stability of this compound was a function of calcination atmosphere as well as of the P/V atomic ratio. These parameter also affects evolution of active phase under working conditions.

When the P/V ratio was close to 1.0 the partial hydrolysis of δ-$VOPO_4$ to α $VOPO_4$ and V_2O_5 occurred, favored by the presence of a steam-containing stream. Under non-oxidizing atmosphere δ-$VOPO_4$ evolved to a disordered layer containing P-OH and V-O-V groups, and the partial reduction of V^{5+} to V^{4+} likely occurred. However, this surface turned out to be extremely reactive, especially when exposed to an oxidizing atmosphere. If catalysts were prepared with an higher excess of phosphorus δ-$VOPO_4$ turned out to be more stable also under hydrolyzing conditions.

Prepared catalysts were active in the oxidation of *n*-butane but poorly selective to maleic anhydride. Consecutive reaction of total combustion to CO_x were favored,

particularly when V_2O_5 was present; catalyst having high excess of P are less active and form also heavy compounds.

Poor catalytic performances of these systems could be related to the loss of P during reaction which could favor the formation of V_2O_5, especially for the sample prepared with P/V ratio close to 1.0. Possible improvements of these systems could be obtained using a P containing support, which might supply the loss of phosphorus and avoid the formation of vanadium oxide. An alternative explanation is that indeed the surface V/P/O (δ-$VOPO_4$) needs the vanadyl pyrophosphate below it, that may act as a sort of in-situ generator of the active compound.

4.5 REFERENCES

[1] Z.Y. Xue, G.L. Schrader, J. Phys. Chem. B 103 (1999) 9459.

[2] N. Duvauchelle, E. Bordes, Catal. Lett. 57 (1999) 81.

[3] N. Ballarini, F. Cavani, C. Cortelli, S. Ligi, F. Pierelli, F. Trifirò, C. Fumagalli, G. Mazzoni, T. Monti, Topics Catal. 38 (2006) 147.

[4] L. O'Mahony, T. Curtin, D. Zemlyanov, M. Mihov, B.K. Hodnett, J. Catal. 227 (2004) 270

[5] L. O'Mahony, T. Curtin, J. Henry, D. Zemlyanov, M. Mihov, B.K. Hodnett, Appl. Catal. A 285 (2005) 36

[6] H. Bluhm, M. Hävecker, E. Kleimenov, A. Knop-Gericke, A. Liskowski, R. Schlögl, D.S. Su, Topics Catal. 23 (2003) 99

[7] M. Hävecker, A. Knop-Gericke, H. Bluhm, E. Kleimenov, R.W. Mayer, M. Fait, R. Schlögl, Appl. Surf. Sci. 230 (2004) 272

[8] M. Hävecker, R.W. Mayer, A. Knop-Gericke, H. Bluhm, E. Kleimenov, A. Liskowski, D.S. Su, R. Follath, F.G. Requejo, D.F. Ogletree, M. Salmeron, J.A. Lopez-Sanchez, J.K. Bartley, G.J. Hutchings, R. Schlögl, J. Phys. Chem. B 107 (2003) 4587

[9] Z.Y. Xue, G.L. Schrader, J. Phys. Chem. B 103 (1999) 9459

[10] N. Ballarini, F. Cavani, C. Cortelli, M. Ricotta, F. Rodeghiero, F. Trifirò, C. Fumagalli, G. Mazzoni, Catal. Today 117 (2006) 174.

[11] H. Abderrazak, M. Dachraoui, M. J. Ayora Cañada, B. Lendi, Appl. spectrosc. 54 (2000) 1610

[12] J. M. Jehng, G. Deo, B. M. Weckhuysen, I. E. Wachs, J. Mol. Catal. A, 110 (1996) 41

[13] X. Gao, I. Wachs, Top. Catal. 18 (2002) 243

[14] N. Magg, B. Immaraporn, J. B. Giorgi, T. Schroeder, M. Bäumer, J. Döbler, Z. Wu, E. Kondratenko, M. Cherian, M. Baerns, P. C. Stair, J. Sauer, H. J. Freund, J. Phys. Chem. B 110 (2006) 14313

[15] M. Bañares, I.E. Wachs, J. Raman Spectr. 33 (2002) 359

[16] I.E. Wachs, Catal. Today 27 (1996) 437

[17] F. Ben Abdelouahab, R. Olier, N. Guilhaume, F. Lefebvre, J. C. Volta, J. Catal. 134 (1992) 151

[18] F. Ben Abdelouahab, R. Olier, N. Guilhaume, F. Lefebvre, J. C. Volta, J. Catal. 148 (1994) 334

[19] F. Trifirò, Catal. Today, 16 (1993) 91.

[20] Z. Y. Xue, G. L. Schrader, J. Catal. 184 (1999) 87.

5

CONCLUSIONS

Selective oxidation of *n*-butane to maleic anhydride is the only industrial example of direct oxidation of paraffins to a chemical intermediate. The reaction has been made possible thanks to the development, in the 70', of an active and selective catalyst, the vanadyl pyrophosphate (VPP). This system is employed both in fixed bed and fluid bed technology. Despite the good performances, the yield value didn't exceed 60% and the system is continuously studied to improve activity and selectivity.

The main open problem is the understanding of the real active phase working under reaction conditions. Several articles deal with the role of different crystalline and/or amorphous vanadium/phosphorus (VPO) compounds. In all cases, bulk VPP is assumed to constitute the core of the active phase, while two different hypotheses have been formulated concerning the catalytic surface. In one case the development of surface amorphous layers that play a direct role in the reaction is described, in the second case specific planes of crystalline VPP are assumed to contribute to the reaction pattern, and the redox process occurs reversibly between VPP and $VOPO_4$. Both hypotheses are supported also by in-situ characterization techniques, but the experiments were performed with different catalysts and probably under slightly different working conditions. Due to the complexity of the system, these differences could be the cause of the contradictions present in literature.

From the literature P/V ratio seems to play an important role on the catalytic performances; for this reason two sample having different P/V ratio were studied. Transformations occurring on the catalytic surfaces under different conditions of temperature and gas-phase composition were studied by means of in-situ Raman

spectroscopy, trying to investigate the changes that VPP undergoes during reaction. Also reactivity tests under steady-state and non-steady state regime were performed in order to understand in which conditions the best active surface develops. VPP showed to be very sensitive to slight changes of catalyst composition and operative conditions. P/V ratio greatly affects the catalytic performances at intermediate reaction temperature (380°C): in presence of air and steam for samples having P/V close to 1.0, α_I-$VOPO_4$ forms, eventually hydrolyzed to [VO_y + $(PO_4)_n$], while with catalyts having a P/V ratio higher then the stoichiometric, the stable compound on the VPP surface at 380°C is δ-$VOPO_4$. At high temperature, however, the two samples behave similarly, and δ-$VOPO_4$ is formed by surface oxidation of VPP.

Reactivity tests showed that the best catalytic performances were obtained when the surface layer contains δ-$VOPO_4$. For catalyst having a slight excess of P, the oxidation to δ-$VOPO_4$ occurs at lower temperature and this ensures good catalytic performances in all the range of temperatures investigated. On the contrary, for samples prepared with stoichiometric P/V ratio, the formation of α_I-$VOPO_4$ or [VO_y + $(PO_4)_n$] at intermediate temperature is responsible for the lower selectivity to MA. Therefore the excess of P favours the formation of δ-$VOPO_4$ and improves its stability under reaction mixture, avoiding its reversible changes under reaction mixture and ensuring high selectivity to MA.

P/V surface ratio can be varied "in-situ" by application of specific treatments. Nevertheless, due to the extremely sensitive nature of VPP, a proper control of each parameter is fundamental for obtain an active and selective catalyst.

The second part of the thesis was dealing with the attempt to project a new catalyst for the oxidation of *n*-butane. The starting point was the idea of reproduce the surface active layer of VPP onto a support. In general, supportation is a way to improve mechanical features of the catalysts and to overcome problems such as possible development of local hot spot temperatures, which could cause a decrease of selectivity at high conversion, and high costs of catalyst.

Precursors of the final catalysts having different P/V ratio (1.1 and 1.5) were prepared by impregnation of monoclinic ZrO_2 (s.s.a. 14 m^2/g) with a solution of NH_4VO_3 and of H_3PO_4. Different thermal treatments were performed and the

evolution of the precursor during the formation of the active phase was followed by means of in-situ Raman spectroscopy.

It was found that a proper control of the parameters during the thermal treatment is essential for the build-up of the desired active phase. Regardless the kind of thermal treatment (dry air, wet air or wet nitrogen), δ-$VOPO_4$ formed. Nevertheless, the stability of this compound was a function of the calcination atmosphere as well as of the P/V atomic ratio. When the P/V ratio was close to 1.0 the partial hydrolysis of δ-$VOPO_4$ to α_I $VOPO_4$ and V_2O_5 occurred, favored by the presence of a steam-containing stream. Under a non-oxidizing atmosphere, δ-$VOPO_4$ evolved to a "disordered" layer containing P-OH and V-O-V groups, and the partial reduction of V^{5+} to V^{4+} likely occurred. However, this surface was extremely reactive, especially when exposed to an oxidizing atmosphere. If catalysts were prepared with an higher excess of phosphorus, δ-$VOPO_4$ turned out to be more stable also under hydrolyzing conditions.

All supported catalysts were active in the oxidation of *n*-butane but poorly selective to maleic anhydride due to the high contribution of consecutive reactions of total combustion to CO_x, particularly favored when V_2O_5 was present. Poor catalytic performances of these systems can be related to the loss of P during reaction which could favor the formation of V_2O_5, especially for the sample prepared with P/V ratio close to 1.0. Possible improvements of these systems could be obtained using a P containing support, which might supply the loss of phosphorous and avoid the formation of vanadium oxide. An alternative explanation is that indeed the surface V/P/O (δ-$VOPO_4$) needs the vanadyl pyrophosphate below it, that may act as a sort of in-situ generator of the active compound.

APPENDIX

Table A.1: UV-Vis bands of different V species

	d-d Transitions (nm)	Charge transefr bands (nm)
V^{5+} (in $VOPO_4$)		320 420
V^{4+} (in $(VO)_2P_2O_7$)	850 d-d 640 d-d	300
V^{3+} (in aqua-complex)	480-500 d-d	

Table A.2: IR-bands and their assignements

$VOHPO_4 \cdot 0{,}5H_2O$ (cm^{-1})	$(VO)_2P_2O_7$ (cm^{-1})
3590 ν_a OH_2	
3370 ν_s OH_2	
3050 ν (P)-OH	
2320 δ (H_2O)	2445 $2*\nu_{as}$ PO_3
2240 $2*\nu_a$ PO_3	2300 $\nu_{as} + \nu_s$ PO_3
2015 $\nu_a+\nu_s$ PO_3	2230 $2*\nu_{as}$ PO_3
1985 $2*\nu_s$ PO_3	1995 ν_{as} PO_3 $+\nu_s$ POP
1950 $2*\nu$ V=O	1940 $2*\nu$ V=O
1818 δ_{ip} POH + δ_{oop} POH	1865 ν PO_3 $+\nu$ POP
1645 δ H_2O	1235, 1220 ν_{as} PO_3
1132 δ_{ip} POH	1140, 1095 ν_{as} PO_3
1194, 1103, 1050 $\nu_{a\,s}$ PO_3	1095 ν_s PO_3
976 ν V=O ($+\nu_s$ PO_3)	966 ν V=O
930 ν P-(OH)	960 ν_{as} POP
686 ω H_2O	792 ν V-(O=V)
641 δ_{oop} POH	740 ν_s POP
548, 531, 483, 416 δ OPO	627, 577, 504, 420 δ OPO

Table A.3: Diffraction patterns of $VOHPO_4 \cdot 0{,}5H_2O$ and of $(VO)_2P_2O_7$

$VOHPO_4 \cdot 0{,}5H_2O$				$(VO)_2P_2O_7$			
d	**2θ**	**I/I**	**hkl**	**d**	**2θ**	**I/I**	**hkl**
5,72	15,5	100		3,87	23,0	100	200
4,53	19,6	40		3,14	28,4	100	024
2,94	30,4	40		2,98	30,0	60	032
3,30	27,0	30		2,66	33,7	60	016
2,66	33,7	30		2,44	36,8	60	230
3,68	24,2	20		2,08	43,5	60	044
3,12	28,6	20		1,57	58,8	60	-
2,80	31,9	10		1,46	63,7	60	-

Table A.4. Diffraction patterns of δ-$VOPO_4$ and α_{II} -$VOPO_4$

δ-$VOPO_4$				α_{II} -$VOPO_4$			
d	**2θ**	**I/I**	**hkl**	**d**	**2θ**	**I/I**	**hkl**
4,53	19,58	24	002	4,42	20,1	64	001
4,02	22,08	100	111	3,56	25,0	100	101
3,68	24,16	36	012	3,06	29,1	47	111
3,12	28,55	85	020	3,00	29,8	24	200
2,95	30,26	19	021	2,21	40,7	38	002
2,57	34,78	13	022	1,96	46,2	31	112
2,18	41,46	8	104	1,90	47,9	5	310
2,13	42,46	11	-	1,82	50,0	8	301

Table A.5: Raman bands of different Vanadium/Phosphorus phases

VPO	>1200	1200- 1100	1100-1000	1000-900	900-400
$(VO)_2P_2O_7$		1190w,1135w, 1109w		930s, 920s	797vw, 457vw, 391vw, 274w
$(VO)HPO_4 \cdot 0.5H_2O$		1155m, 1110m	1009w	985vs, 915	517vw, 466w, 342m, 289w
$VOHPO_4 \cdot H_2O$			1002w	983w	888vs, 342w, 297m br
β $VOHPO_4 \cdot 2H_2O$		1121m,	1037w	969s, 927m sh	284m
α $VOHPO_4 \cdot 2H_2O$		1135w, 1117w	1048m br	930sh, 913vs	360w, 320w, 289m, 231m
$VOHPO_4 \cdot 4H_2O$			1084vs, 1055s,	998vs, 982vs	509s, 402m, 321s, 266vs
$VO(H_2PO_4)_2$		1151m br		935vs, 900m sh	575m, 224m,141m
$VO(PO_3)_2$	1271m, 1255s, 1216s	1109w	1065w	957vs	692m, 459w, 397w, 345w,
$V(PO_3)_3$	1229s, 1215s	1180m, 1127w	1070w, 1020w		669s, 503m, 420m, 395m
$VOPO_4 \cdot 2H_2O$			1039s	988m, 952vs	658w, 542s, 451w,
α_I -$VOPO_4$		1143w	1038s	965m, 944m, 928vs, 905w	663w, 579s, 541s, 458m, 433w, 302m
α_{II} -$VOPO_4$			1091s	993s, 979m, 945vs	650vw, 619w, 587w, 466m, 433m, 399m
δ-$VOPO_4$	1200vw		1090m, 1075m, 1020m	977w, 936s	655w, 590m, 482w, 444vw
β-$VOPO_4$		1110vw	1075s	997m, 986vs	892s, 804vw, 782vw, 741vw, 656m, 599m, 435s, 368m

γ-$VOPO_4$		1188w	1096s,1040s, 1022m	996w, 958m, 951vs	656s, 638w, 596s, 556w, 454m, 390s

w: weak, m: medium, s: strong

Part B

Selective oxidation of *o*-xylene to phthalic anhydride

1

INTRODUCTION

1.1 PHTHALIC ANHYDRIDE: PRODUCTION AND USES

Phthalic Anhydride, isobenzofuran-1,3-dione, is a white solid formed by needles or platelets.

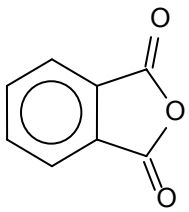

Figure 1.1: Phthalic Anhydride structure.

The most important physical-chemical characteristics of phthalic anhydride (PA) are listed in Table 1.1.

Table 1.1: Physical-chemical features of phthalic anhydride [1, 2].

Molecular Weight (g/mol)	148.12
Melting Point (°C)	131.6
Boiling Point (°C)	295.1
Combustion heat (KJ/g)	22.16
Explosion limits (%V)	Lower: 1.7 Upper: 10.5
Solubility in water (g/l at 25°C)	6
Density (g/cm^3 at 4°C)	1.527

1.1.1 Phthalic anhydride uses [1]

Total worldwide phthalic anhydride capacity amounts to a little over 5 million tons/year; around 60% of total global phthalic demand, approaching 3.7 million tons annually, is used to produce phthalate plasticisers with almost 15% going to both unsaturated polyester and alkyd resins manufacture [3].

As all cyclic anhydrides, phthalic anhydride is a reactive compound, but in addition, the otherwise very stable aromatic ring is capable of reaction. Phthalic anhydride reactions which have achieved commercial importance are summarized below.

1. The most important is the reaction with alcohols or diols to give esters or polyesters; unsaturated polyester resins are obtained by polycondensation in the presence of maleic anhydride or fumaric acid.
2. One or both of the carboxy groups can react with ammonia to give phthalic monoamide and phthalimide or phthalonitrile.
3. Phthalein and rhodamine dyes are obtained by reaction of phthalic anhydride with phenols, aminophenols or quinaldine derivatives.
4. The Friedel–Crafts reaction of PA with benzene derivatives followed by ring closure to form anthraquinone derivatives is of importance as a route to Indanthrene dyes.
5. Much attention has been devoted to the rearrangement of dipotassium phthalate to produce terephthalic acid, but due to technical problems the process is no longer used.
6. 3,5-Dihydrophthalic acid can be produced by electrochemical hydrogenation of phthalic anhydride; hydrogenation with a nickel catalyst produces phthalide.

1.1.2 Phthalic anhydride production [1]

Phthalic anhydride is predominantly produced on industrial scale by gas-phase oxidation of *o*-xylene or naphthalene; actually, over 90% of world production is based on *o*-xylene with the remainder using naphthalene feedstock [3].

The selective oxidation of naphthalene (Figure 1.2) was the most important production way of phthalic anhydride until 1960.

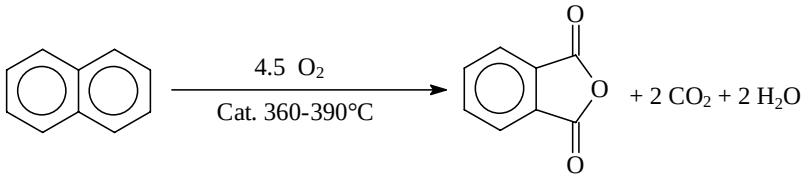

Figure 1.2: Selective oxidation of naphthalene to phthalic anhydride.

The reaction is carried out in gas phase in a multitubolar fixed bed reactor, using a catalyst based on V_2O_5 and TiO_2 deposited on an inert ring-type support. The heat of formation is 1788 KJ/mol, while the combustion heat reach 5050 kJ/mol. Depending on the yield achieved and the byproducts formed, a heat of reaction of 2100–2500 kJ/mol is expected. Besides maleic anhydride, naphthoquinone is also formed as a byproduct, which requires a high performance of the purification stage. According to the literature, yields of up to 102 wt% are achievable in commercial plants, but the final product yields generally do not exceed 98 wt%.

Starting from 1965, *o*-xylene became the most used feedstock for PA production. The changeover to *o*-xylene was inevitable because the quantities of naphthalene derived from coal tar depend on the production of coke and these were unable to keep pace with the increasing demand for naphthalene. Moreover, feeding *o*-xylene the number of byproducts is reduced, the yield by weight is increased and environmental problems are smaller. The reaction scheme is shown in Figure 1.3.

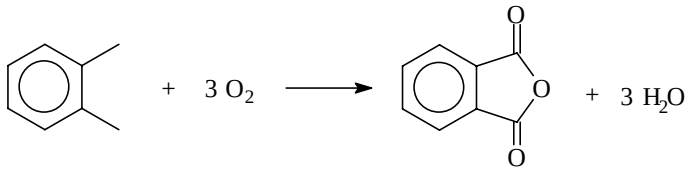

Figure 1.3: Selective oxidation of *o*-xylene to phthalic anhydride.

The reaction is carried out in multitubolar fixed bed reactor. Commercial catalysts are normally formed by a ring of inert material (such as steatite, alumina, etc…) on which is supported the real active phase, constituted of TiO_2, V_2O_5 and different promoters.

The formation heat of phthalic anhydride starting from *o*-xylene is -1108.7 kJ/mol, while the total combustion heat reaches values of -4380 kJ/mol; normally in the multitubolar reactor the reaction heat is about 1300-1800 kJ/ mol.

The best performing catalysts allow to reach yields about 115%wt, with a complete conversion of *o*-xylene (necessary also to avoid emission of *o*-xylene, not allowed for environmental laws) [4].

The most important gas-phase processes are described in the following section and differs from each other for:

- Feed (*o*-xylene or naphthalene or both)
- type of reactor (fluid or fixed bed)
- *o*-xylene concentration in feed (low or high)

Polynt Process

In the so called LAR (low air ratio) process high load of *o*-xylene is fed in the reactor (134 g/m^3). Also naphthalene could be used as staring material [5, 6].

Flow sheet is reported in Figure 1.4: air and *o*-xylene are mixed and preheated in a carburator before being fed in the multitubolar reactor; reaction temperature is kept constant by a fused salts circuit [7].

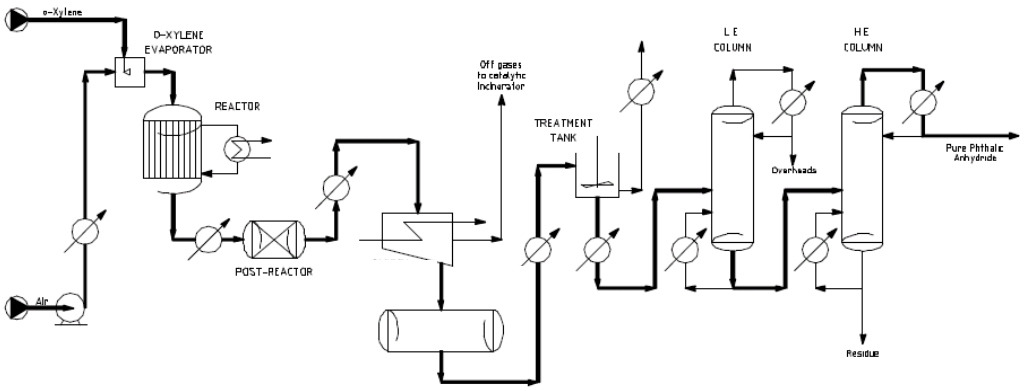

Figure 1.4: Flow sheet of Polynt Process [elaborated from 8].

BASF Process [1, 9]

The BASF Process is described in Figure 1.5. Preheated *o*-xylene is fed in a mulitubolar fixed bed reactor, temperature is maintained at 380°C through a fused salts circuit. The concentration of *o*-xylene in the feed is very variable, due to the use of a very active and selective catalyst formed of TiO_2 and V_2O_5 deposed on an inert and non porous support.

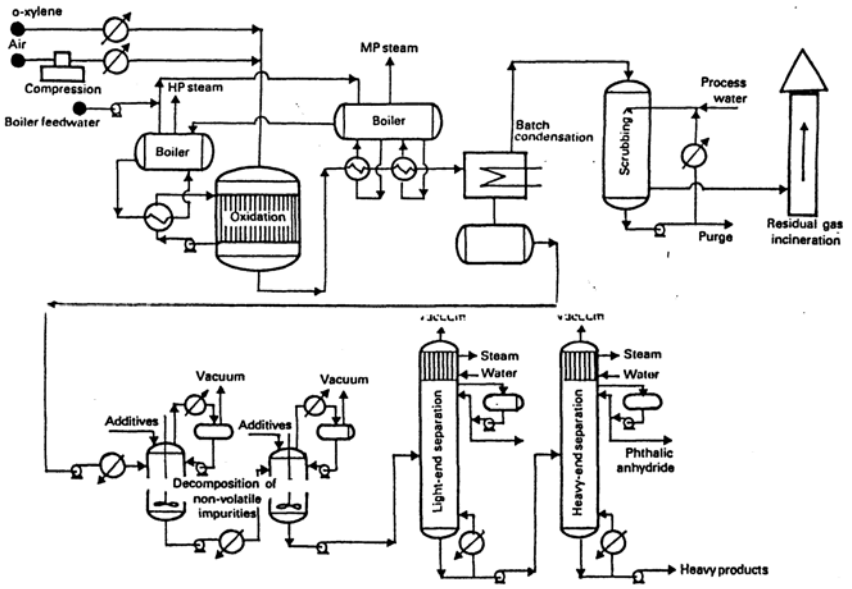

Figure 1.5: BASF process for production of phthalic anhydride in a fixed bed reactor [elaborated from 9].

Sherwin-Williams/Badger process

This is the only process carried out in a fluid bed (Figure 1.6).

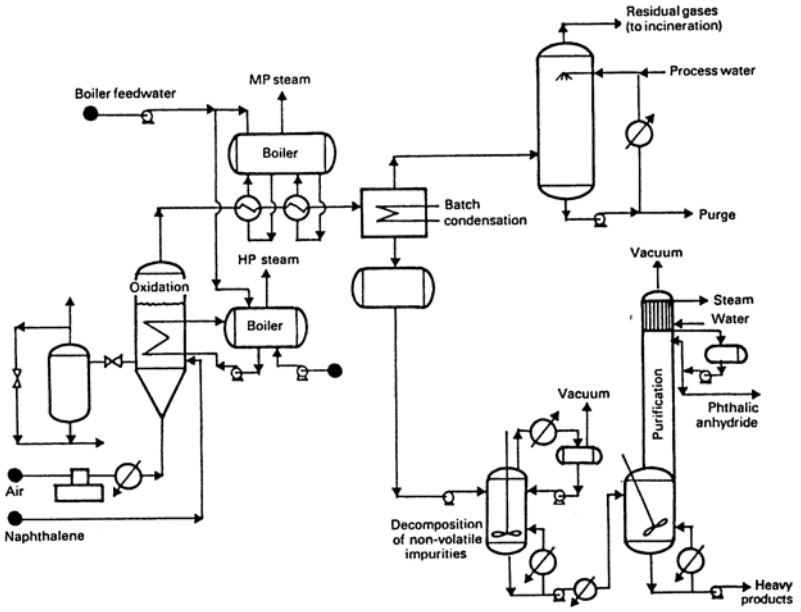

Figure 1.6: SherwinWilliams/Badger process for production of phthalic anhydride in a fluid bed reactor [elaborated from 9].

The starting material is naphthalene, the catalyst is a vanadium/titanium system supported on silica. The reaction temperature is very uniform, between 340 and 385°C, and no hot spots are present (contrary to the case of fixed bed process). Yield in phthalic anhydride is lower with respect to the one obtained in the fixed bed, mainly starting from *o*-xylene.

1.2 CATALYTIC SYSTEM

In the old processes ex naphthalene the catalyst was only formed by vanadium pentoxide [10], the use of *o*-xylene as starting material for the production of phthalic anhydride was possible only when a new generation of catalysts was introduced in the '60, constituted of spheroidal particles on which it was applied a thin thick of V_2O_5-TiO_2 [11-21]. The introduction of TiO_2 modified the activity allowing the feed of high volumes of *o*-xylene [22-31]. Today all the industrially used catalysts are based on V_2O_5 supported on TiO_2 and also different elements are added to promote the catalytic activity, the selectivity to phthalic anhydride and also the catalyst life. This active phase is sprayed on an inert support (rings or spheres) of ceramics or steatite; a very high amount of support, with respect to the real active phase, is necessary to dissipate the reaction heat and stabilize the thermal conditions of the catalyst. To bind the active phase to the support different kinds of binders are employed, normally formammide, acrylic or stearic acids.

The main characteristics of the industrial system are listed in Table 1.2.

Table 1.2: Characteristics of industrial TiO_2-V_2O_5.

%wt TiO_2	60-98
Crystalline phase of TiO_2	Anatase
%wt V_2O_5	2-15
Thick of catalytic layer (mm)	0.08-1.5
Support	Spheres or rings of porcelain, quartz or steatite
Dimensions of support (mm)	diameter: 4-12 hight: 6-12

1.2.1 Structural properties of V_2O_5-TiO_2 system

Despite the large number of studies dealing the catalytic system, it is not really clear how the behaviours of V_2O_5 are modified by the spreading on TiO_2 [32]. It is known that the interaction with the titania surface greatly affects the structural features and the reactivity of V_2O_5. Specific interaction oxide-oxide leads to dispersion of vanadium and favours the formation of a bidimensional structure, called monolayer [33-35]. Probably, the higher activity of supported systems is related to a variation of the bond energy between the oxygen and the catalyst surface [36].

Theoretical monolayer is calculated by a series of simplifications and geometrical approximations. It is supposed that only a type of surface sites geometry is present and that porosity does not affect the distribution of active species; actually, the system is constituted by different crystallographic planes, having different surface density [37]. Theoretical monolayer is also defined as the amount of V_2O_5 units necessary to completely cover the TiO2 surface (that is 0.146% by weight of V_2O_5 per m^2 of support) [38-39]. Different hypotheses have been formulated on the way in which vanadium dispersion takes place. Vejux e Courtine [40-41] have suggested a preferential interaction between (010) planes of V_2O_5 and (001) planes of TiO_2 anatase. This leads to an increase in surface density of V=O groups, that are considered the active sites for *o*-xylene oxidation.

For Kozlowski and co-workers [42] and Haber [43] the dispersion of vanadium oxide is due to a chemical reaction between V_2O_5 and TiO_2, with formation of isolated and polymeric V species (as example is reported the formation of VO_4 units, having two terminal oxygen atoms in the group V=O and two bridge oxygen atoms in the group V-O-Ti).

Using characterization tecniques such RAMAN Spectroscopy [39, 44-47], UV-Vis Spectroscopy [48], FT-IR Spectroscopy [49,50], TPR-O [51-55], different vanadium species have been identified on TiO_2 surface (Figure 1.7).

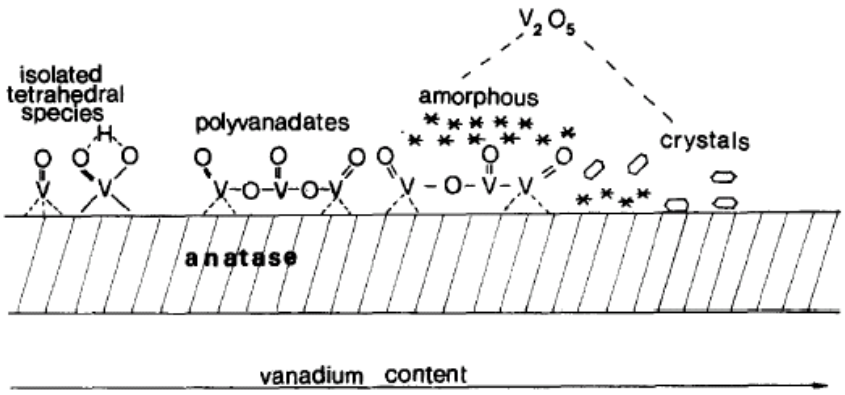

Figure 1.7: Schematic representation of the different vanadium species present on TiO_2 anatase as function of V content [55].

Three different vanadium species could be identify:

- ✓ monomeric and isolated VO_X species, strongly bonded to the support;
- ✓ polymeric $[VO_x]_n$ species, bonded with the surface;
- ✓ cristalline or amorphous V_2O_5.

At very low vanadia content (about 10% of the monolayer), only isolated vanadium species are observed. With increase in loading, beginning from about 20% of the mnl the appearance of polymeric species has been observed. At loading exceeding 1 mnl amorphous and crystalline V_2O_5 are also observed [55].

Very few works were dealing with the correlation of catalytic performances with the presence of different kinds of vanadium. It was found that polyvanadate are more active than V in bulk vanadia and for lower amount of vanadium the terminal V=O oxygen is more active then the bridged V-O-Ti oxygen [37]. In a recent work [56], it was reported that monomeric vanadyl (V=O) is the most active specie in the selective oxidation of toluene to benzoic acid, and that it is the species responsible for the catalytic activity of V/Ti/O in this reaction. Bond and co-workers [23,38,57] showed that very good catalytic performances in *o*-xylene oxidation could be obtained at vanadia loading corresponding approximately to a monolayer.

1.2.2 Redicibility of V/Ti catalysts

Reduction of V/Ti/O catalysts has been studied by means of thermogravimetric tecniques [43], reduction in programmed temperature [23,45,52-55] or using

hydrogen or CO as reducing agent [55]. All authors agreed that the lower is the vanadium content, the higher is its reducibility.
Following this rule the reducibility scale of Vanadium is:

monolayer > polyvanadates > amorphous or cristalline V_2O_5

In the '80 a very deep work was done on V/Ti/O system; so called "EUROCAT" catalysts were analyzed and tested in the *o*-xylene oxidation in different European laboratories [58]. Two V/Ti/O samples with the same TiO_2 surface area (10.3 m^2/g) and different vanadium content (1%wt and 8%wt V_2O_5) were prepared. On these samples also reduction in programmed temperature analysis were carried out [54].
The three different kinds of vanadium were distinguished by TPR, due to their different reduction temperatures [53,54,59-60]:

- isolated monomeric species show a maximum reduction peak above 500 – 510 °C
- reduction of polymeric specie occurs at 540 °C
- V_2O_5 is reducible only starting from 580°C

The identification of monomeric species from polyvanadates by TPR is quite complex, but it is possible to solubilize polymeric species and V_2O_5 with diluted HNO_3; with this treatment only isolated vanadium (not soluble in acid ambient) remains on the surface and in this case only a reduction peak at low temperature is visible [59]. From all these considerations, it seems that terminal V=O oxygen atoms are easily removed from the surface with respect to V-O-V oxygen. As the rate limiting step is (under normal conditions) the break of C-H bond, the most active samples may present more isolated vanadium than polyvanadates or V_2O_5.

1.2.3 Vanadium oxidation state

Vanadium oxidation state in V/Ti/O systems, particularly at low vanadia content, is a controversial subject. Some authors [23,61] agreed that monolayer contains only V^{5+}; on the contrary, it has been demonstrated by UV-Vis spectroscopy [62,63] and ESR [64,65] that also in fresh samples vanadium is partially reduced.
Most authors agreed that the soluble vanadium species are mainly in the 5+ oxidation state; while oxidation state of insoluble V species is a point of discussion. Trifirò and co-workers [65] maintain that in the insoluble V species

only V^{4+} is present. For Gasior [66] e Anderson [67] in the monolayer only 20% of vanadium is in a reduced form.

1.2.4 Comparison between V_2O_5 supported on TiO_2 anatase and rutile

Several studies have demonstrated a decrease of activity and selectivity of V/Ti/O system for temperatures higher than 500°C [16,68]. This effect is due to:

- ✓ decrease of catalyst surface area
- ✓ transformation of TiO_2 anatase to rutile, promoted by the presence of V and followed by partial reduction of vanadium atoms
- ✓ decrease of active site, because of incorporation of reduced V ions into rutile lattice

In general, V/Ti/O catalysts on anatase are more active and selective with respect to V/Ti/O on rutile [69,70]. This is due to the better spreading of V_2O_5 on anatase, while on rutile V^{4+} are incorporated in the lattice; in this case vanadium is more stable toward oxidation and reduction, and so less active. Therefore, properties of vanadium on rutile are similar to which of pure V_2O_5.

1.2.5 Role of dopants

Industrial V/Ti/O systems always contain a low amount of promoters, generally less than 1%wt. The role of these components is to improve selectivity to phthalic anhydride, avoiding total combustion to CO and CO_2 and limiting the presence of reaction intermediates; moreover, promoters can increase activity or catalyst life avoiding phase transition from anatase to rutile.

An important parameter which determine type and amount of promoters is the Tamman temperature, T_T [71]

$$T_T = (T_M + 273)/2 - 273$$

in which T_M is the melting temperature (in °C) of promoter. For V_2O_5-TiO_2 system, Tamman temperature can not exeed 500°C.

The most used promoters are oxides or salts of Na, K, Rb, Cs, Sb, Sn, Nb, P, Mo; each elements has a particular role, for example:

- potassium and cesium improve selectivity to phthalic anhydride, decreasing activity;

- molibdenum stabilizes anatase form and increases catalyst activity and selectivity;
- silver increases selectivity limiting total oxidation of *o*-xylene to CO_x.

Deo e Wach**s** [18] studied the effect of several dopants on V/Ti/O system. Two classes of additives have been found:

- non interacting dopants (such as WO_3, Nb_2O_5, SiO_2) which coordinate only to the support, not changing the bond length of vanadia species;
- interacting dopants (K_2O and P_2O_5) coordinated to V ion which greatly affect redox properties of the system.

Van Hengstum et al. [72] studied the effect of K and P: the presence of P causes an increase of surface acidity, while K modifies the nature if active sites. Other studies showed that K easly interacts with vanadium forming KVO_3. This leads to a decrease of vanadium reducibility, that means lower catalyst activity and higher selectivity to phthalic anhydride [23,73].

The addition of Cs oxide causes a change in the rate-determining step of the reaction [74]. With the unpromoted catalyst the rate-determining step is the reduction of the active site by *o*-xylene, while with the Cs-promoted catalyst, vanadium re-oxidation becomes the rate-determining step of the reaction. On the other hand, the presence of increasing amounts of Cs accelerates the re-oxidation of reduced V sites by O_2.

Antimony enhances catalyst activity, maintainig a higher dispersion of vanadium oxide and a high surface concentration of isolated sites [74,75].

It is clear that the role of promoters is crucial to improve process performance[18,76]. In the industrial catalytic, which is subdivided into several different layer, the relative amount of all the components is optimised for each catalyst layer. In fact, the effect of the promoters may differ in relation to the gas-phase composition; moreover in each section of the reactor, different stages of the reaction require that catalyst components facilitate specific steps in the reaction network. Table 1.3 compares a few patents from the literature [77-79]; the amount of every component is reported for each catalytic layer in a three-bed reactor.

Table 1.3: Catalyst compositions for V/Ti/O catalysts used in *o*-xylene oxidation, in each layer of a three-bed reactor with downstream flow.

	Ref 77	Ref 78	Ref 79
Component, wt%	**Top layer**		
TiO_2	95,60	91,92	90,10
V_2O_5	4,00	4,84	7,12
Cs_2O	0,54	0,62	0,35
Sb_2O_3	-	1,93	2,37
P_2O_5	-	0,29	-
K_2O	-	0,01	-
Nb_2O_5	-	0,39	-
	Middle layer		
TiO_2	89,05	92,05	88,91
V_2O_5	7,50	4,84	7,12
Cs_2O	0,14	0,48	0,10
Sb_2O_3	3,20	1,94	2,37
P_2O_5	0,34	0,29	0,92
K_2O	-	0,01	-
Nb_2O_5	-	0,39	-
	Bottom layer		
TiO_2	90,30	92,30	78,63
V_2O_5	7,00	4,86	19,81
Cs_2O	-	0,21	-
Sb_2O_3	2,50	1,94	-
P_2O_5	0,46	0,29	1,03
K_2O	-	0,01	-
Nb_2O_5	-	0,39	-

The three layers may contain different amounts of vanadium oxide, with the catalyst in the top layer having the lowest amount. In such a case, the catalyst is designed so as to maintain a lower temperature in the hot-spot, distribute the reaction heat more evenly all along the reactor, and to have a positive effect on the catalysts' lifetime. The amount of cesium oxide decreases from the top downwards, to the bottom layer.

In the third (bottom) layer the main requisite is to convert as much of the *o*-xylene as possible (environmental legislation in Italy allows no more than 50 ppm of residual hydrocarbon to be released in the stream vented into the atmosphere), while limiting the oxidative degradation of intermediates and PA. Fore this reason the amount of Sb, promoter of activity, increase along the catalytic bed.

1.2.6 Deactivation and regeneration

One of the most important causes of catalyst deactivation is the reaction temperature: temperature profiles are depending on several process parameters, such as salts bed temperature and *o*-xylene concentration [58].

The high reaction temperatures are the main cause of the rutilization of TiO_2 anatase: Courtine and Vejux [40] have determined the activation energy of anatase-rutile phase transition in TiO_2-V_2O_5 (15 kcal/mol), but in absence of V_2O_5 the transformation occurs at higher temperature and with a higher activation energy (150 kcal/mol) [80]. In practice, V_2O_5 catalyzes the TiO_2 rutilization [41, 81]: Grzybowska [49] and co-workers have observed that V could migrate inside the titania lattice and at the same time the rutilization occurred, with the formation of solid solution of V^{4+} in TiO_2 rutile. The presence of this solid solution of V^{4+} in rutile is, for Schulz and co-workers [82], the cause of catalytic activity decreasing, because of V^{4+} is more stable to oxidation.

1.3 REACTION SCHEME AND MECHANISM

1.3.1 Reaction scheme

The *o*-xylene oxidation is a quite complex reaction, which involves different intermediates and includes different steps. In this reaction 12 electrons are involved: 6 hydrogen atoms are extracted from the organic molecule, while 3 oxygen atoms are added.

The reaction intermediates are o-toluic aldheyde, o-toluic acid and phthalide, while by-products are CO and CO_x and also maleic anhydride and benzoic acid, the last two in low amounts.

Different hypotheses of reaction mechanism have been formulated; due to the different reaction conditions and also the different employed catalyst

(promoters, surface area, etc.), comparisons between the proposed mechanisms are very difficult.

In the scheme reported in Figure 1.8 the different possible steps are summarized.

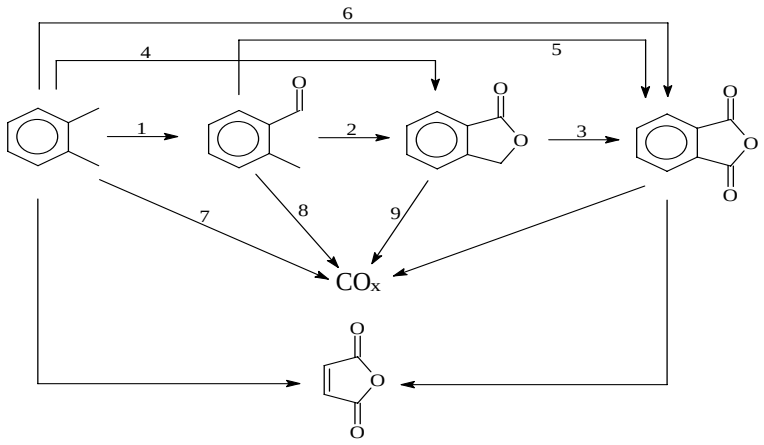

Figure 1.8: Reaction scheme proposed in the literature [55,83].

Different authors agree that phthalic anhydride is formed in two different ways: directly from *o*-xylene (step 6) or through the different intermediates (steps 1, 2, 3 and 5 in Figure 1.7) [84-88]. On the contrary, for Anastasov et al. [25], the only possible way to produced phthalic anhydride is passing through the intermediates (step 1, 2, 3). All the authors agree that CO_x are coming not only from *o*-xylene, but also from all the others organic molecules [89-94]. In a paper is reported that reaction to phthalic anhydride and maleic anhydride are competitive and so parallel [92].

1.3.2 Reaction mechanism and active sites

In general all authors are in agreement, that at least three different sites have to be present on the catalytic surface:

- ✓ sites in which the C-H bond is activated (in quite all oxidation processes this is the rate limiting step)
- ✓ sites for the Oxygen insertion
- ✓ re-oxidation sites (in which the molecular oxygen has to be adsorbed)

The *o*-xylene oxidation follows the Mars and Van Kreveken mechanism [93]. It was demonstrated that the lattice oxygen present on the surface is the active site for the C-H broken. After this step the oxygen atom is inserted in the molecules and finally the catalyst is reoxidized by the molecular oxygen fed with *o*-xylene.

The nature of the real active phase was studied by different authors, with different results:

- For Courtine [28,41] and Murakami the active sites are V=O groups, present on the TiO_2 surface in the 010 plan of V_2O_5.
- For others authors the real active sites are $[VO_x]_n$ species present on the TiO_2 surface. In particular, for Bond [94] the only active site is an oxo-hydroxy $O=V_5$-OH group, while other authors think that polyvanadates could be the real active sites [45,46].
- Finally, for Trifirò and co-workers [65] the atoms forming the monolayer are not active in the *o*-xylene oxidation, while are used as "secondary support" for three-dimensional layer of V_3O_7.

Anyway, all the hypotheses underline the key role of V=O group in the different kind of vanadium (isolated or polyvanadates).

As proposed by Bond, four different Vanadium sites could participate in the reaction (from A to D in Figure 1.9).

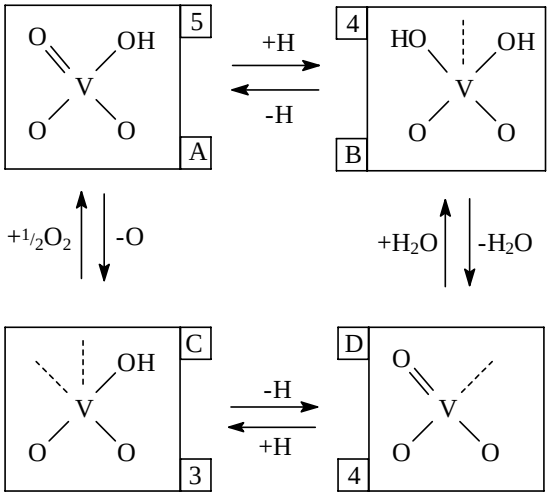

Figure 1.9: structure of different active species. Numbers represent the Vanadium oxidation state, while dotted lines are the possible bonding points for methyl groups [99].

Site A is the most predominant one and actively participates in the reaction, while site B is the initial form of V/Ti/O [94]. The H atoms are originally in the methyl groups of *o*-xylene; the re-oxidation of the reduced species C by molecular oxygen is relatively fast and not rate-determining, since the order in Oxygen is

about 0.5 suggesting that reaction of second order an "adsorbed" O atom, as in species A, with an adsorbed *o*-xylene molecule is the rate-limiting step. Structures A and B would have tetrahedral geometry. These reactive groups are chemically bonded to the anatase support, the electrical conductivity of which is thereby affected. One important consequence of this catalytic structure is that all the chemical action has to occur in or on the monolayer, re-oxidation of which must take place with gaseous molecular O and not by lattice oxide ions diffusing from below.

1.4 REFERENCES

[1] Ulmann's Chemical Encyclopedia, Vol A20, page 182.

[2] MSDS of Phthalic Anhydride.

[3] Tecnon Orbichem, London SW11 3TN, UK

[4] T. Heidemann, H. Wanjek, EP1084115 assigned to BASF AG

[5] Alusuisse Italia S.p.A., EP 37492, 1980 (A. Neri et al.).

[6] Alusuisse Italia S.p.A., US 4489204, 1980 (A. Neri et al.).

[7] I. Pasquon, GF. Pregalia: Prodotti e processi dell'industria chimica.

[8] www.polynt.com

[9] A. Charevel, G. Lefebvre: Petrochemical Process major oxygenated, clorinated and nitrated derivates.

[10] H. Sutter, Phthalsaureanhydride, Munchen Verlag, 1973.

[11] G.C. Bond, A.J. Sarkany, G.D. Parfitt, J. Catal., 57 (1979) 476.

[12] A.J. Van Hengstun, J.C. Ommen, H. Bosh, P.J. Gellings, Appl. Catal., 8 (1983) 369.

[13] S. Lars, J. Anderson, J. Chem. Soc. Farad. Trans. I, 75 (1979) 1356.

[14] A. Andersson, S.T. Lundin, J. Catal., 65 (1980) 9.

[15] A. Andersson, S.L.T. Andersson, in Solid State Chemistry and Catalysis, R.K. Grasselli, J.F. Brazdil Eds., American Chemical Society Pub.: Washington D.C. 1985, ACS Series nr. 279, page 121.

[16] B. Grzybowska, M. Czerwenska, J. Sloczynski, Catal. Today, 1 (1987) 157.

[17] G. Deo, I. E. Wachs, J. Catal., 129 (1991) 307.

[18] G. Deo, I. E. Wachs, J. Catal., 146 (1994) 323.

[19] G. Busca, A. S. Elmi, P. Forzatti, J. Phys. Chem., 91 (1987) 5263.

[20] A.S. Elmi, E. Tronconi, C. Cristiani, J.P.C. Martin, P. Forzatti, G. Busca, Ind. Eng.Chem. Res., 28 (1989) 387.

[21] W.E. Slinkard, P.B. Degrott, J. Catal., 68 (1981) 423.

[22] G.C. Bond, S. Flamerz, R. Shukri, Farad. Discuss. Chem. Soc., 87 (1989) 65.

[23] G.C. Bond, S.F. Tahir, Appl. Catal., 71 (1991) 1.

[24] J.P. Gellings, in Specialist Periodical Report-Catalysis, G.C. Bond, G. Webb Eds., Royal society of Chemistry, London 1985, Vol. 7, p. 105.

[25] V.N. Nikolov, D. Klissurski, A Anastasov, Catal. Rev.-Sci. Eng., 33 (1991) 319.

[26] M.S. Wain Wright, N.R. Foster, Catal. Rev.-Sci. Eng., 19 (1979) 211.

[27] J. Haber, Pure Appl. Chem., 56 (1984) 1663.

[28] P. Courtine, in Solid State Chemistry in Catalysis, R.K. Grasselli, J.F. Brazdil Eds., American Chemical Society Pub.: Washington D.C. 1985, ACS Series nr.279, page 37.

[29] G. Deo, I.E. Wachs, J. Haber, Crit. Rev. Surf. Chem., 4 (1994) 141.

[30] B. Grzyboska, J. Haber, in Vanadia Catalysts for Processes of Aromatic Hydrocarbons, Polish Scientific Pub., Krakow, 1984.

[31] G. Centi, S. Perathoner, F. Trifirò, Res. Chem. Intermediates, 15 (1991) 49.

[32] M. Gasior, B. Grzybowska, Vanadia Catalysts for processes of oxidation of aromatic hydrocarbons (B.Gryzbowska-Swierkosz e J.Haber eds.), Warszawa, 1984, p.133

[33] D. Honicke, J. Xu, J. Phys. Chem., **92** (1988) 4699.

[34] J. Haber, Proc. 8th International Congress on Catalysis, Berlin 1984, Dechema Pub., Frankfurth AM 1994, Vol.1, p. 85.

[35] Y.C. Xie, Y.Q.Y. Tang, Adv. Catal., **37** (1990) 221.

[36] G. Louguet, Ph.D. Thesis, L'Universite de Poitiers (1972)

[37] G. Centi Appl. Catal. A: General 147 (1996)267-298.

[38] G. C. Bond, K. Bruckmann, K. Faraday Discuss. Chem. Soc., **72** (1981) 235.

[39] F. Roozeboom, C. Mittelmejer-Hazeleger, A. Moulijn, J. Medema, V. H. J. de Beer, P. J. Gellings, J. Phys. Chem., **84** (1980) 2783.

[40] A. Vejux, P. Courtine, C.R. Acad. Sci. Ser.C., **286** (1978) 135.

[41] A. Vejux, P. Courtine, J. Solid State Chem., **23** (1978) 93.

[42] A. Kozlowski, R. F. Pettifer, J. M. Thomas, J. Phys. Chem., **87** (1963) 5176.

[43] J. Haber, A. Kozlowska, R. Kozlowski, J. Catal., **102** (1986) 52.

[44] G. Deo, I.E. Wachs, J. Haber, Crit. Rev. Surf. Chem., **4** (1994) 141.

[45] G.T. Went, L. J. Leu and Bell, J. Catal., **134** (1992) 479.

[46] G.T. Went, S.T. Oyama and A. T. Bell, J. Phis. Chem. **94** (1990) 4240.

[47] T.Machej, J. Haber, A.M. Turek and J.E.Whacs, Appl. Catal., **70** (1991) 115.

[48] K. Dyrek, E. Serwicks and B. Gzybowska, React. Kinet. Catal. Lett., **10** (1979) 93.

[49] J. Gasior, M. Gasior, B. Gzybowska, R. Kozlowski and J. Sloezynski, Bull. Acad. Polon. Sci, Ser. Chim., **27** (1979) 829.

[50] M. Gasior and B. Gzybowska, Bull. Acad. Polon. Sci, Ser. Chim., **27** (1979) 835.

[51] D.A. Bulushev, L.Kiwi-Minsker, F. Rainone and A. Renken, J. Catalysis **205**, 115.

[52] R. A. Koeppel, J. Nickl, A. Baiker, Catalysis Today, **20** (1994) 45.

[53] S. Besselmann, C. Freitag, O. Hinrichsen and M. Muhler, Phys. Chem., 2001, 3, 4633.

[54] G.C. Bond, J.C. Vedrine, Catalysis Today **20** (1994) 171.

[55] B. Grzybowska-Swierkosz Appl. Catal. A: General **157** (1997) 263.

[56] C. Freitag, S. Besselmann, E. Löffler, W. Grünert, F. Rosowski, M. Muhler, Catal. Today, 91–92 (2004) 143.

[57] G.C. Bond and E König, J. Catal., 77 (1982) 309.

[58] V. Nikolov, D. Klissurski, K. Hadjiivanov, in Catalyst Deactivation (1987), Proc. 4-th Int. Symp., Antwerp, Sept. 29-October 1, (B. Delmon and G. Froment, eds.) Elsevier, Amsterdam, 1987, p.173.

[59] D.A. Bulushev, L.Kiwi-Minsker, F. Rainone, A. Renken, J. Catal. 205 (2002) 115.

[60] R. A. Koeppel, J. Nickl, A. Baiker, Catal. Today, 20 (1994) 45-52.

[61] M.G. Nobbenhuis, P. Hug, T.Mallat and A. Baiker, Appl. Catal. A, 108 (1994) 241.

[62] G. Busca and E. Giamello, Mater. Chem. Phys., 25 (1990) 475.

[63] G. Busca, L. Marchetti, G. Centi and F. Trifirò, J. Chem. Soc. Faraday Trans. I, 81 (1985) 1003.

[64] M. Rusiecka, B. .Gzybowska and M. Gasior, Appl.Catal., 10 (1984) 101

[65] G. Centi, E. Giamello, D. Pinelli, F. Trifirò, J. Catal, 130 (1991) 220
G. Centi, D. Pinelli, F. Trifirò, D. Ghoussoub, M. Guelton, L. Gengembre, ibid. 130 (1991) 238.

[66] M. Gasior, I. Gasior and B. Gzybowska, Appl. Catal., 10 (1984) 87.

[67] M. Inomata, K. Mori, A. Miyamoto, T. Ui, Y. Murakami, J. Phys. Chem., 87 (1983) 754 and references therein.

[68] R.Y. Saleh, I.E. Whacs, S.S. Chan and C.C. Chersich, J. Catal., 98 (1986).

[69] M. Sanati, L. R. Wallenberg, A. Andersson, S. Jansen, Y. Tu, J. Catal., **132** (1985) 128.

[70] L. R. Wallenberg, M. Sanati, A. Andersson, J. Catal., **126** (1991) 246.

[71] W. Adamson, Physical Chemistry of Surfaces, 3rd ed., Wiley, New York, 1976, p.250.

[72] A. van Hengstum,J. Pranger, V Fedorov, Neftekhim 17 (1977) 34.

[73] H. Eckert, G. Deo, I. E. Whacs, A.M. Hirt, Colloids surf. 45 (1990) 347.

[74] S. Anniballi, F. Cavani, A. Guerrini, B. Panzacchi, F. Trifirò, C. Fumagalli, R. Leanza, G. Mazzoni, Catal. Today 78 (2003) 117

[75] F. Cavani, C. Cortelli, A. Frattini, B. Panzacchi, V. Ravaglia, F. Trifirò, C. Fumagalli, R. Leanza, G. Mazzoni, Catal. Today 118 (2006) 298

[76] B. Grzybowska-Swierkosz, Topics Catal. 21 (2002) 35

[77] P. Reuter, G. Voit, T. Heidemann (2004) US Patent 6,774,246, assigned to BASF

[78] M. Okuno, T. Takahashi (2000) Eur Patent 1,063,222, assigned to Nippon Shokubai

[79] S. Neto, J. Zühlke, S. Storck, F. Rosowski (2005) WO Patent Appl 2005/011862, assigned to BASF

[80] R. Shanon, J. Pask, Amer. Mineral., 49 (1964) 1707.

[81] D. J. Cole, C.F. Cullis, O. J. Hucknall, J. Chem. Soc. Farad. Trans., 1 (1976) 2185.

[82] R. Haase, U. Illgen, J. Scheve, I. W. Schulz, Appl. Catal.,19 (1985) 13.

[83] R.Y.Saleh, I.E.Wachs, Appl.Catal., 31 87 (1987).

[84] P.H. Calderbank, Chem. Eng. Sci., 32 (1977) 1435.

[85] A. Yabrov, A. Ivanov, React. Kinet. Catal. Lett., 14 (1980) 347.

[86] K. Chandrasekharan, P. Calderbank, Chem. Eng. Sci., 35 (1980) 1523.

[87] O. Il'inich, G. Boreskov, A. Ivanov, V. Lyahova, H. Belyaeva, Neftekhimia, 18 (1978) 270.

[88] J. Skrzypek, Chem. Eng. Sci., 40 (1985) 611.

[89] T. Sato, Y. Nakanishi, K. Maruyama, T. Suzuki, U.S. Patent 4481304 (1984) assigned to Nippon Shok. Kag. Kog. Co.

[90] J.K. Burdett, T. Hughbanks, G.J. Miller, J.W. Richardson Jr., J.V. Smith, J. Am. Chem. Soc., 109 (1987) 3639.

[91] F. Cavani, E. Foresti, F. Parrinello, F. Trifirò, Appl. Catal., 38 (1988) 311.

[92] G. Busca, Catal.Today, 27 (1996) 457.

[93] P. Mars, D. van Krevelen, Chem. Eng. Sci. Spec. Supl., 3 (1954) 41.

[94] G.C. Bond, J. Catal., 116 (1989) 531.

2

EXPERIMENTAL

2.1 CATALYSTS SYNTHESIS

Catalysts were prepared by the wet impregnation technique: an aqueous solution containing the desired amount of NH_4VO_3 (and $CsNO_3$, when necessary) was added to the support (TiO2 anatase, having a specific surface area of 22.5 m^2/g). Water was evaporated under mild evacuation at 70°C. The wet solid was dried at 150°C for 3h, and calcined at 450°C for 5h in static air, with the following steps:

- 10° C/min from room temperature to 150°C
- at 150° C for 3 h
- 10° C/min from 150°C to 450°C
- at 450°C for 5h

During the thermal treatment the ammonium metavanadate was transformed into V_2O_5 and released ammonia and water:

$2\ NH_4VO_3 \rightarrow V_2O5 + 2\ NH_3 + H_2O$

Samples were loaded in the reactor in form of pellets with a diameter between 590 and 250 μm (30-60 mesh).

2.2 SAMPLES CHARACTERIZATION

FT-IR Spectroscopy

The IR-spectra were recorded using a FT-IR Perkin-Elmer spectrometer, with the KBr method, with a resolution of 4cm^{-1}, using 10 scansions, between 4000 and 400 cm^{-1}.

UV-VIS Spectroscopy

UV-Vis spectra were recorded in diffuse reflectance using a Perkin-Elmer UV/VIS/NIR Lambda 19 instrument, equipped with an integrating sphere, between 190 and 1500 nm. After recording, spectra were transformed in F(R) by the Kubelka-Munch law.

RAMAN Spectroscopy

Raman studies were performed using a Renishaw 1000 instrument, equipped with a Leica DMLM microscope, laser source Argon ion (514 nm) with power <25 mW. Generally for all samples different spectra were recorded. "*In-situ*" analysis were performed using a commercial Raman cell (Linkam Instruments TS1500).

Specific surface area

The specific surface area was determined by N_2 adsorption at 77K (the boiling T of nitrogen), with a Sorpty 1700 Instrument (Carlo Erba), using BET equation.

X-Ray Diffraction

The XRD measurements were carried out using a Philips PW 1710 apparatus, with Cu K_α (λ = 1.5406 Å) as radiation source in the range of $5°<2\theta<80°$, with steps of 0.1 grade and acquiring the signal for 2 seconds for each step.
Reflects attribution was done by the Bragg law, using the d value. ($2d\ sen\theta = n\lambda$)

2.3 CATALYTIC TESTS

2.3.1 Bench scale plant

Catalytic tests were carried out in a continuous-flow, fixed bed, stainless steel reactor. Different parameters could be varied, such as the feed composition, residence time and temperature inside the reactor

The laboratory plant is schematized in Figure 2.1 and could be divided in three main different parts:

4) "feed"
5) "reaction"
6) "downstream"

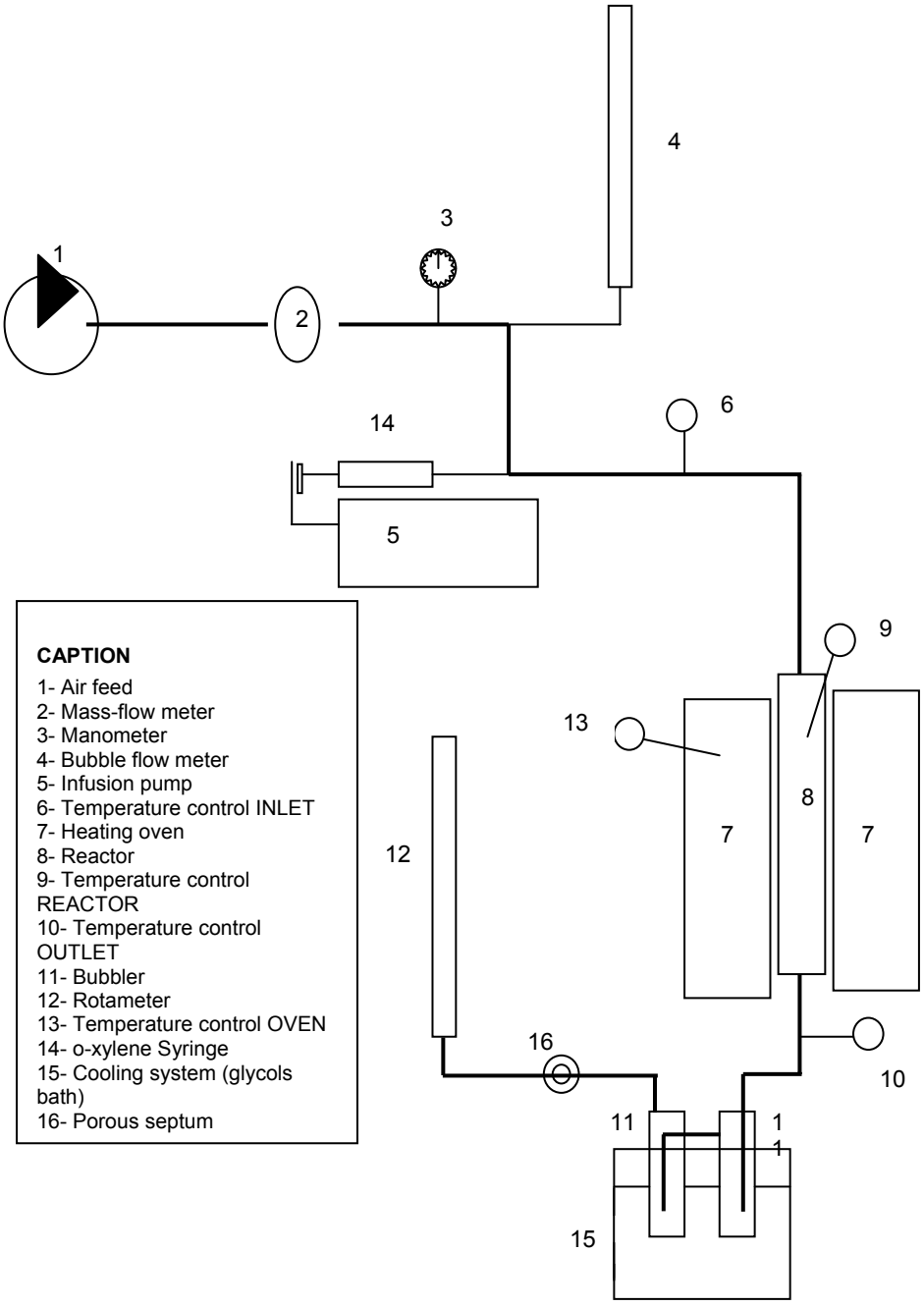

Figure 2.1: Scheme of the bench scale plant.

1) Feed:

Air was coming from an apposite bottle and the flux was regulated by a mass flow meter, while *o*-xylene was fed through a high precision infusion pump. The pipe was heated at 150°C to allow the vaporization of *o*-xylene.

2) Reaction:

The fixed bed reactor was constituted by a stainless pipe with a diameter of ¼ inches and of 25 cm length. Inside the reactor a bed of corundum was loaded, to allow the positioning of the catalyst in the isothermal zone. The reactor was located inside an oven that allows the heating up to a 450°C. The catalytic bed temperature was controlled by a thermocouple. The outlet was maintained at 280°C, thanks to the presence of a heating string, temperature of which was also controlled by a thermocouple.

3) Downstream:

Products in the outlet stream were condensed in acetone; all the organic compounds (and the non reacted *o*-xylene) were collected for at least 30 minutes. After the bubbler it was possible to sample incondensable products (such as unreacted air, CO, CO_2), using a syringe of 500µl volume, through a porous septum.

2.3.2 Analytical system

The quantitative analysis of products (and non converted *o*-xylene) was done by gas chromatography using the internal standard method. The outlet gas was collected in acetone, cooled by a glycol bath. After the desired time, the content of the bubbler was transferred in a 100 ml glass reactor, in which 50 µl of tridecane (the internal standard) were added.

By gascromatography were analyzed reactants and products. In the FISONS Instruments GC MEGA 2 two different columns were located:

1) Semicapillar CP-Sil8 column, of 30 m length, with an internal diameter of 0.53 mm and stationary phase of 5% diphenyl methylsiloxane. In this column were separated all the organic compounds, the connected detector being a FID.

2) Packed Carbosieve SII column, of 2 m length, with a stationary phase formed by active carbons. In this column CO, CO_2, H_2O, O_2 and N_2 were separated and detected by a TCD.

For both columns Helium was employed as carrier gas.

The oven temperature program was: 5 minutes at 45°C, heating up to 100°C (heating rate of 20°C/min), isothermal step at 100°C for 2 minutes, heating at 220°C (heating rate of 30°C/min) and final isothermal step at 220°C for 5 minutes.

Phthalic acid was quantified by titration with a solution of triethylamine in acetone (0.007 mol/l), using bromophenol blue as indicator.

3

THE ROLE OF VANADIUM OXIDE LOADING ON V/Ti/O REACTIVITY

3.1 INTRODUCTION

The main component of the industrial catalyst for *o*-xylene oxidation to phthalic anhydride is vanadium oxide, dispersed over TiO_2 anatase support. The amount of vanadium oxide loading is one important parameter [1-12]; in fact, as described in Chapter 1 it affects the kind of V species which develops on the titania surface. The interaction between vanadium oxide and titania generates: (i) V species that are chemically bound to the support via oxo bridges (isolated V in octahedral or tetrahedral coordination, depending on the hydration degree), (ii) polymeric species spread over titania, and (iii) bulk vanadium oxide, either amorphous or crystalline The relative amount of the different V species is a function of the surface area of support and of the vanadium loading. At low vanadium loading only isolated or polymeric V species are formed, which generate the so-called monolayer; a further increase of V content leads to the segregation of bulk V_2O_5. Experimental determinations agree that for the TiO_2 support, the monolayer corresponds to approx 7.9 V atoms per nm^2, that is about 0.146 wt% V_2O_5 per square meter of titania [13-16].

Industrial catalyst has to be designed to maintain a lower temperature in the hot-spot, distribute the reaction heat more evenly all along the reactor, and to have a positive effect on the catalysts lifetime. For this reason, catalytic bed is constituted by different layers which may contain different amounts of vanadium oxide, with the catalyst in the top layer having the lowest amount [17-20].

Vanadium loading is usually comprised between 5 and 10 wt% V_2O_5 (titania surface areas range between 15 and 30 m^2/g); these values are close to or higher than that one corresponding to the monolayer coverage of the support. This is necessary in order to minimize the reactivity contribution of the bare support that can be detrimental for the selectivity to phthalic anhydride. Furthermore, it is believed that a high surface density of vanadium ions sites is necessary for this complex reaction, which requires the transfer of several O^{2-} species from the solid to the alkylaromatic. It is clear that a better comprehension of the specific reactivity of each kind of vanadium is not only interesting from the scientific point of view, but could also be extremely useful to design a better catalyst and improve catalytic performances of industrial systems.

This section of my thesis is dedicated to the study of the effect of V loading, with the aim of find a correlations between V/Ti/O catalytic activity and the amount of the different vanadium species.

3.2 EXPERIMENTAL

Catalysts were prepared with the wet impregnation technique: an aqueous solution containing the desired amount of NH_4VO_3 was added to the TiO_2 support (anatase, s.s.a. 22.5 m^2/g). After evaporation of water the solid calcined at 450°C for 5 h in static air.

The composition of the prepared samples is summarized in Table 3.1.

Table 3.1: Prepared samples.

Sample Code	V_2O_5 (wt.%)
V1	1
V2	2
V3.5	3.5
V5	5
V7	7
V10	10
V15	15
V100	Pure V_2o_5

Catalysts were characterized by means of Raman spectroscopy, *in-situ* measurements were performed by feeding vapours of wet air, containing either 1 or 3 vol% water; the concentration of steam was varied by bubbling the dry air stream in a water-containing vessel, maintained at controlled temperature.
Catalytic tests were carried out in a laboratory continuous-flow, fixed-bed reactor at atmospheric pressure. The feed composition was 1 mol.% *o*-xylene in air.

3.3 RESULTS AND DISCUSSION

3.3.1 Effect of the vanadia loading on the nature of V species

The effect of an increasing loading of vanadium oxide on the nature of the V species, with a TiO_2 of 22.5 m^2/g, is illustrated in Figure 3.1, showing the Raman spectra recorded at 360°C, i.e., under conditions at which the VO_x species are dehydrated.

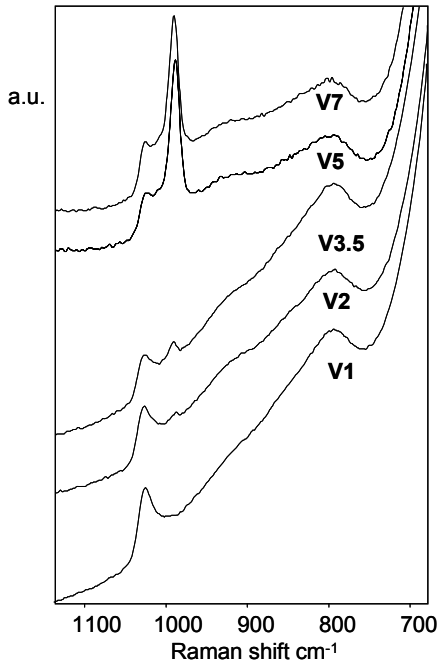

Figure 3.1: Raman spectra of dehydrated V/Ti/O catalysts having increasing amounts of V_2O_5 loading.

It can be notice that for a V_2O_5 content of 1 and 2 wt%, the predominant band was that at approximately 1030 cm^{-1}, assigned to the symmetric stretch of mono-oxo terminal V=O bond [13-16, 21]. In literature a slight shift of this band, from 1028 to 1032 cm^{-1}, with increased vanadia loading, has been reported [16]. In studied

samples, the band fell at 1029 ± 1 cm^{-1}, and apparently there was no shift of the band for increasing vanadium loading; therefore the attribution either to monomeric isolated VO_4 species or to polymeric species is uncertain. The 1 wt% V_2O_5 corresponds to approx the 40% of the theoretical monolayer, that would indicate the preferred formation of oligomeric species; however, in previous works, evidences were obtained that in this sample the monomeric, isolated species was the prevailing one [22].

The broad band between 900 and 1000 cm^{-1} is attributable to the internal vibration of the V-O-V bond in oligomeric vanadium species [13,21].

The band at 997 cm^{-1} is typical of bulk vanadium oxide; it was observed already in the sample containing the 2 wt% V_2O_5, and its intensity grew remarkably when the vanadia loading was increased. For these samples theoretical monolayer corresponds to 3.4 wt.% of V_2O_5, however, the maximum vanadium oxide loading dispersed on anatase, without the formation of bulk vanadium oxide, may be a function of the preparation procedure adopted [1,23].

3.3.2 Effect of the vanadia loading on reactivity

All the samples were tested in the oxidation of *o*-xylene. Figure 3.2 plots the rate of *o*-xylene transformation per mol of V (TOF) at 334°C as a function of the vanadia loading; the figure also compiles the temperature at which 60% *o*-xylene conversion was obtained. It is shown that the TOF decreased when the vanadia loading was increased; the most relevant decrease of activity was observed for the sample containing the 3.5 wt% V_2O_5, in which the formation of bulk vanadia was evident.

A decrease of the activity for vanadia contents above the monolayer is expected, because bulk vanadia is less active than polyvanadate due to the exposure of fewer sites per unit weight of active phase. Furthermore, the vanadia crystallites are sitting on top of the surface vanadium oxide monolayer and further decrease the number of exposed surface vanadia sites. Due to these reasons, the experimental TOF indeed is an apparent value when measured for samples having supra-monolayer vanadium oxide loading.

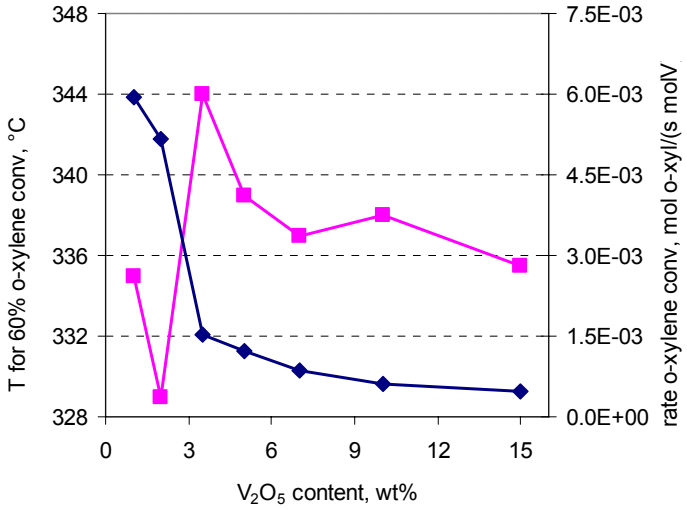

Figure 3.2: Integral rate of *o*-xylene conversion at 334°C per unit mole of V (◆) and temperature for 60% *o*-xylene conversion (■) as function of the overall vanadia loading.

In the case of *o*-xylene oxidation with sub-monolayer V/Ti/O catalysts, in general higher vanadium oxide loading lead to an increase of conversion [24,25], but a comparison of the V specific activity was not reported. It is worth reminding that the presence of bare titania surface may lead to the deposition of heavy compounds on the catalyst surface, responsible for missing C in the C balance, that poison the isolated V species and lead to quick catalyst deactivation [2]; the characteristics of the titania support may greatly affect these deactivation phenomena. With samples V1 and V2 (sub-monolayer samples), the C balance was around 96-98%, when the by-products phthalic acid and phthalaldehyde (products that have never been taken into consideration before in the literature) were also included [26]. Therefore, deactivation with 1 and 2 wt% V_2O_5 catalysts was negligible; this made possible to evaluate the catalytic activity in the absence of phenomena that might affect it.

The plot of Figure 3.2 indicates that the most reactive species is the dispersed VO_4. The decrease of activity shown in the sub-monolayer region may be attributed either to a lower activity of the V-O bond involved in the rate-determining step of the reaction, or to a lower accessibility of the active sites due to the development of polymeric species. A possible involvement of the V-O-Ti bond in *o*-xylene activation, as proposed for methanol oxidation catalysed by monolayer vanadium oxide [27], may also fit with the experimental trend; in fact,

the number of V-O-Ti bonds per V atom decreases with an increase of the degree of condensation of VO_4 units.

The effect of the vanadium oxide loading on selectivity is shown in Figure 4.3, that reports the overall selectivity to *o*-tolualdehyde + *o*-toluic acid + phthalide + phthalaldehyde + phthalic anhydride + phthalic acid (that is, the overall selectivity to C_8 oxygenates, including reaction intermediates precursors of phthalic anhydride formation) at 40-55% *o*-xylene conversion and at 98% *o*-xylene conversion; under the latter conditions, the selectivity to the intermediates was close to zero.

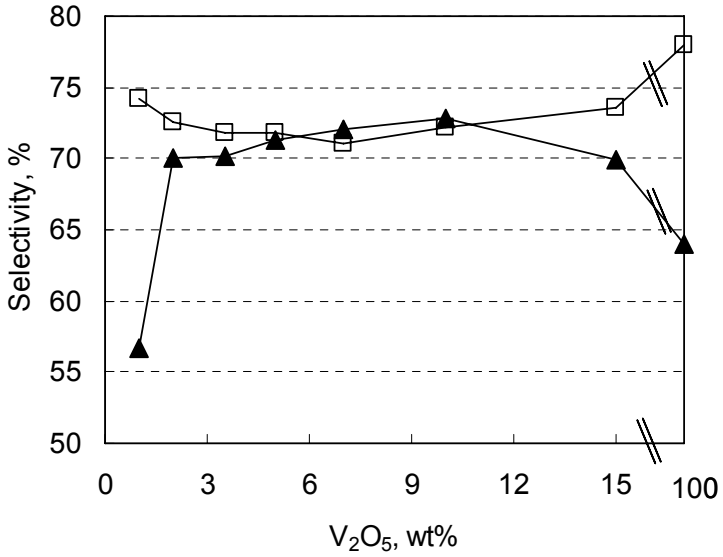

Figure 3.3: Selectivity to *o*-tolualdehyde + *o*-toluic acid + phthalaldehyde + phthalide + phthalic anhydride + phthalic acid at 40-55% *o*-xylene conversion (□) and selectivity to phthalic anhydride + phthalic acid at 98% *o*-xylene conversion (▲) as functions of the overall vanadia loading in V/Ti/O catalysts.

The trend at moderate conversion is different from that one previously reported in the literature [25], especially if the sub-monolayer catalysts are taken into consideration; this discrepancy may be attributed to a different role of the bare titania support, whose characteristics may greatly affect the performance.

The 1 wt% V_2O_5 catalyst gave the best overall selectivity at moderate *o*-xylene conversion, but showed the lowest selectivity to phthalic anhydride + phthalic acid at high hydrocarbon conversion. The increase of the vanadia content led to a

small but non-negligible decrease of the selectivity at moderate conversion, the minimum being observed with the catalyst having the 5 wt% V_2O_5.

The selectivity at high conversion, on the contrary, was the highest with catalysts having the 7 and the 10 wt% V_2O_5.

The following considerations can be done:

1. the best performance is shown by catalysts having more than the monolayer coverage. Apparently, this is necessary in order to limit undesired consecutive reactions occurring on phthalic anhydride, such as combustion or hydrolysis to yield phthalic acid, that at high temperature may be the precursor for the formation of carbon oxides.
2. With catalysts having 5-to-10 wt% V_2O_5 the selectivity at high *o*-xylene conversion was similar to the overall selectivity to C_8 compounds obtained at medium conversion. This suggests that with these catalysts there is no important contribution of consecutive reactions limiting the selectivity to phthalic anhydride.
3. With catalysts having less than 5 and more than 10 wt% V_2O_5, the selectivity at high conversion was lower than that obtained at medium *o*-xylene conversion. This confirms the role of crystalline V_2O_5 and of anatase in promoting the high-temperature consecutive reactions on phthalic anhydride [1,2,28].
4. Unsupported bulk V_2O_5 gave 44% conversion at 388°C, with an overall selectivity to phthalic anhydride + intermediates of 79%, and of 64% at 98% conversion (413°C). Although much less active than titania-supported vanadium oxide [29], the selectivity shown by bulk V_2O_5 at moderate conversion was even better than that one of the monolayer catalyst.
5. The performance of the 1 wt% V_2O_5 indicates that a high surface density of VO_x species is not a requisite for the selective transformation of *o*-xylene to phthalic anhydride, in contrast with the general belief [1,30]. These data suggest that when the reaction network includes kinetically consecutive steps, and each reaction intermediate has to desorb into the gas phase before being re-adsorbed on another oxidized V sites and over there be transformed to the successive compound, almost isolated vanadium or oligomerized VO_4 units can perform this multi-step reaction, provided (a) the catalytically active surface is not saturated by reactants

and intermediates, and (b) the rate-determining step in the redox process is the reduction of V sites by the hydrocarbon. This makes the majority of active sites be present in the oxidized form and hence be available for the interaction with *o*-xylene or with the intermediates.

3.4 CONCLUSIONS

In this section the effect of the loading of vanadium oxide in V/Ti/O catalyst has been studied. It was found that in unpromoted samples the activity (TON) of VO_x species decreased when the vanadium oxide loading was increased from the sub-monolayer to the monolayer content, indicating that the activity of the highly dispersed (isolated and oligomerized) VO_x species is higher than that of the polymeric vanadate. A further decrease of the TON in the supra-monolayer region was due to the formation of bulk vanadium oxide.

The overall selectivity to C_8 oxygenates was a function of both the vanadium oxide loading and of the conversion. The best selectivity to phthalic anhydride + phthalic acid at high *o*-xylene conversion was offered by the catalyst well above the monolayer, also containing bulk vanadium oxide; on the other hand, the catalyst having the lower amount of vanadium oxide loading (approximately 40% of the monolayer coverage) provided an excellent selectivity to C_8 oxygenates at 50-60% *o*-xylene conversion.

3.5 REFERENCES

[1] B. Grzybowska, Appl. Catal. A. 157 (1997) 263.
[2] G.C. Bond, J. Chem. Tech. Biotechnol. 68 (1997) 6.
[3] V. Nikolov, D. Klissurski, A. Anastasov, Catal. Rev.-Sci. Eng. 33 (1991) 319
[4] M.S. Wainwright, N.R. Foster, Catal. Rev.-Sci. Eng. 19 (1979) 211
[5] P.J. Gellings, in Catalysis (Specialist Periodical Report). Roy. Soc. Chem., London, 1985, Vol. 7, p. 105
[6] G.C. Bond, S.F. Tahir, Appl. Catal. 71 (1991) 1
[7] Catal. Today, 20 (1994) Special Issue on Eurocat Oxide VTiO catalyst
[8] I.E. Wachs, B.M. Weckhuysen, Appl. Catal. A 157 (1997) 67
[9] C.R. Dias, M.F. Portela, G.C. Bond, Catal. Rev.-Sci. Eng. 39(3) (1997) 169
[10] G. Centi, Appl. Catal. A 147 (1996) 267
[11] P. Courtine, E. Bordes, Appl. Catal. A 157 (1997) 45

[12] G.C. Bond, Appl. Catal. A 191 (2000) 69
[13] I.E. Wachs, Catal. Today 27 (1996) 437
[14] G. Deo and I.E. Wachs, J. Catal. 129 (1991) 307
[15] G. Deo and I.E. Wachs, J. Catal. 146 (1994) 323
[16] L.J. Burcham, G. Deo, X. Gao, I.E. Wachs, Topics Catal. 11/12 (2000) 85
[17] P. Reuter, G. Voit, T. Heidemann, US 6774246, 2004, assigned to BASF
[18] M. Okuno, T. Takahashi, EP 1063222, 2000, assigned to Nippon Shokubai
[19] S. Neto, J. Zühlke, S. Storck, F. Rosowski, WO 2005/011862 A1, assigned to BASF
[20] C. Gückel, M. Niedermeier, M. Estenfelder, WO Patent Appl 2006/125468, assigned to Süd-Chemie AG
[21] M. Bañares, I.E. Wachs, J. Raman Spectr. 33 (2002) 359
[22] F. Cavani, C. Cortelli, A. Frattini, B. Panzacchi, V. Ravaglia, F. Trifirò, C. Fumagalli, R. Lenza, G. Mazzoni, Catal. Today, 118 (2006) 298
[23] B.M. Weckhuysen, D.E. Keller, Catal. Today 78 (2003) 25
[24] I.E. Wachs, R.Y. Saleh, S.S. Chan, C.C. Chersich, Appl. Catal. 15 (1985) 339.
[25] R.Y. Saleh, I.E. Wachs, Appl. Catal. 31 (1987) 87
[26] N. Ballarini, A. Brentari, F. Cavani, S. Luciani, C. Cortelli, F. Cruzzolin, R. Leanza, Catal. Today in press
[27] K. Routray, L.E. Briand, I.E. Wachs, J. Catal. 256 (2008) 145
[28] G. Deo, I.E. Wachs, J. Haber, Crit. Rev. Surf. Chem. 4 (1994) 141
[29] M. Gasior and T. Machej, J. Catal., 83 (1983) 472
[30] B. Grzybowska-Swierkosz, Appl. Catal. 157 (1997) 409.

4

DYNAMIC BEHAVIOR OF V/Ti/O CATALYSTS: EFFECT OF STEAM

4.1 INTRODUCTION

In literature, several papers discuss the chemical-physical features and catalytic properties of titania-supported vanadium oxide-based catalysts (V/Ti/O) in oxidation catalysis [1-12]. On the contrary, little attention has been given to one aspect that may have profound implications on the catalytic performance, the role of gas-phase components. In fact, in the industrial practice, the vanadium oxide-based catalysts need the addition of gas-phase promoters in the feed stream, that although do not have a direct role in the reaction stoichiometry, when present give a considerable improvement of catalytic performance.

Among these, steam (a component of the reaction environment in oxidation reactions) could play an important role.

In literature, the effect of steam on the nature of V sites in supported vanadium oxide catalysts has been investigated by Wachs et al [13,14]. It was found that moisture makes hydrogen bonding to the oxygen functionalities of the surface vanadia species; the H bonding was observed for the terminal V=O bond, the corresponding Raman band shifting to lower wavenumbers. Below 230°C, water was also able to hydrolyse the V-O-support bond, while at higher temperatures, no appreciable modification of the V surface species was found.

Oxidation of *o*-xylene is carried out at temperature higher than 360°C, therefore a deeper understanding of the changes of the V species occurring at high temperature is certainly interesting. In this section, the dynamic phenomena

occurring at the V/Ti/O surface at temperature between 350°C and 450°C were investigated in the presence of steam. Moreover a correlation between the amount of the different vanadium species and catalytic performances have been searched for.

4.2 EXPERIMENTAL

A catalyst containing 7 wt.% V_2O_5 on TiO_2 anatase (s.s.a. 22.5 m^2/g) was prepared with the wet impregnation technique as described in Chapter 2.1, and calcined at 450°C for 5 h in static air.

In-situ measurements were performed by feeding vapours of wet air, containing either 1 or 3 vol.% water; the concentration of steam was varied by bubbling the dry air stream in a water-containing vessel, maintained at controlled temperature. In Table 4.1 are listed all the Raman experiments carried out.

Table 4.1: *In-situ* Raman experiments

Test code	First step: Temperature/feed	Second step: Temperature/feed
1	360°C/3% steam in air	-
2	400°C/3% steam in air	400°C/dry air
3	450°/3% steam in air	-
4	400°C/3% steam in air	360°C/dry air
5	400°C/3% steam in air	450°C/dry air
6	400°C/dry air	-

Catalytic tests were carried out in a laboratory continuous-flow, fixed-bed reactor at atmospheric pressure. The size of catalyst particles ranged from 250 to 590 μm. The feed composition was either 1 mol.% *o*-xylene in air, or 1 mol% *o*-xylene and 3 mol% steam in air.

4.3 RESULTS AND DISCUSSION

4.3.1 Characterization

Prepared catalyst was characterized by means of different techniques, to control its chemical-physical characteristics.

Figure 4.1 shows the X-Ray diffractogram of the sample containing 7 wt.% V_2O_5 on titania, after calcination.

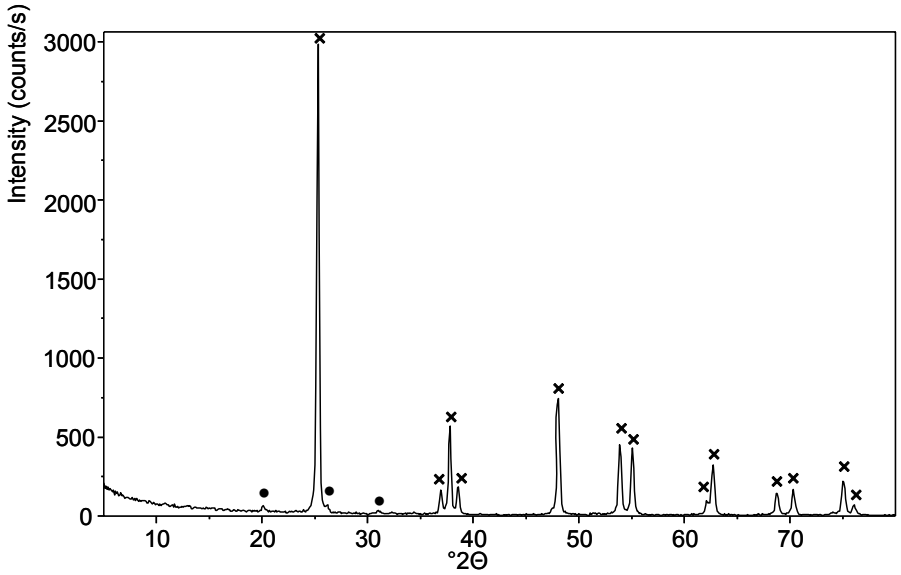

Figure 4.1: X-Ray diffraction pattern of calcined sample. Symbols: × TiO_2 (JCPDS 21-1272), ● V_2O_5 (JCPDS 41-1426)

The diffraction pattern showed the reflections of TiO_2 anatase used as support and much less intense reflections of V_2O_5 shcherbinaite.

The presence of bulk vanadium oxide was confirmed also by spectroscopic tecniques (UV-Vis DRS, FT-IR, Raman).

In particular, Figure 4.2 reports the FT-IR spectum of the sample after calcination.

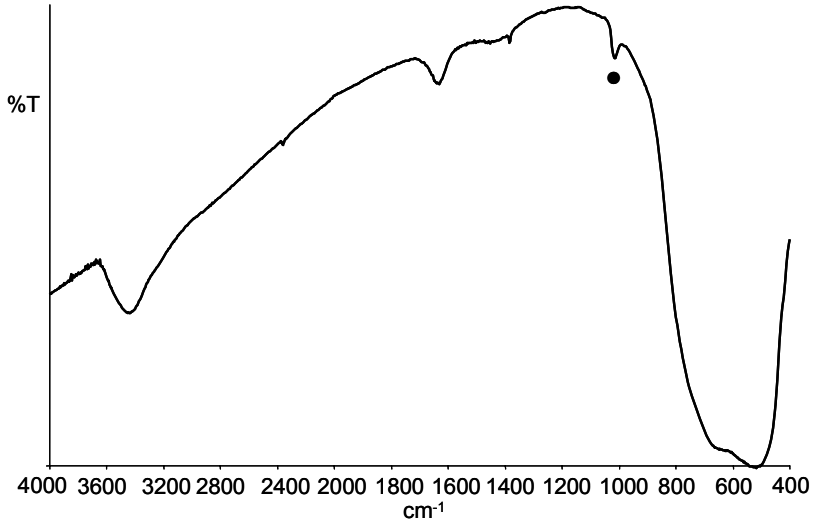

Figure 4.2: FT-IR spectrum of calcined sample. Symbols:● V_2O_5

The absorption band in the range 400-800 cm^{-1} is typical of titanium oxide, while the bands at 3600 and 1600 cm^{-1} are due to the presence of adsorbed water. Concerning the vanadium species, the band at 1020 cm^{-1} is relative to the stretching of V=O bond in V_2O_5 [15].

The presence of V^{5+} oxide is also detected by UV-Vis spectroscopy; the spectrum (Figure 4.3) shows TiO_2 band between 190 and 350 nm and a band at 470 nm attributable to crystalline V_2O_5 [16].

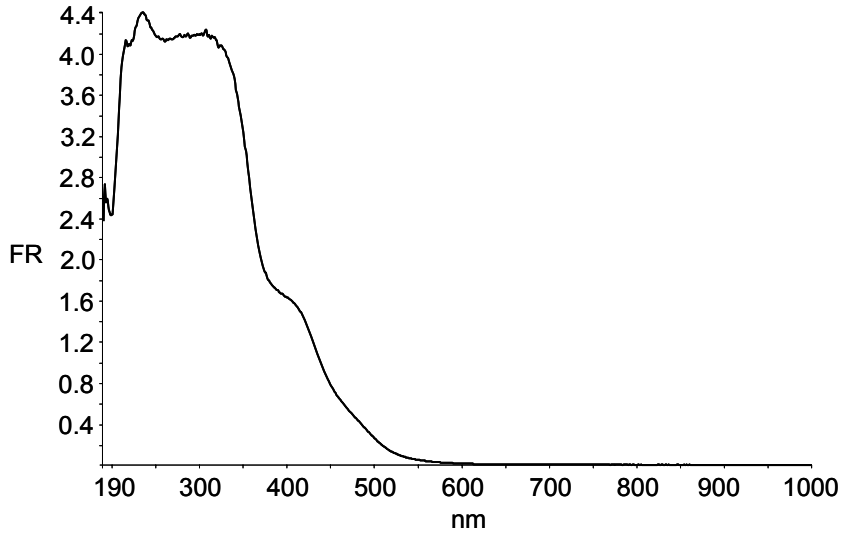

Figure 4.3: UV-Vis DR spectrum of calcined sample.

The formation of vanadium oxide in this sample was quite expected, being the amount of vanadium more than twice the theoretical monolayer value for a titania having specific surface area 22.5 m^2/g (3.4 wt.% V_2O_5 [6]).

To investigate the possible changes of the vanadium species when exposed to the reaction mixture, the sample was characterized before and after catalytic tests under different conditions.

Figure 4.4 reports the Raman spectra recorded after calcination, after equilibration in mixture o-xylene/air and after reaction with air enriched in steam. Spectra of calcined and "used" sample had similar features. In all cases the typical bands of TiO_2 anatase support (at Raman shift 180, 380, 520, 640 cm^{-1}) were present. In addition the calcined sample showed bands at 997, 705, 483, 305, 285 cm^{-1} attributable to bulk V_2O_5.

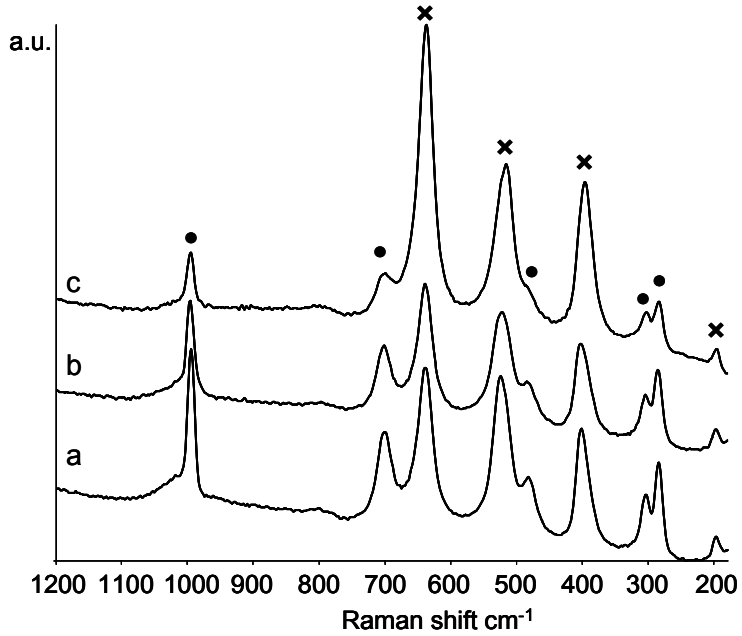

Figure 4.4: Raman spectra of sample after calcination (a), after equilibration in mixture *o*-xylene/air (b) and after reaction with 3%steam/air/*o*-xylene (c). Symbols: × TiO_2, ● V_2O_5

After working under different reaction conditions the catalyst seems not to undergo any dramatic modifications; spectra collected both after equilibration (*o*-xylene/air) and after reaction with steam, still showed the band of V_2O_5.

This could means that (i) the reaction atmosphere not modify the nature of the active phase, or (ii) changes of the surface layer occur only at high temperature in presence of *o*-xylene and air and the phenomenon is reversible.

4.3.2 The effect of steam on catalytic performances

Figure 4.5 reports the effect of temperature on *o*-xylene conversion and on the distribution of products for the sample containing 7 wt.% V_2O_5. Tests were carried out feeding 1 mol.% *o*-xylene in air, residence time 0.13 s. The sample was first equilibrated at 400°C, under reaction mixture for about 10 hours. After this period, the catalyst had a quite stable catalytic performance.

Conversion of *o*-xylene increased with temperature, total conversion was reached at 360°C.

Selectivity to intermediates (such as o-toluic acid, o-toluic aldehyde, phthalaldehyde and phthalide) was relatively high at low temperature, while decreased at high temperature. In correspondence with the decrease of

selectivity to these intermediates, phthalic anhydride selectivity increased. Selectivity to intermediates became nil at total *o*-xylene conversion.

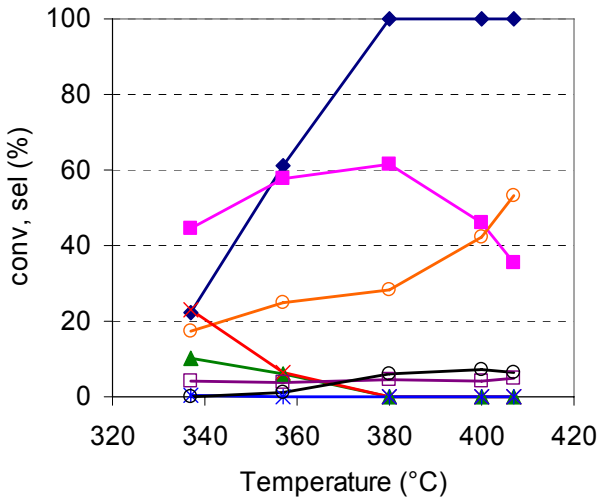

Figure 4.5: Conversion of *o*-xylene (♦) and selectivity to phthalic anhydride (■), phthalide (▲), $CO+CO_2$ (●), o-tolualdehyde + o-toluic acid (×), maleic anhydride + benzoic acid (□), phthalaldehyde (✳) and phthalic acid (○)as a function of temperature. Catalyst: 7wt.% V_2O_5 on TiO_2.

Selectivity to maleic anhydride and benzoic acid was quite not affected by temperature and it was lower than 5% in all the temperature range studied.

Selectivity to total oxidation products (CO and CO_2) increased with the temperature and became quite high for T>340°C.

The trend of phthalic anhydride selectivity showed a maximum at 340°C: the increase of selectivity at low temperature was depending on the decrease of selectivity to intermediates, while at high temperature the selectivity decrease of phthalic anhydride was compensated by the increase of selectivity to CO and CO_2.

When PA selectivity was higher than 50%, also phthalic acid formed. Selectivity to acid increased up to 7 % at 400°C, then it decreased due to the consecutive oxidation to CO_x.

The effect of steam has been studied feeding to the reactor a flow of air enriched with 3% steam; this value corresponds to approximately twice the amount of water generated by the reaction itself at these reaction conditions. Transient reactivity at 360°C was followed along with time on stream. At this temperature, working under classical conditions (i.e. feed composition: 1 mol.% *o*-xylene/air, Figure 4.5) conversion of *o*-xylene was about 60%, so it should be possible to

evidence the effect of steam both on activity and selectivity to phthalic anhydride.

Figure 4.6 shows the effect of steam on the catalytic performance of the 7 wt% V_2O_5 catalyst.

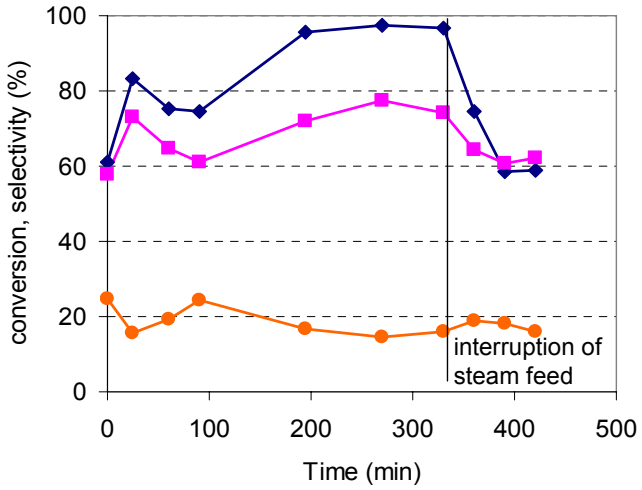

Figure 4.6: *o*-xylene conversion (◆), selectivity to phthalic anhydride (▲) and to CO_x (●) at 360 °C as functions of time-on-stream after addition of 3 vol% steam to the reactor inlet feed. Catalyst: 7wt.% V_2O_5 on TiO_2.

It is shown that a progressive modification of the catalytic performance occurred within a few hours. After an initial rapid variation, the trend experimentally observed was that of an increase of *o*-xylene conversion; the latter finally reached a stable value after approximately 3-4 hours of reaction with the steam-enriched feed. The increase of conversion also led to a better selectivity to phthalic anhydride, because of the lower selectivity to the reaction intermediates. Moreover, the interruption of the steam addition in the feed led to the recovery of the initial performance within less than 2 hour time-on-stream. This means that the effect of steam was reversible.

Different phenomena may be responsible for the effect experimentally observed:

(a) a change of the catalyst surface temperature due to the different heat conduction properties of steam, as compared to the mixture of *o*-xylene and air; however, in this case a decrease of the surface temperature and a decrease of the conversion would be the expected effects;

(b) an effect of surface "cleaning", favouring the desorption of reaction intermediates and products and hence rendering the active sites more

available for the activation of the alkylaromatic; it also may reduce carbon deposition;

(c) a modification of the characteristics of the active sites;

(d) an increase of the number of the active sites.

To discriminate between these hypotheses, *in-situ* Raman measurements were performed by feeding vapours of wet air at high temperature.

4.3.3 The effect of steam on the nature of V species

Several *in-situ* Raman experiments were carried out on a catalyst containing 7 wt.% V_2O_5, after equilibration; temperature and steam concentration were varied for a better comprehension of the dynamic occurring on catalyst surface.

In all tests, the sample was first heated in dry air up to the desired temperature, then maintained at this temperature for a few hours (during this step steam was eventually fed).

As an example, to study the effect of steam at 400°C, the catalyst was heated under flow of dry air up to 400°C; Raman spectra collected at 25°C and at increasing temperature are shown in Figure 4.7.

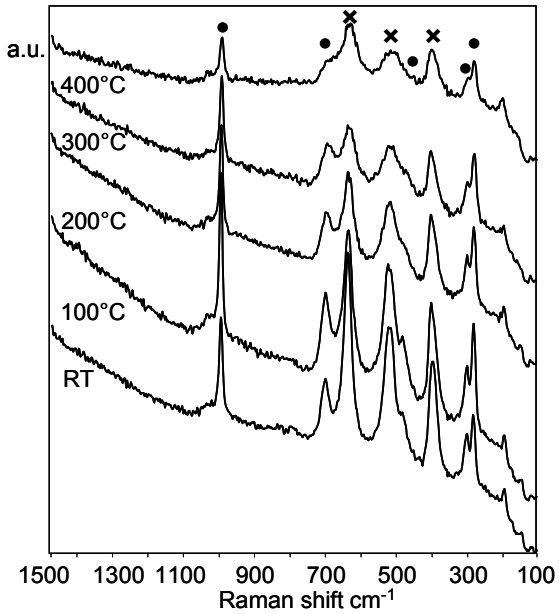

Figure 4.7: Raman spectra collected at increasing temperature in flow of dry air. Symbols: × TiO_2, ● V_2O_5

The spectrum collected at room temperature (RT in Figure 4.5) was typical of a VTiO system having vanadium content higher than the monolayer value. The

bands at Raman shift 180, 380, 520, 640 cm^{-1} are relative to the anatase support, while the bands at 997, 705, 483, 305, 285 cm^{-1} are attributable to the presence of bulk V_2O_5. As expected, increasing temperature all the bands became broader and less intense; however the band attributable to vanadium oxide were still evident up to 400°C.

Then 3% of steam was added and the sample was maintained at 400°C under wet air for about 4 hours; the spectra recorded under these conditions are reported in Figure 4.8.

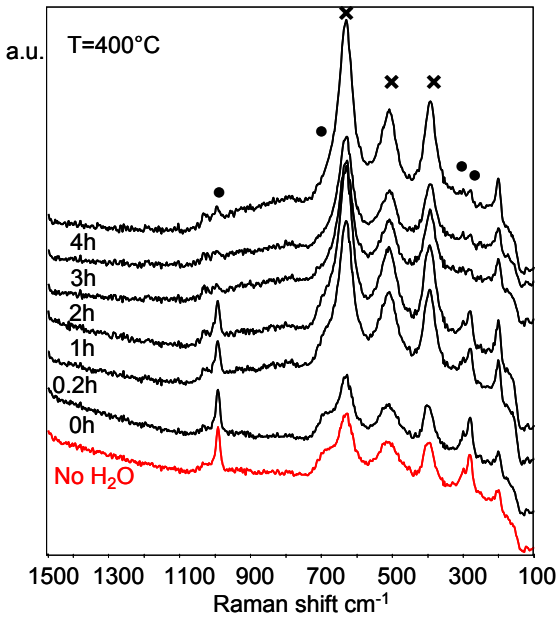

Figure 4.8: Raman spectra collected at 400°C in flow of 3%steam in air. Symbols: × TiO_2, ● V_2O_5.

The spectra recorded at increasing time of exposure to the wet stream (T=400°C) evidenced a progressive decrease of the intensity of the band at Raman shift 997 cm^{-1} associated to bulk vanadium oxide and of the other bands attributed to the latter compound as well, and an increase of intensity of the broad band falling between 900 and 1000 cm^{-1} and attributable to the internal vibration of the V-O-V bond in oligomeric vanadium species [13,17]. The band assigned to the symmetric stretch of mono-oxo terminal V=O bond [13,14,17-20] at 1029 cm^{-1} did not apparently undergo any modification.

After this experiment, the temperature was lowered down to 360°C, and dry air was fed to the catalyst; Figure 4.9 compiles the Raman spectra recorded under the latter conditions. It is shown that after the interruption of the steam feed, the

intensity of the band at 997 cm^{-1} increased; the spectrum originally recorded under a dry atmosphere was observed after 1 hour the steam feed had been interrupted.

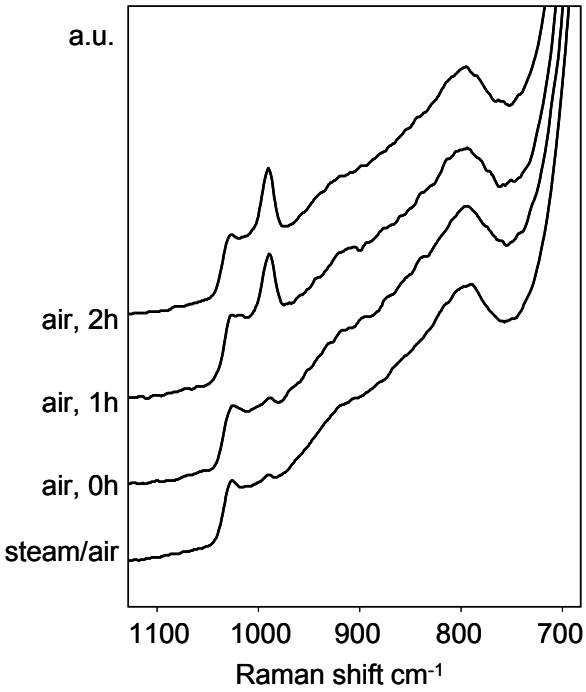

Figure 4.9: Raman spectra collected at 360°C after interruption of steam feed.

These results indicate that steam may favour the spreading of bulk vanadium oxide, with a corresponding increase of the number of active sites, and possibly also the formation of sites that are intrinsically more active than those in bulk vanadium oxide (Chapter 3). The formation of smaller V_2O_5 nanoparticles, with an increased number of edge sites that give higher activity, also cannot be excluded.
It is well known that heating V_2O_5 at temperatures higher than the Tamman temperature (482K) causes the spreading of the oxide over supports [21-23]. The driving force for this phenomenon is the lowering of the surface free energy by formation of the monolayer. However, high temperatures are required for surface diffusion or migration to occur at an appreciable rate. On the other hand, reaction-induced spreading of bulk metal oxides onto the surface of supports may occur during exothermal reactions, at temperatures lower than that required for thermal spreading [24]. Vanadia migration is favoured over well-developed anatase crystal planes [24]; at 450°C spontaneous spreading takes place, controlled by diffusion of V species through the monolayer. It is worth noting that

after reaction in microreactor, the sample, containing bulk vanadia, still showed a Raman spectrum quite similar to that one before reaction. This means that the temperature that develops at the catalyst surface during the exothermal oxidation reaction is likely higher than 400°C; the latter conditions may thermodynamically favour segregation phenomena of vanadium oxide rather than its dispersion.

The effect of the steam added could be that one of lowering the catalyst surface temperature during reaction, that becomes closer to the temperature at which spreading phenomena may be both kinetically and thermodynamically favoured, i.e., approximately 400°C.

For this reason the evolution of catalyst under steam/air was studied also at 450°C.

Figure 4.10 shows the Raman spectra recorded at 450°C under 3% steam in air.

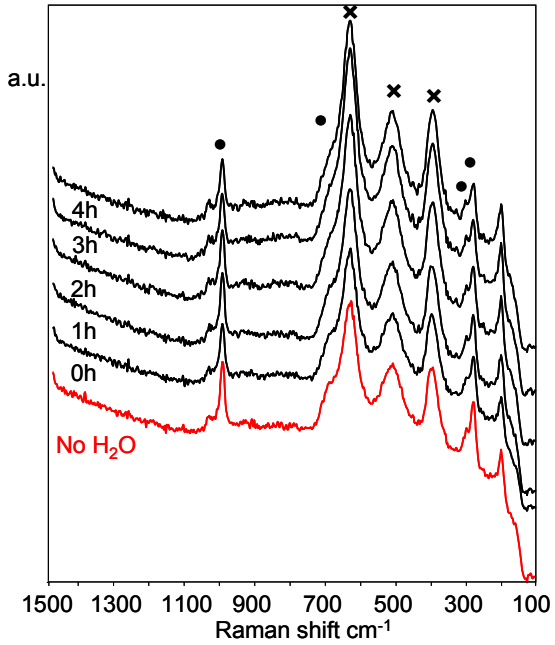

Figure 4.10: Raman spectra collected at 450°C in flow of 3%steam in air. Symbols: × TiO_2, ● V_2O_5

In this case the Raman bands of bulk V_2O_5 were still evident after 4 hours of exposure to steam; also their intensity did not decrease so rapidly as in the experiment in Figure 4.8 (400°C). It is evident that a 450°C the spreading phenomena that at 400°C had occurred in a few hours did not occur at an appreciable extent within the same period of time.

Moreover, the same experiment of Figure 4.7 and 4.8 was carried out with only ≈1% steam in air, or with no steam at all.

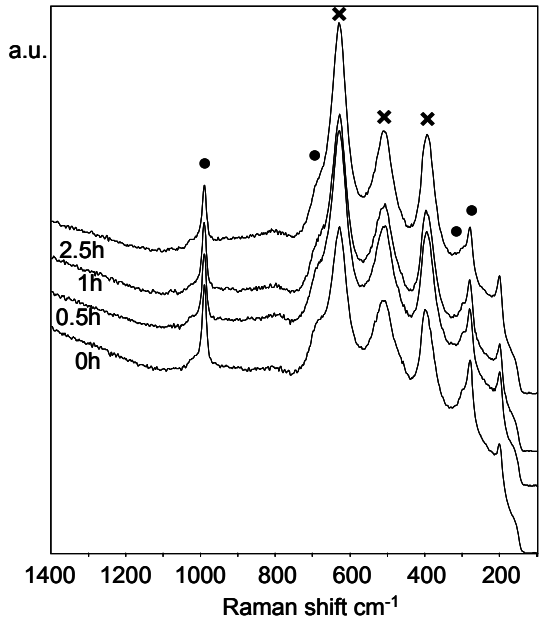

Figure 4.11: Raman spectra collected at 400°C in flow of dry air. Symbols: × TiO_2, ● V_2O_5

Flowing dry air, no spreading of vanadium oxide was observed by *in-situ* Raman measurements (Figure 4.11); this means that the partial pressure of water is important in determining the kinetics of the transformation.

This suggests that the main role of water was that of favouring the hydrolysis of V-O-V bonds in bulk vanadium oxide, with generation of mobile and reactive species. This caused an increase of the number of available active sites, and hence an enhancement of the catalytic activity. The formation of stable V-O-Ti bonds (e.g., in polyvanadate) is unlikely, for two reasons: (i) due to the relatively high amount of vanadium oxide loading, most likely no titania surface was available for bonding with additional VO_x species; and (ii) the formation of a stable structure would not explain why the phenomenon was reversible.

In fact, when water was withdrawn from the feed, V species re-aggregated to yield back bulk vanadium oxide; in the reactor, this corresponded to a progressive lowering of the catalytic activity (Figure 4.6).

Noteworthy, the segregation of vanadium oxide after water withdrawal was experimentally observed during Raman *in-situ* experiments only when the temperature in the cell was lowered down to 360°C. In fact at 400°C, that is the

temperature at which under wet stream spreading phenomena had occur, no formation of bulk vanadium oxide was observed within a few hours after withdrawal of steam. This confirms that the two events, i.e. vanadium oxide dispersion and re-aggregation, are function of the water partial pressure and of temperature; they only occur at well defined conditions, being the result of contrasting driving forces. When the temperature is close to 400°C, in fact, the hydrolysis of V-O-V bonds and the dispersion of V species, induced by the presence of steam, is kinetically favoured over the segregation into a bulk compound. On the other hand, at about 450°C dehydration and segregation are favoured for thermodynamic reasons over hydrolysis and spreading, even in the presence of steam.

4.4 CONCLUSIONS

The role of steam, as gas-phase promoter for VTiO system, was studied. It has been demonstrated that this component modifies the relative amount of the V species present on the support and consequently affects the catalytic performance. In particular, carrying out the reaction in the presence of 3 vol% steam in the inlet feed, this amount being higher than that one generated during the reaction, led to a remarkable improvement of catalytic activity.

In-situ Raman measurements evidenced that this effect was due to a dispersion of bulk vanadium oxide to generate a higher number of active sites. However, vanadium oxide spreading was greatly dependent on the water partial pressure and of the temperature. The effect was quite reversible, and the interruption of the steam feed led to a recover of the initial catalytic activity owing to the re-aggregation of dispersed V species into bulk vanadium oxide.

Vanadium oxide dispersion and re-aggregation are the result of contrasting driving forces: for kinetically reason the dispersion is favoured only at relative high temperature (400°C), on the other hand if the temperature is too high (450°C) segregation of bulk vanadia is thermodynamically favoured.

4.5 REFERENCES

[1] B. Grzybowska, Appl. Catal. A. 157 (1997) 263.

[2] G.C. Bond, J. Chem. Tech. Biotechnol. 68 (1997) 6

[3] V. Nikolov, D. Klissurski, A. Anastasov, Catal. Rev.-Sci. Eng. 33 (1991) 319.

[4] M.S. Wainwright, N.R. Foster, Catal. Rev.-Sci. Eng. 19 (1979) 211

[5] P.J. Gellings, in Catalysis (Specialist Periodical Report). Roy. Soc. Chem., London, 1985, Vol. 7, p. 105.

[6] G.C. Bond, S.F. Tahir, Appl. Catal. 71 (1991) 1

[7] Catal. Today, 20 (1994) Special Issue on Eurocat Oxide VTiO catalyst

[8] I.E. Wachs, B.M. Weckhuysen, Appl. Catal. A 157 (1997) 67.

[9] C.R. Dias, M.F. Portela, G.C. Bond, Catal. Rev.-Sci. Eng., 39(3) (1997) 169

[10] G. Centi, Appl. Catal. A 147 (1996) 267

[11] P. Courtine, E. Bordes, Appl. Catal. A 157 (1997) 45

[12] G.C. Bond, Appl. Catal. A 191 (2000) 69

[13] M. Bañares, I.E. Wachs, J. Raman Spectr. 33 (2002) 359

[14] J.-M. Jehng, G. Deo, B.M. Weckhuysen, I.E. Wachs, J. Mol. Catal. A 110 (1996) 41

[15] I.L. Botto, M.B. Vassallo, E.J. Baran, G. Minelli, Mater. Chem. Phys. 50 (1997) 267

[16] G. Catana, R.R. Rao, B.M. Weckhuysen, P. Der Voort, E. Vansant, R.A. Schoonheydt, J. Phys. Chem. B 102 (1998) 8005
J.G. Eon, R. Oliver, J.C. Volta, J. Catal., 145, 1994, 318

[17] I.E. Wachs, Catal. Today 27 (1996) 437.

[18] G. Deo and I.E. Wachs, J. Catal. 129 (1991) 307

[19] G. Deo and I.E. Wachs, J. Catal. 146 (1994) 323

[20] L.J. Burcham, G. Deo, X. Gao, I.E. Wachs, Topics Catal. 11/12 (2000) 85.

[21] J. Haber, Pure Appl. Chem. 56 (1984) 1663

[22] D.A. Bulushev, L. Kiwi-Minsker, A. Renken, Catal. Today 57 (2000) 231

[23] C.B. Wang, Y. Cai, I.E. Wachs, Langmuir 15 (1999) 1223

[24] J. Haber, T. Machej, E.M. Serwicka, I.E. Wachs, Catal. Lett. 32 (1995) 101.

5

THE MECHANISM OF *O*-XYLENE OXIDATION TO PHTHALIC ANHYDRIDE: THE ROLE OF CS

5.1 INTRODUCTION

The selective oxidation of *o*-xylene to phthalic anhydride (PA), catalyzed by titania (anatase)-supported vanadium oxide, has been investigated by several authors in latest decades, and all main aspects concerning the catalyst properties necessary to obtain an active and selective V/Ti/O system are well known since long time [1-9]. The research carried out so far has been dealing mainly with the nature of the V species and the interaction that develops between the latter and the titania support, both affecting the catalytic performance. Much less investigated has been the role of promoters, fundamental components of the industrial catalyst [1,10,11]. As described in Chapter 1.5, promoters playing a fundamental role are Cs, Sb and P, but also several other elements are reported in the patent literature. The role of promoters is crucial, and the proper control of the relative amount of each component in the catalytic bed, subdivided into several layers having different composition, is fundamental for the process performance. Furthermore, since the reaction network for PA formation is very complex and includes several parallel and consecutive reactions, a proper understanding of the role of each dopant cannot be separated from the analysis of the reaction scheme. In this section are showed the results of an investigation aimed at understanding the role of Cs in V/Ti/O catalysts, in order to evidence in which step of the reaction network this promoter play its role.

5.2 EXPERIMENTAL

Catalysts were prepared using the wet-impregnation technique, as described in chapter 2.1. Two samples were studied:

(a) an undoped V/Ti/O catalyst containing 7 wt.% V_2O_5,

(b) a Cs-doped V/Ti/O catalyst containing 7 wt.% V_2O_5 and 0.35 wt.% Cs_2O.

The surface area of TiO_2 was 22 m^2/g. Samples were calcined in air at 450°C for 5 hours.

For catalytic measurements, a mixture of *o*-xylene vapors in air (either 1 or 0.5 mol.% hydrocarbon) was continuously fed to tubular-flow stainless steel reactor operating at atmospheric pressure; variable amounts of catalysts were loaded in order to carry out tests under isothermal conditions and with variation of the residence time. Some tests were carried out by feeding phthalic anhydride vapors; the compound was first dissolved in toluene (0.1% of anhydride), and then 1% of the solution was vaporized in air.

5.3 RESULTS AND DISCUSSION

5.3.1 The reaction network at 320°C

The effect of Cs was investigated in relation to the reaction network at 320°C. Both catalysts were tested in *o*-xylene oxidation varying the residence time, at 320°C, feed composition being 1 mol.% hydrocarbon in air.

Figures 5.1-5.3 compare the conversion of *o*-xylene and the selectivity to the products as a function of residence time.

The two catalysts gave the same *o*-xylene conversion up to residence time 0.4 s. However, the two systems showed a great difference for residence time higher than 0.4 s; in fact, the Cs-doped catalyst showed a remarkable increase of conversion, from 34% to 100%, for an increase of 0.1 s residence time only. On the contrary, the undoped catalyst showed an increase of conversion of only the 10% when the residence time was increased from 0.4 to 0.7 s. It is worth mentioning that the experimental trends reported in Figure 5.1 were totally reproducible, and were perfectly replicated when the residence time was first increased and then decreased.

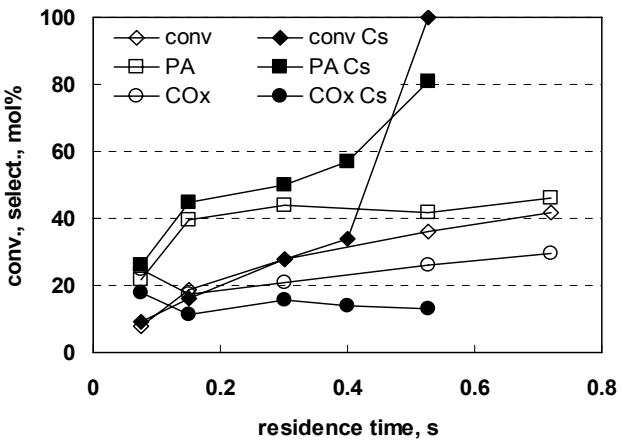

Figure 5.1: Conversion of *o*-xylene and selectivity to phthalic anhydride (PA) and carbon oxides (CO_x) for the undoped (open symbols) and Cs-doped (full symbols) catalysts as functions of the residence time. Feed composition: 1 mol% o-xylene in air. Temperature 320°C.

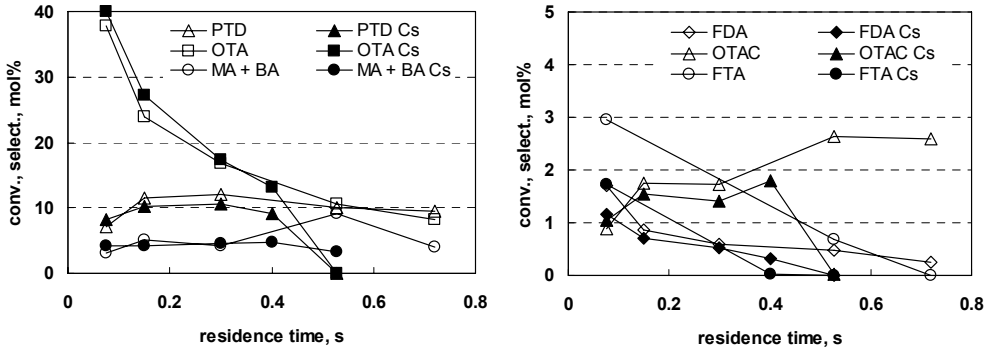

Figure 5.2 (left): Selectivity to phthalide (PTD), *o*-tolualdehyde (OTA), maleic anhydride (MA) and benzoic acid (BA) for the undoped (open symbols) and Cs-doped (full symbols) catalysts as functions of the residence time. Feed composition: 1 mol% *o*-xylene in air. Temperature 320°C.
Figure 5.3 (right): Selectivity to phthalaldehyde (FDA), *o*-toluic acid (OTAC) and phthalic acid (FTA) for the undoped (open symbols) and Cs-doped (full symbols) catalysts as functions of the residence time. Feed composition: 1 mol% *o*-xylene in air. Temperature 320°C.

With both catalysts, primary products were *o*-tolualdehyde, phthalaldehyde, carbon oxides, phthalic acid, benzoic acid and maleic anhydride. Secondary products were phthalide, *o*-toluic acid and PA. At these conditions phthalaldehyde and phthalic acid underwent consecutive transformations. Selectivity to phthalic acid showed a minimum at intermediate values of residence time; this indicates that this compound is also formed by consecutive transformation of a secondary product, most likely PA.

With the undoped catalyst, both phthalide and *o*-toluic acid did not undergo any consecutive reaction, whereas with the Cs-doped catalyst the selectivity to both compounds became nil, and that to PA correspondingly increased, when *o*-xylene reached complete conversion.

The reaction network that can be inferred from the experimental results agrees with that one reported in the literature [2-4]; however new aspects, never reported previously, can be inferred (Figure 5.4).

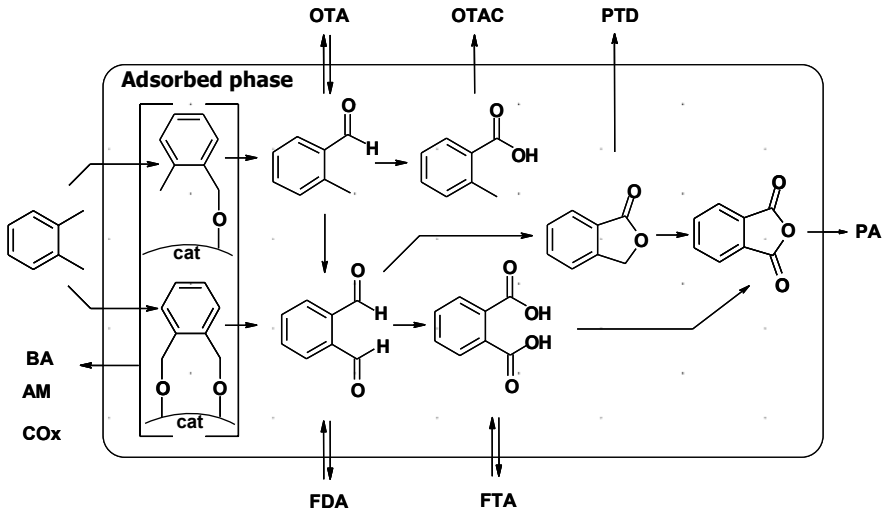

Figure 5.4: Reaction scheme of *o*-xylene oxidation on V/Ti/O catalyst at 320°C. PA: phthalic anhydride; PTD: phthalide; OTA: *o*-tolualdehyde; MA: maleic anhydride; BA: benzoic acid; FDA: phthalaldehyde; OTAC: *o*-toluic acid; FTA: phthalic acid.

At 320°C, there are two main direct selective pathways for *o*-xylene transformation. The main one likely occurs by interaction of the alkylaromatic with the catalyst surface through one methyl group, which is then oxidized to yield *o*-tolualdehyde; the latter compound desorbs into the gas-phase. A less important path occurs by interaction of both methyl groups [3], and oxidation of the hydrocarbon to phthalaldehyde. In fact, both *o*-tolualdehyde and phthalaldehyde are primary products. Unselective parallel reactions of combustion to CO_x, and of formation of maleic anhydride and benzoic acid occur by oxidative scission of the C-C bond and decarboxylation, and by electrophylic oxidative attack on the aromatic ring of the adsorbed alkylaromatic.

The *o*-tolualdehyde desorbs into the gas phase and may then re-adsorb and yield *o*-toluic acid; the re-adsorption of phthalaldehyde may yield phthalic acid; the

latter, however, is apparently formed by direct reaction, probably because of the strong interaction of the dialdehyde with the catalyst surface which favors the consecutive oxidation of this compound before it may desorb into the gas phase. Concerning the formation of phthalide, this compound is not apparently formed by intramolecular disproportionation and condensation of *o*-toluic acid, but rather seems to form by direct transformation of *o*-tolualdehyde. One possible route from *o*-tolualdehyde to phthalide is by oxidation of the second methyl group and rapid intramolecular Tishchenko-like condensation. It is in fact known, that aldehydes could undergo isomerization to the corresponding esthers (for instance, formaldehyde dimerizes to methyl formiate) [12]. The same intramolecular reaction may obviously occur on phthalaldehyde; the low selectivity to this compound experimentally observed is likely due to the fact that the Tishchenko reaction is fast.

With the undoped catalyst, phthalide and *o*-toluic acid are not re-adsorbed on the catalyst surface and therefore are not consecutively transformed to PA. Indeed, under these conditions the main route to PA apparently is the re-adsorption of *o*-tolualdehyde and the direct transformation of this compound. This may occur via oxidation to phthalaldehyde, which may then be successively transformed through two different pathways, both occurring without the desorption of any intermediate compound: (a) the oxidation of the dialdehyde to phthalic acid, which then dehydrates to PA, and (b) the intramolecular condensation to yield phthalide, which is then oxidized to PA. The former reaction may give the greater contribution, as suggested by the fact that gas-phase phthalide does not interact (i.e., is not re-adsorbed) with the catalyst under these conditions.

5.3.2 The role of Cs at 320°C

One major result of catalytic tests is that the undoped catalyst works at a surface-saturation state, that means at conditions of maximal coverage of the surface with the organic reactant and the intermediates. This is demonstrated by the trend of the *o*-xylene conversion in function of the residence time; the re-adsorption and oxidation of gas-phase phthalide and *o*-toluic acid is hindered likely because of the scarceness of oxidizing sites available on the catalyst surface at 320°C. The main role of Cs, therefore, is to maintain a cleaner and more oxidized active surface, by accelerating the re-oxidation of reduced V sites and

hence by favoring the desorption of intermediate compounds and their re-adsorption and consecutive oxidation to PA. This agrees with the role of Cs in doped V/Ti/O catalysts, which was found to accelerate the catalyst re-oxidation by O_2 [10,11]. In fact, it was found with the Cs-promoted catalyst the rate-determining step of the reaction becomes catalyst re-oxidation; moreover, TPR/TPO measurements evidenced that the presence of increasing amounts of Cs enhanced the rate of the rate-determining step, accelerating the re-oxidation of reduced V sites by O_2.

This effect however becomes evident at 320°C only when *o*-xylene conversion is higher than the 30%. This is likely due to the fact that an increase of the hydrocarbon conversion causes an increase of the O_2/*o*-xylene ratio in the gas-phase; only when this ratio becomes higher than a defined value, does the enhancement effect of Cs on V re-oxidation rate become effective and play a role on catalytic performance. To confirm this hypothesis catalytic tests feeding a lower amount of hydrocarbon were carried out. Using a hydrocarbon-leaner feedstock, the surface concentration of reactants and intermediates is lower, so no activity enhancement effect by Cs should be observed.

Figures 5.5-5.7 report the results obtained at 320°C, feeding 0.5 mol.% *o*-xylene in air.

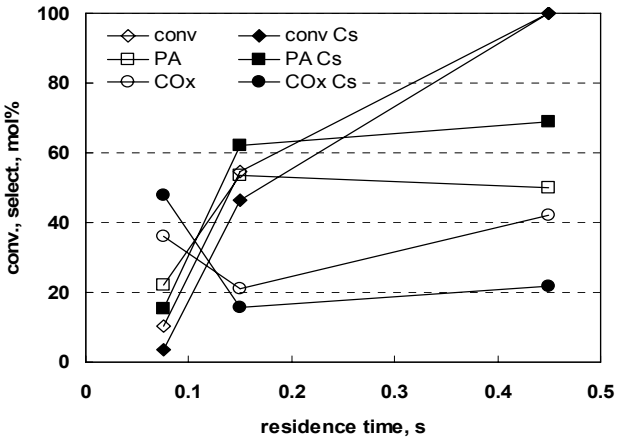

Figure 5.5: Conversion of *o*-xylene and selectivity to phthalic anhydride (PA) and carbon oxides (COx) for the undoped (open symbols) and Cs-doped (full symbols) catalysts as functions of the residence time. Feed composition: 0.5 mol% *o*-xylene in air. Temperature 320°C.

The two catalysts gave the same conversion, and under these conditions all the reaction intermediates were re-adsorbed and successively oxidized to PA. With

the undoped catalyst, the conversion of *o*-xylene at 0.15 and at 0.45 s residence time, under *o*-xylene–lean conditions, was much greater than that observed with 1% *o*-xylene in feed. This indicates that under the latter conditions the catalyst surface is saturated by the adsorbed reactant and intermediates.

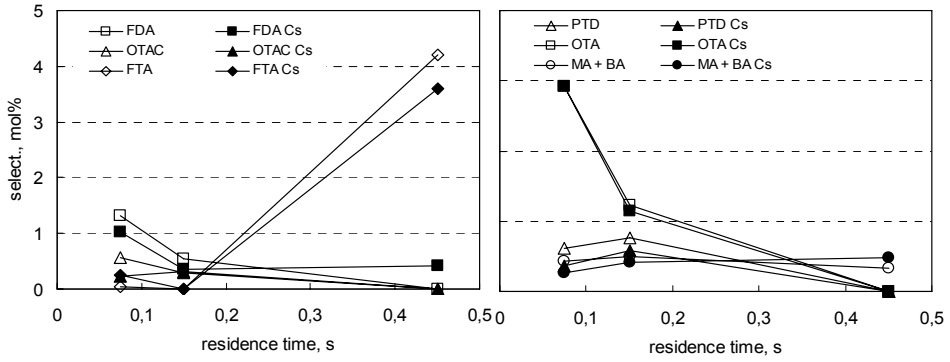

Figure 5.6 (left): Selectivity to phthalide (PTD), o-tolualdehyde (OTA), maleic anhydride (MA) and benzoic acid (BA) for the undoped (open symbols) and Cs-doped (full symbols) catalysts as functions of the residence time. Feed composition: 0.5 mol% *o*-xylene in air. Temperature 320°C.
Figure 5.7 (right): Selectivity to phthalaldehyde (FDA), o-toluic acid (OTAC) and phthalic acid (FTA) for the undoped (open symbols) and Cs-doped (full symbols) catalysts as functions of the residence time. Feed composition: 0.5 mol% *o*-xylene in air. Temperature 320°C.

The Cs-doped catalyst showed to be more selective to PA at all conversion levels, at both conditions of inlet *o*-xylene concentration tested. This corresponded to a lower selectivity to CO_x, even at very low *o*-xylene conversion.
The other consecutive transformations were apparently not remarkably affected by the presence of Cs. This indicates that the higher availability of surface oxidizing sites lowers the contribution of parallel combustion by non-selective oxygen species, and favors the reaction pathway of oxidation of adsorbed *o*-xylene.

5.3.3 The reaction network at 400°C

Reaction network at high temperature was also investigated; these conditions are similar to the actual ones (industrially it is necessary to work at temperatures higher than 350°C to ensure almost total conversion of *o*-xylene). Catalytic tests were carried out feeding 1 mol% *o*-xylene at 400°C and varying the residence time. Because of the catalysts were very active, also test with very short residence time were carried out (<0.001s), to control the distribution of products at very low o-

xylene conversion and to determine the primary and secondary compounds formed from *o*-xylene. Results of test are reported in Figure 5.8-5.11.

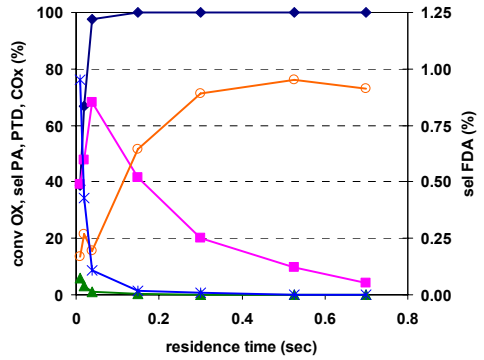

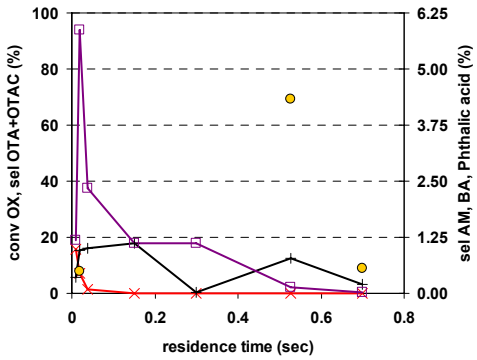

Figure 5.8 (left): *o*-xylene conversion (◆) and selectivity to phthalic anhydride (PA, ■), phthalide (PTD, ▲) and CO + CO_2 (○)and phthaldialdehyde (FTA, ✳) as function of residence time, T: 400°C. undoped sample.
Figure 5.9 (right): Selectivity to *o*-toluic aldehyde + *o*-toluic acid (OTA+OTAC, ×), maleic anhydride (AM, □), benzoic acid (BA, +) and phthalic acid (FTA, ●) as function of residence time, T: 400°C. undoped sample.

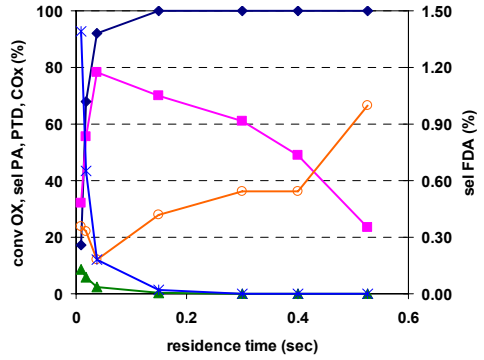

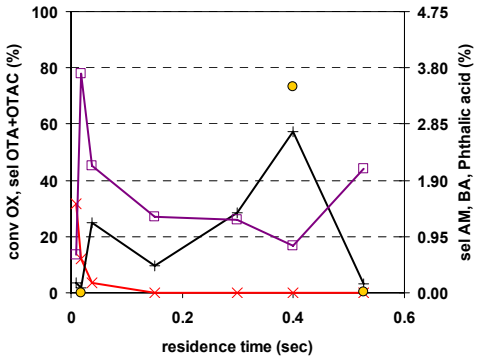

Figure 5.10 (left): *o*-xylene conversion (◆) and selectivity to phthalic anhydride (PA, ■), phthalide (PTD, ▲) and CO + CO_2 (○)and phthaldialdehyde (FTA, ✳) as function of residence time, T: 400°C. Cs-doped sample.
Figure 5.11 (right): Selectivity to *o*-toluic aldehyde + *o*-toluic acid (OTA+OTAC, ×), maleic anhydride (AM, □), benzoic acid (BA, +) and phthalic acid (FTA, ●) as function of residence time, T: 400°C. Cs-doped sample.

In both samples *o*-xylene conversion rapidly increased with the residence time, reaching values near 100% already at residence time lower than 0.04 s; hence, at this temperature no saturation effect of the catalyst surface was evident.
Cs doped sample was slightly more active at low contact time; this may suggest that at high temperature and low contact time sample containing Cs favours a second way of activation and transformation of *o*-xylene, likely the oxidation to phthalaldehyde.

With both catalysts, primary products were *o*-tolualdehyde and phthalaldehyde to confirm that *o*-xylene can interact with the catalyst surface through one or both methylic groups. Products that underwent consecutive reaction were phthalaldehyde, *o*-tolualdehyde, phthalide and phthalic acid.

A difference with respect to the reaction scheme proposed in Figure 5.4 concerns the trend of selectivity to phthalide. In fact at 400°C this compound seems to be a primary product, because its selectivity was not zero at nil residence time. Then it derives from *o*-tolualdehyde and/or *o*-toluic acid, but also may form from phthalaldehyde by intramolecular Tishchenko-like reaction. Due to the elevated availability of oxidizing sites formation of dialdehyde is favored, its strong interaction with the catalyst surface causes its consecutive transformation to phthalide before it may desorb into the gas phase. Moreover, at 400°C, phthalide is consecutively oxidized to phthalic anhydride. Therefore two kinetically independent reaction pathways lead to the formation of phthalic anhydride at 400°C: (a) the oxidation of *o*-tolualdehyde to phthalaldehyde and phthalic acid, and the dehydration of the acid to phthalic anhydride, and (b) the oxidation of phthalide. Maleic anhydride is a final, secondary product, which didn't undergo other reaction, while benzoic acid underwent a side reaction and is probably degraded to CO_x.

Selectivity to phthalic anhydride showed a maximum for both samples. The initial increasing in selectivity was due to the transformation of intermediates to phthalic anhydride, while at high residence time was due to the side reaction on phthalic anhydride to CO and CO_2. Cs-doped catalyst was more selective than the undoped sample; the difference of selectivity to phthalic anhydride between the two samples was great especially at high residence time, when the contribution of the side reaction to CO_x was much more higher in the case of undoped catalyst. Also at low residence time, Cs-doped sample was more selective than the undoped one; this means that Cs not only decreases the undesired contribution of side reaction on phthalic anhydride, but also increases the rate of a reaction responsible for its formation.

Tests carried out at high temperature varying the residence time confirmed the reaction scheme proposed in Figure 5.4; in addition also the direct oxidation of *o*-xylene to yield phthalide (via phthalaldehyde and/or *o*-tolualdehyde) is possible.

Moreover, at this temperature phthalide was easily oxidized to phthalic anhydride.

5.3.4 The role of Cs at 400°C

The most relevant difference between the undoped catalyst and the Cs-doped one was the presence, in the former, of a consecutive reaction of phthalic anhydride combustion to CO_x. With the undoped catalyst, this reaction greatly contributed to the decrease of the selectivity to phthalic anhydride at high temperature.

A possible explanation is that at high *o*-xylene conversion, phthalic anhydride hydrolyses to form phthalic acid; in these conditions a not negligible amount of water is present in the reaction atmosphere (water is a co-product of the reaction). Cs could inhibit the hydrolysis of phthalic anhydride.

To better understand which kind of reaction was responsible for the degradation of phthalic anhydride, catalytic test feeding this compound were carried out. Phthalic anhydride was first dissolved in toluene (concentration: 0.1 mol% anhydride), then of the solution was vaporized and fed to the reactor. To simulate the reaction atmosphere a flow of wet air was used; 3 mol.% of steam was fed saturating the flow of dry air by bubbling it in water. Because V/Ti/O systems catalyzes oxidation of toluene to benzaldehyde [1,13], separate tests were carried out feeding toluene vapors in wet air. The yield to products so obtained (CO_2, maleic anhydride, benzoic acid) was subtracted from the corresponding yield obtained by feeding the toluene/phthalic anhydride mixture at the same reaction conditions.

Results obtained with the undoped sample are shown in Table 5.1.

Table 5.1: Phthalic anhydride conversion and yield to phthalic acid (undoped sample)

T (°C)	PA conversion (%)	Phthalic acid yield (%)
360	80	55
380	100	-

Phthalic anhydride was hydrolyzed to phthalic acid: at 360°C the yield to this product was 55 mol.%. At higher temperature, phthalic acid underwent

consecutive oxidation to CO_x. On the contrary, with the Cs-doped sample no formation of phthalic acid was evident.

This confirms that the hydrolysis of phthalic anhydride to phthalic acid is the key reaction determining catalytic performances at high temperature, in term of selectivity. Phthalic acid, in fact, can easily undergoes decarboxylation to form CO_x. The presence of Cs inhibits the hydrolysis to phthalic acid and guarantees high selectivity to phthalic anhydride, also at high *o*-xylene conversion.

5.4 CONCLUSIONS

The effect of the dopant Cs on the catalytic performance of a titania (anatase)-supported 7 wt% V_2O_5 catalyst in *o*-xylene oxidation to PA has been investigated in relation to the reaction network at 320°C and 400°C.

The reaction scheme proposed for *o*-xylene oxidation is shown In Figure 5.12.

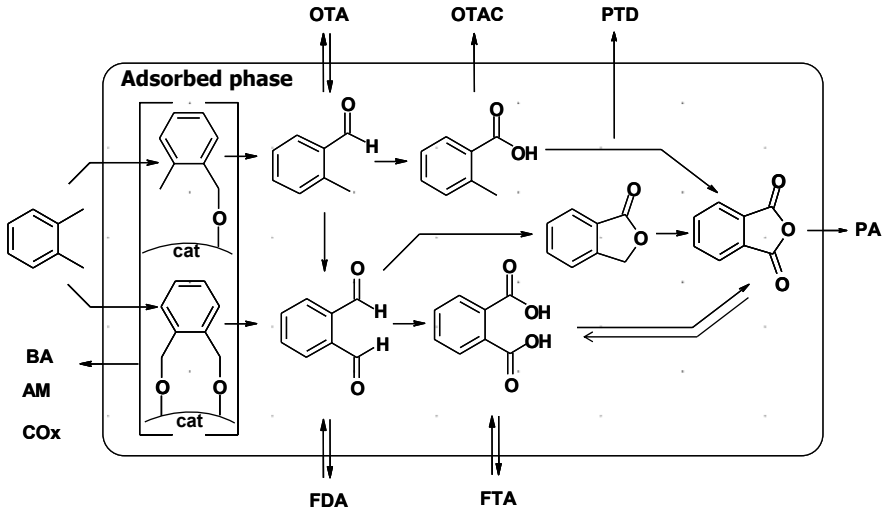

Figure 5.12: Hypothesized reaction schema for *o*-xylene oxidation to phthalic anhydride. Oxygen and water are not indicated.

Two new reaction intermediates were observed, such as phthaldialdehyde and *o*-phthalic acid; phthaldialdehyde is formed both from *o*-toluic aldehyde and *o*-xylene, and is transformed into phthalide by Tishchenko reaction and in *o*-phthalic acid by oxidation. Phthalic anhydride was formed both by oxidation of the dialdehyde to phthalic acid, which then dehydrates to PA, and oxidation of phthalide. The main route of degradation of phthalic anhydride is its hydrolysis to phthalic acid, precursor of CO_x.

Cs was found to play different role depending on working conditions:

(i) at low temperature (under conditions of incomplete hydrocarbon conversion) favors the formation of phthalic anhydride with respect to parallel reactions to CO_x and avoid the saturation effect maintaining a cleaner and more oxidizing catalyst surface;

(ii) at high temperature inhibits the hydrolysis of the anhydride to phthalic acid, precursor of CO_x.

5.5 REFERENCES

[1] B. Grzybowska, Appl. Catal. A. 157 (1997) 263.

[2] C.R. Dias, M.F. Portela, G.C. Bond, Catal. Rev.-Sci. Eng. 39(3) (1997) 169.

[3] G.C. Bond, J. Chem. Tech. Biotech. 68 (1997) 6

[4] G. Centi, Appl. Catal. A 147 (1996) 267.

[5] P. Courtine, E. Bordes, Appl. Catal. A 157 (1997) 45.

[6] V. Nikolov, D. Klissurski, A. Anastasov, Catal. Rev.-Sci. Eng. 33 (1991) 319.

[7] G.C. Bond, Appl. Catal. A 191 (2000) 69.

[8] I.E. Wachs, B.M. Weckhuysen, Appl. Catal. A 157 (1997) 67.

[9] B. Grzybowska, Top. Catal. 21 (2002) 35.

[10] S. Anniballi, F. Cavani, A. Guerrini, B. Panzacchi, F. Trifirò, C. Fumagalli, R. Leanza, G. Mazzoni, Catal. Today 78 (2003) 117.

[11] F. Cavani, C. Cortelli, A. Frattini, B. Panzacchi, V. Ravaglia, F. Trifirò, C. Fumagalli, R. Leanza, G. Mazzoni, Catal. Today 118 (2006) 298.

[12] K. Tanabe, K.Saito, J. Catal., 35 (1974) 247]

[13] A. J. Van Hengstum, J. G. Van Ommen, H. Boseh and P. J. Gellings, Appl. Catal, 8 (1983) 369-382

6

EFFECT OF SUPPORT

6.1 INTRODUCTION

Titanium oxide is widely used as support for metal or metal oxide catalytic elements such as in the case of *o*-xylene selective oxidation. Besides, TiO_2 is also a well-known photocatalyst with applications ranging from water purification to health protection (indoor and outdoor air purification), H_2 production (by water photodissociation) and preparation of advanced materials (self-cleaning glasses and tissues, etc.) [1–6]. Recently, growing interest on these materials regards the possibility of nanostructuring titania, especially for photocatalytic applications. Titanium dioxide nanoparticles have been shown to possess highly efficient photocatalytic activity [7]. It is known that decreasing particle size improves the catalytic performance of this system, not only because of an increase in surface area, but also by modification of the band gap and/or introduction of intermediate states which modify the pathways of photocatalytic processes. In general, nanoparticles have been under intense examination due to their ability to possess properties that vary from the bulk material. Consequently, it may be interesting to investigate the behaviour of this kind of systems also as support for metal oxides (e.g. V_2O_5). In particular, different crystal sizes could affect the nature of the V species that form over titania. However, nanosized TiO_2 has high specific surface area, while titania used as the support for vanadium oxide based catalysts (for the selective oxidation of *o*-xylene to phthalic anhydride) has a specific surface area lower than 30 m^2/g in order to avoid consecutive reactions on the desired product and ensure high selectivity to phthalic anhydride. To decrease the specific surface area, freshly precipitated titania is usually calcined at

high temperature. In this section is reported an attempt to obtain samples of nanocrystalline TiO_2, in the anatase form and having (i) comparable surface area, but (ii) different crystal size, in order to study the effect of the latter parameter on the nature of the V species and finally on the catalytic performance. To this purpose, starting from two samples of TiO_2 synthetized in organic solvent, calcination treatments were carried out, while checking for the variation of the crystallites size.

6.2 EXPERIMENTAL

Samples were prepared by the group of Dr. M. Niederberger under solvothermal conditions [8]. The solvent was mixed with titanium tetraisopropoxide in a glove box under Ar (molar ratio solvent/Ti =10). The reaction mixture was transferred into a steel autoclave equipped with a Teflon liner, which was sealed, removed from the glove-box and heated in an oven for 1 day. The yellow suspension obtained, was separated by centrifugation. The precipitate was washed with chloroform and dichloromethane, and then dried in vacuum. Details about the synthesis conditions are summarized in Table 6.1.

Table 6.1: Studied samples.

Sample code	Solvent	Synthesis Temperature
Sample1	2-butanone	180°C
Sample2	benzaldehyde	200°C

Thermogravimetric analysis (TGA) were performed using a TA instrument (TGA2050) under flow of air.

6.3 RESULTS AND DISCUSSION

The samples were analyzed by means of thermogravimetric analysis (TGA) in order to identify the temperature at which the organic residuals are eliminated and the amount of the latter. Titania was heated in flow of air from room temperature up to 600°C for 30 min (heating rate: 10°C/min). Analysis conditions are similar to those usually used for calcination of samples, then also indications

of the minimal temperature at which the thermal treatment should be performed could be obtained.

Figure 6.1 shows the thermograms of the two samples.

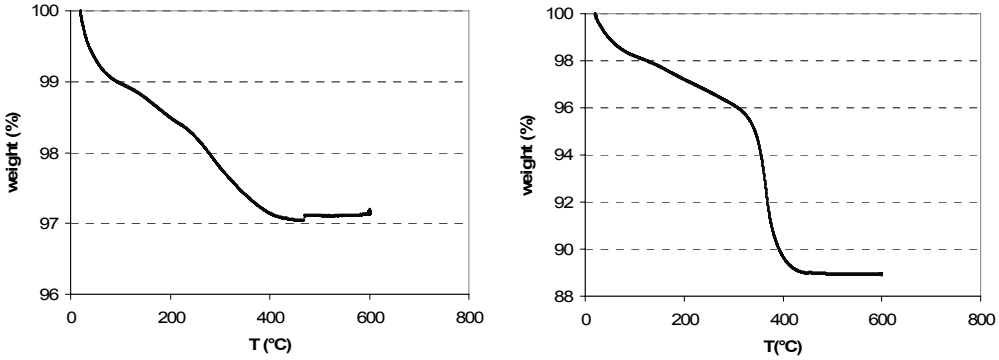

Figure 6.1: Thermograms of Sample1 (left) and Sample2 (right)

TiO_2 synthetized in benzaldehyde (Sample2) showed a considerable decrease of weight at 360°C (ca. 11%), while for TiO_2 synthetized in 2-butanone the weight loss was gradual, not so accentuated (only 3%) and started at lower temperature. It is evident that when butanone was used for the synthesis (Sample1) a lower amount of solvent was adsorbed on titania and that it was bound more weakly.

Both samples have been characterized by SEM and Raman spectroscopy before and after TGA.

Figures 6.2 and 6.3 show SEM images of the samples.

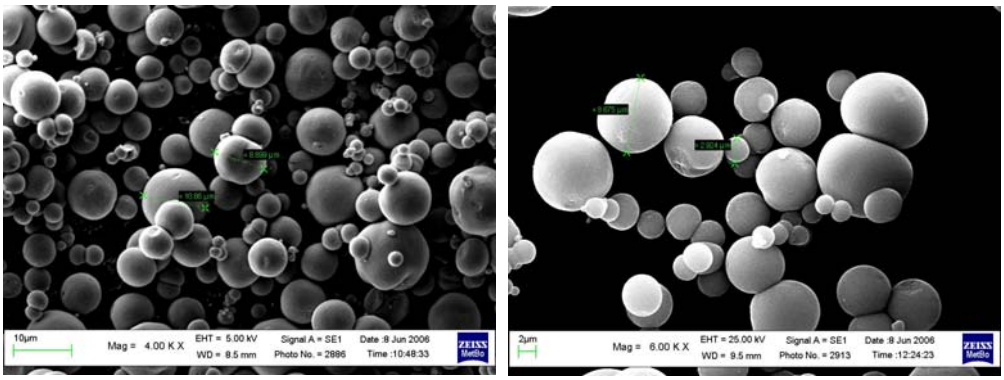

Figure 6.2: SEM images of Sample1 before (left) and after (right) TGA.

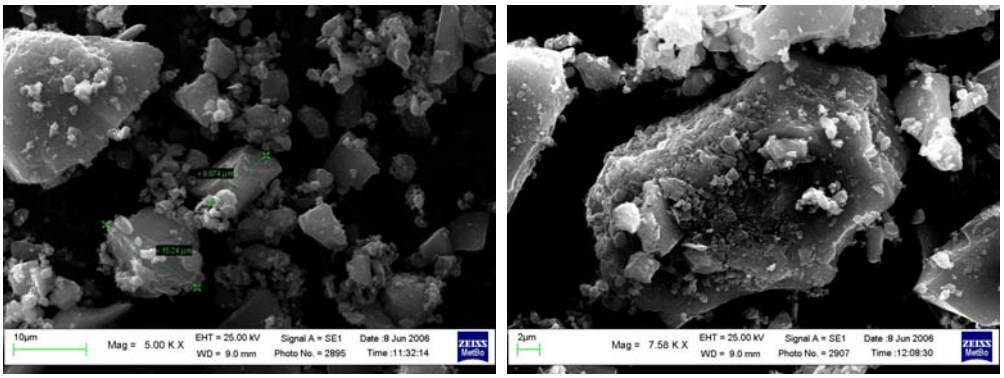

Figure 6.3: SEM images of Sample2 before (left) and after (right) TGA.

Morphology of the samples was quite different: Sample1 (solvent: 2-butanone) was constituted of spherical particles of 2-8 μm of diameter, while Sample2 was less "homogenous" in shape and size of particles. In both cases, morphology was not much affected by thermal treatment at high temperature.
In Figure 6.4 are reported Raman spectra of the samples before and after TGA.

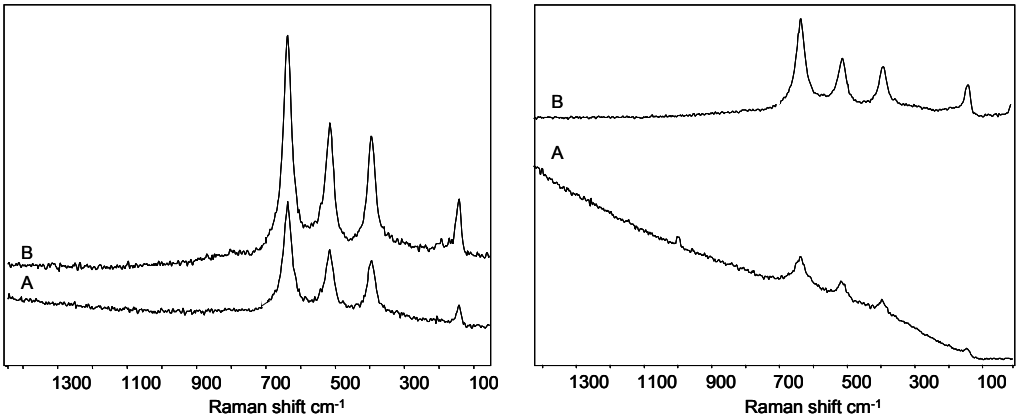

Figure 6.4: Raman specrta of Sample1 (left) and Sampl 2 (right), before (A) and after (B) TGA.

In all spectra the typical bands of TiO_2 anatase (at 180, 380, 520 and 640 cm^{-1}) were present, therefore the treatment at 600°C did not cause the transformation of titania anatase into rutile form. In the spectra of fresh samples (A) a rising of the baseline going to higher values of Raman shift was observed; this effect is typical of fluorescence phenomena that are promoted by organic compounds present as impurities. Indeed, fluorescence was more pronounced for Sample2 that from TGA analysis turned out to contain contained an higher amount of

residual solvent. Raman spectrum of this sample, collected before TGA, also showed a band at 1000 cm^{-1}, typical of benzaldehyde used as solvent.

Since after the treatment at 600°C TiO_2 was still in anatase form, samples were calcined at this temperature according to the following procedure:

- heating in static air from room temperature up to 600°C (rate 10°C),
- isothermal step at 600°C for 1 hour.

Figures 6.5 and 6.6 compares the X-ray diffraction patterns of the samples before and after the thermal treatment: all reflections corresponde to pure anatase, to confirm that the calcination temperature does not promote the anatase-rutile phase transition.

However, after calcination diffractograms showed more defined reflections to indicate an increase of crystallinity.

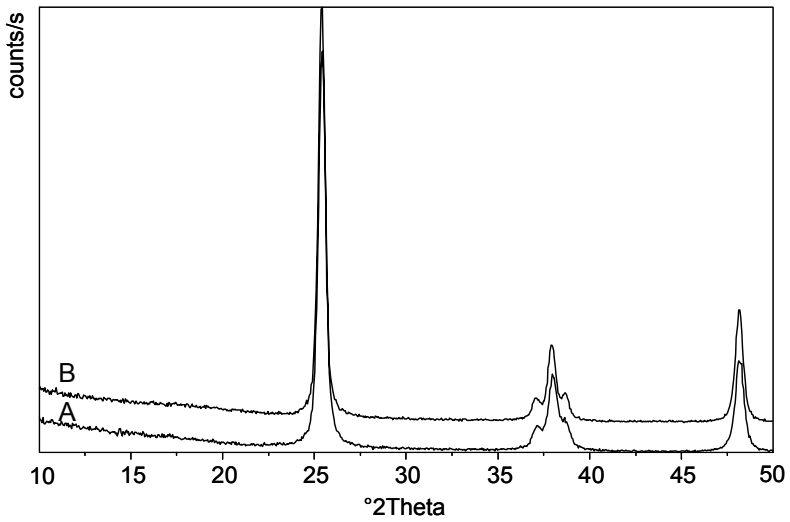

Figure 6.5: XRD patterns of Sample1 before (A) and after (B) the thermal treatment at 600°C

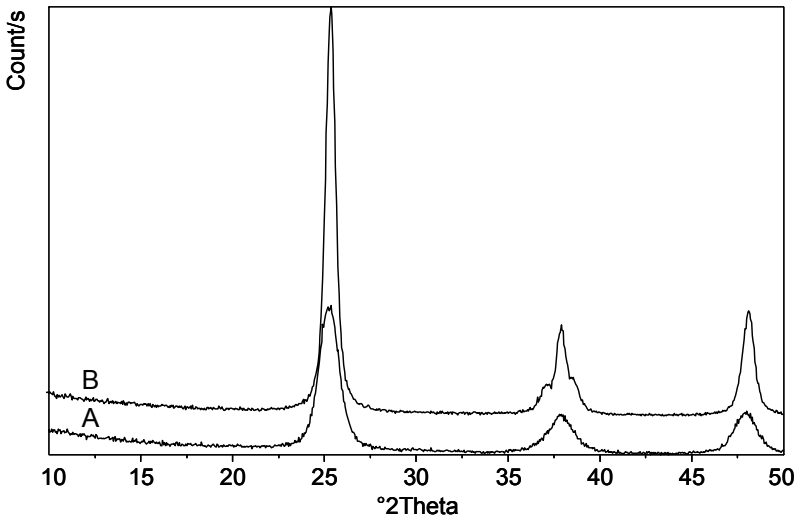

Figure 6.6: XRD patterns of Sample2 before (A) and after (B) the thermal treatment at 600°C.

Variation in crystal size of sample due to calcination was investigated calculating the crystallites size from Scherrer equation using the reflection at 25 °2theta as reference. The specific surface area was determined by N_2 adsorption at 77K (by BET equation). Table 6.2 summarizes the surface areas and the crystallites size of samples before and after calcination. As reference also features of a typical TiO_2 support are reported.

Table 6.2: Crystal size and specific surface areas of samples

Sample code	Solvent	Size[a] (nm)	Size[b] (nm)	Area[b] (m^2/g)
Sample1	2-butanone	21.6	23.8	50
Sample2	benzaldehyde	6.8	14.4	76
Commercial TiO_2	-	n.d.	60	30

[a] **fresh sample**
[b] **calcined sample**

Before calcination both samples had nanosized particles; Sample1, prepared with butanone, had crystallites larger than Sample2. The differences between fresh samples were maintained even after thermal treatment; in both cases crystallites size increased slightly after calcination, more for Sample2 than for Sample1. As expected, surface area was higher for the sample having lower crystallinity. However these values were still high with respect to those typically used in industrial catalysts for *o*-xylene oxidation. We tried to lower surface area of

Sample2 to approx 50 m^2/g by calcination at 600°C for prolonged time, while leaving crystal size close to 15 nm. These samples will be less meaningful from the industrial point of view, because of the high surface area, nevertheless they will be quite meaningful for characteristics/activity relationship study. After calcination at 600°C for 7 hours Sample2 had crystallites size of 18 nm, being surface area still high (65 m^2/g).

6.4 CONCLUSIONS

In this section, a preliminary study on the effect of calcination procedure on crystal size of anatase was reported. Two samples synthetized with different solvents, and having different crystallinity were calcined to obtain systems still having nanometric crystallites but relatively low surface area. This is necessary in order to evaluate the effect of titania crystal size on the nature of V species, and consequently on catalytic performances of VTiO systems in selective oxidation reactions. It was found that, depending on the solvent, samples show different crystallinity. In particular using benzaldehyde smaller particles can be obtained. Calcination at 600°C, also for a long period, slightly affects crystallites size; nevertheless, specific surface areas are still to high to allow the use of these materials as support for o-xilene oxidation catalysts.

6.5 REFERENCES

[1] K. Kabra, R. Chaudhary, R.L. Sawhney, Ind. Eng. Chem. Res. 43 (2004) 7683

[2] A. Kudo, Catal. Surveys Asia 7 (2003) 31.

[3] D. Bahnemann, Sol. Energy 77 (2004) 445.

[4] M. Anpo, Bull. Chem. Soc. Jpn. 77 (2004) 1427

[5] M. Anpo, Pure Appl. Chem. 72 (2000) 1265

[6] H. Gnaser, B. Huber, C. Ziegler, Encyclopedia of Nanoscience and Nanotechnology, vol. 6, American Scientific Publisher, Los Angeles, 2004, p. 505

[7] S. Weaver, G. Mills, J Phys Chem B 101 (1997) 3769

[8] G. Garnweitner, M. Antonietti, M. Niederberger, Chem. Commun., (2005) 397

7

CONCLUSIONS

Phthalic anhydride is produced by gas-phase selective oxidation of *o*-xylene; the catalysts is a supported system formed by V_2O_5 on TiO_2 (V/Ti/O). Interaction between V_2O_5 and the support generates different V species: (i) V species which is chemically bound to the support via oxo bridges (isolated V in octahedral or tetrahedral coordination, depending on the hydration degree), (ii) a polymeric species spread over titania, and (iii) bulk vanadium oxide, either amorphous or crystalline. The amount of different vanadium species is function of vanadium content and of the titania surface area. The different species could have different catalytic properties, therefore changes of the relative amount of V species can affect catalytic performances of the system.

A series of sample containing increasing amount of vanadium (1-15wt% V_2O_5) were prepared by impregnation procedure and tested in the *o*-xylene oxidation reaction, with the aim of investigate the effect of vanadium loading. In this way information about the intrinsic reactivity of each vanadium species could be obtained. It was found that the activity of VO_x species decreases when the vanadium oxide loading is increased, indicating that the activity of the highly dispersed (isolated and oligomerized) VO_x species is higher than that of the polymeric vanadate. When the formation of bulk vanadium oxide occurs, a further decrease of activity is observed. Concerning the selectivity to C_8 oxygenates, it is a function of both the vanadium oxide loading and of the conversion. At high *o*-xylene conversion, the best selectivity to phthalic anhydride + phthalic acid is offered by the catalysts containing bulk vanadium oxide; on the other hand, the sample having the lower amount of vanadium oxide loading provides an excellent selectivity to C_8 oxygenates at 50-60% *o*-xylene conversion.

Another important aspect that I studied in my PhD was dealing with the changes that the catalytic surface can undergo under working conditions. In fact, the high temperature and a different gas-phase composition could have an effect also on the formation of different V species, and consequently on the catalytic performances. Steam is a gas phase component always present in the reaction atmosphere, then it could have an effect on the catalytic behaviour of V/Ti/O system. The dynamic phenomena occurring at the surface of a 7wt% V_2O_5 on TiO_2 catalyst in the presence of steam was investigated by means of Raman spectroscopy and reactivity tests. It has been demonstrated that this gas-phase component modifies the relative amount of V species present on the support and consequently affects catalytic performances. If the reaction is carried out in presence of 3 vol% steam in the inlet feed (during reaction the amount of steam does not exceed 2%) a remarkable improvement of the catalytic activity is observed. *In-situ* Raman measurements evidenced that this effect is due to the dispersion of bulk vanadium oxide to generate a higher number of active sites. The effect is quite reversible, and the interruption of the steam feed leads to a recover of the initial catalytic activity owing to the re-aggregation of dispersed V species into bulk vanadium oxide. Vanadium oxide spreading and re-aggregation are the result of contrasting driving forces: for kinetically reason the dispersion is favoured only at relative high temperature (400°C), on the other hand if temperature is too high (450°C) the segregation of bulk vanadia is thermodynamically favoured.

Finally, the effect of Cs on the reaction mechanism of *o*-xylene oxidation was investigated at two different temperatures with the aim of evidencing in which step of the reaction network this promoter plays its role. Two new reaction intermediates were observed: phthaldialdehyde and *o*-phthalic acid. Phthaldialdehyde is formed both from *o*-toluic aldehyde and *o*-xylene, and is transformed into phthalide or phthalic acid. The main route of degradation of phthalic anhydride is its hydrolysis to phthalic acid, precursor of CO_x.

Cs was found to play different roles depending on working conditions: at low temperature it avoids the saturation maintaining a cleaner and more oxidizing catalyst surface; at high temperature it inhibits the hydrolysis of the anhydride to phthalic acid, precursor of CO_x.

Ringraziamenti

Pensavo di non riuscire ad arrivarci più... invece, finalmente, l'ultima pagina!
Questi tre anni di dottorato sono stati per me un'esperienza bellissima. Ho imparato tante cose, e sono cresciuta tanto sia dal punto di vista scientifico che da quello umano. E se questo è stato possibile è grazie all'aiuto di tante persone.
Grazie alla mia meravigliosa famiglia, per avermi sempre lasciata libera di decidere cosa volessi fare da grande e per avermi appoggiato e supportato in tutte le mie scelte.
Grazie al Prof. Cavani, per aver creduto in me e quando forse neanche io ci credevo troppo, per avermi trasmesso la passione e l'entusiasmo che servono per fare questo "lavoro" e per la fiducia che continua ad avere in me nonostante a volte avrebbe fatto bene a licenziarmi!
Grazie a Polynt SpA, non solo "per il supporto scientifico e finanziario al progetto di ricerca", ma per avermi insegnato a guardare le cose da una prospettiva diversa, al mio grande capo Carbotta, a Federico, Roberto, Tiziana, il Dott. Piola e il Dott. Mazzoni.
Grazie ai ragazzi che hanno avuto la sfortuna di lavorare con me in questi anni, perché senza di loro la mia tesi sarebbe stata molto più corta da scrivere. Grazie ai "miei" uomini del VPO per avermi fatto cominciare e finire in bellezza ed allegria questo dottorato. A Davide, per avermi fatto fare amicizia con l'impianto maleica e per avermi insegnato a non prendere tutto sempre troppo sul serio, e a Fede, per l'entusiasmo e le battute grezze, ma anche per i discorsi seri e per quelle domande di chimica che mi fanno venire mille dubbi e mi costringono a riflettere sulle cose... che magari così mi viene anche qualche bella idea! Grazie alle ragazze: ad Ali, perché la sua voglia di fare e di imparare mi ha aiutato a superare quei momenti in cui il dottorato non sembrava un'esperienza poi così fantastica; ad Auro, per aver cercato di mettere un po' di ordine tra i miei fogli e nella mia vita (ma forse sono troppo vecchia per cambiare!); ad Elisa, perché se oggi sono così è un po' anche colpa o merito suo.
Un grazie enorme a tutti i ragazzi che in questi anni sono passati per il lab, a partire dai miei compagni di scrivania. A Stefaniù, per le interminabili chiacchierate sul lab, sulla vita e sul mondo (il tutto alle 7 di sera sulle scale della facoltà!); a Stefano e al suo non arrendersi mai e combattere per cambiare le cose che non vanno, ma soprattutto per avermi aperto gli occhi sul fantastico mondo della tecnologia... e di UBUNTUUUUU!! A miei compagni di sventura Gamba, Dario, Saurino e "l'amico dottorando" Andrea. E a tutti gli altri: Ros, Peppino (anche se forse ti ho fatto lavorare troppo la copertina è fantastica, grazie!), Alle, Kate, il Naz, Simon, Irene, Patricia... Grazie anche ai "vecchi", Mattia, Ale, Antonio, Carlo, Max, Jo... e a tutti i giovani...
Grazie davvero perché questi tre anni saranno indimenticabili, ed è tutto merito vostro!